

**Characterising vascular changes in the spinal cord after injury  
as a novel therapeutic target**

**Nicole Jade Smith**

PhD Thesis

Submitted in accordance with the requirements for a degree of Doctor in  
Philosophy

University of Leeds

Biomedical Sciences

October 2021

## **Intellectual property rights**

The candidate confirms that the work submitted is her own and that appropriate credit has been given where reference has been made to the work of others.

This copy has been supplied on the understanding that it is copyright material and that no quotation from the thesis may be published without proper acknowledgement.

The right of Nicole Jade Smith to be identified as Author of this work has been asserted by her in accordance with the Copyright, Designs and Patents Act 1988.

© The University of Leeds and Nicole Jade Smith

## Acknowledgements

Firstly, I would like to thank my supervisor Professor Stuart Egginton for his support and guidance throughout my project. Thank you for helping me to persevere and showing me how to always keep learning. I hope I can go on as many adventures in my career as you!

To Nat Doody, I will never be able to thank you enough for your friendship and teamwork throughout our PhDs; I couldn't have done it without you. I have loved going on this journey with you and seeing the researchers and people we have grown into. Thank you for keeping me sane, and I hope the dream team comes back together in the future!

Thank you to Dr Jessica Kwok and Professor Ronaldo Ichiyama for your advice and expertise; I have learnt a huge amount from you both. To Dr Sîan Irvine and Dr Roger Kissane, thank you for teaching me all the lab techniques I needed to know, and a few extra ones too, and for the fun along the way. I would also like to thank all the staff in CBS (particularly Neil and Andy) for making this project possible and providing such knowledgeable insight along the way. To Martin in the electron microscopy department, thank you for all of your hard work and perseverance; you allowed me to get some great images and some interesting data! Thank you to Dr Pete Tickle and Hakam Nazir for providing the tissue and making my first experiments at Leeds possible. Thank you also to Kateřina Štěpánková and Eliane Vitoriano for helping with the stereology data collection.

To Maddie, Varinder, Sîan, and Dani, thanks for all of the lunch dates and chats, and making my time at Leeds memorable. I would also like to thank Jess, Maddie, and Nat (again) for somehow making PhD life in lockdown as fun as

possible and learning so many new things together. Suzie and Liv, thanks for all of the very belated birthdays across cities and for always being great friends, regardless of how often we actually see each other! Thank you also to my friends outside the lab for all of your support; even if it was just a random coffee date, you all helped me get through it.

Finally, I would like to thank my family for always believing in me. You have taught me to never give up, and your love and support means the world to me. Mum, Dad, and Jennifer, thank you for putting up with the grumpy chats and for always helping me to get to the other side. To Tom, thank you for being the light at the end of this long journey and for keeping me going through these last years. I love you all.

## Abstract

After spinal cord injury (SCI), vascular integrity is disrupted by the primary mechanical trauma and secondary biochemical insult, impeding neuronal regeneration and functional recovery. A systematic analysis of changes within the capillary bed following common angiogenic treatments in rats before and after moderate/severe T10 contusion injury aimed to identify potential targets for vascular regeneration. A combined intrathecal delivery of angiopoietin-1 (Ang1) and vascular endothelial growth factor (VEGF) may stabilise damaged microvessels and promote angiogenesis.

Intact rats received prazosin administration or wheel running for 10 days before perfuse fixation. Animals with an SCI were perfuse-fixed on days 2, 5, 15, and 45 post-injury. A parallel group of animals also had a subdural osmotic pump inserted delivering Ang1/VEGF or a vehicle intrathecally for 14 days, and were perfuse-fixed at days 5 and 15. Capillary number, surface area, areal density, and feret diameter were measured. Transmission electron microscopy (TEM) was used to characterise vessel microstructure.

Accurate and reliable capillary staining was optimised, however no angiogenesis was observed in intact spinal cords following angiogenic stimuli. Adverse, widespread changes in injured spinal vasculature showed some recovery with time. Capillary collapse close to the injury epicentre partially resolved by day 15, however vessel abnormalities were present at day 45. TEM confirmed severe vessel damage at day 2; endothelial cell tight junction structure was significantly compromised. Ang1/VEGF delivery led to improved vascular morphology compared to vehicle controls, particularly at T11. However, TEM measurements were variable following Ang1/VEGF treatment

between regions and timepoints, potentially indicating the balance of Ang1/VEGF needs optimising.

These studies demonstrated acute regression or collapse of capillaries after SCI, with abnormal vessels persisting for at least 45 days. Stabilising the capillaries and promoting angiogenesis using Ang1 and VEGF respectively showed promise as an approach to reduce this damage and potentially encourage functional recovery after SCI.

## Table of contents

<b>Intellectual property rights</b> .....	<b>i</b>
<b>Acknowledgements</b> .....	<b>ii</b>
<b>Abstract</b> .....	<b>iv</b>
<b>Table of contents</b> .....	<b>vi</b>
<b>Table of figures</b> .....	<b>xi</b>
<b>Table of tables</b> .....	<b>xiii</b>
<b>List of abbreviations</b> .....	<b>xiv</b>
<b>Chapter 1 : General introduction</b> .....	<b>1</b>
1.1 Spinal cord injury .....	2
1.2 Angiogenesis .....	6
1.3 The blood spinal cord barrier .....	12
1.4 Vascular response to SCI .....	16
1.5 Current vascular treatment strategies .....	20
1.5.1 Vasodilators .....	20
1.5.2 Exercise .....	22
1.5.3 Growth factors.....	25
1.6 Aims and objectives .....	29
1.6.1 Overall objectives.....	29
1.6.2 Promoting spinal cord angiogenesis via systemic stimulation...29	
1.6.3 Characterising vasculature after SCI .....	30
1.6.4 Stabilising capillaries after SCI using Ang1 and VEGF .....	30
<b>Chapter 2 : General materials and methods</b> .....	<b>32</b>
2.1 Ethics .....	33
2.2 Animals .....	33
2.3 Solutions .....	33
2.3.1 Phosphate buffer.....	33
2.3.2 Paraformaldehyde.....	34
2.3.3 Sucrose.....	34
2.3.4 Phosphate buffered saline .....	34
2.3.5 Tris non-saline .....	34
2.3.6 Dextran .....	34
2.3.7 Heparin and sodium nitroprusside .....	35
2.4 Spinal cord preparation.....	35
2.4.1 Snap freezing.....	35

2.4.2 Perfuse fixation .....	35
2.5 Acute contusive spinal cord injury .....	36
2.6 Cyrosectioning .....	38
2.7 Immunohistochemistry .....	38
2.8 Microscopy .....	39
2.9 Analysis .....	39
2.9.1 Stereology .....	39
2.9.2 Minimum feret diameter .....	41
2.9.3 Statistics .....	41
<b>Chapter 3 : Spinal cord microcirculation and angiogenic stimuli .....</b>	<b>42</b>
3.1 Introduction .....	43
3.2 Aims .....	46
3.3 Methods .....	47
3.3.1 Spinal cord preparation .....	47
3.3.1.1 Snap freezing .....	47
3.3.1.2 Perfuse fixation .....	47
3.3.2 Optimisation of dextran labelling .....	47
3.3.2.1 Dextran perfusion .....	47
3.3.2.2 Dextran surgery .....	48
3.3.3 Cyrosectioning .....	48
3.3.4 Lectin histology .....	48
3.3.5 Immunohistochemistry optimisation .....	49
3.3.6 Microscopy .....	50
3.3.7 Analysis optimisation .....	50
3.3.7.1 Co-localisation .....	50
3.3.7.2 Stereology .....	50
3.3.7.3 Minimum Feret Diameter .....	51
3.3.7.4 Statistics .....	51
3.4 Results .....	52
3.4.1 Optimising immunohistochemistry .....	52
3.4.1.1 Fixed vs frozen tissue .....	52
3.4.1.2 Specificity and co-localisation .....	53
3.4.1.3 Dextran perfusion .....	55
3.4.2 Effects of known angiogenic promoters on microvasculature ...	55
3.5 Discussion .....	60

<b>Chapter 4 : Timeline of vascular changes following SCI.....</b>	<b>65</b>
4.1 Introduction .....	66
4.2 Aims.....	69
4.3 Methods .....	70
4.3.1 Surgery .....	70
4.3.2 Spinal cord preparation.....	70
4.3.3 Transmission electron microscopy.....	70
4.3.3.1 Fixative solution .....	70
4.3.3.2 Tissue preparation .....	71
4.3.3.3 Transmission electron microscopy.....	71
4.3.4 Cyrosectioning .....	72
4.3.5 Immunohistochemistry .....	72
4.3.6 Fluorescence microscopy .....	72
4.3.7 Analysis .....	72
4.3.7.1 Stereology.....	72
4.3.7.2 Minimum feret diameter .....	72
4.3.7.3 Transmission electron microscopy measurements .....	73
4.3.7.4 Statistics .....	73
4.4 Results.....	74
4.4.1 Contusion force.....	74
4.4.2 Stereological analysis .....	75
4.4.2.1 Vessel number decreases after injury.....	75
4.4.2.2 SCI compromises vessel surface area.....	78
4.4.2.3 Vessel areal density is more variable following SCI.....	80
4.4.2.4 Surface:volume ratio decreases acutely post-SCI at the injury epicentre .....	83
4.4.3 Minimum feret diameter remains unchanged following SCI .....	84
4.4.4 Injury epicentre is highly variable following SCI .....	86
4.4.5 Transmission electron microscopy demonstrates significant ultrastructural changes to microvasculature following SCI .....	89
4.5 Discussion .....	92
4.5.1 Summary .....	97
<b>Chapter 5 : Stabilising capillaries and promoting angiogenesis                 following SCI.....</b>	<b>99</b>
5.1 Introduction .....	100
5.2 Aims.....	104
5.3 Methods .....	105

5.3.1 Growth factor preparation .....	105
5.3.2 Osmotic pump preparation.....	106
5.3.3 Surgery .....	106
5.3.3.1 Osmotic pump implantation .....	106
5.3.3.2 Osmotic pump implantation optimisation .....	107
5.3.4 Locomotor testing .....	108
5.3.5 Spinal cord preparation.....	109
5.3.6 Transmission electron microscopy.....	110
5.3.7 Cyrosectioning .....	110
5.3.8 Immunohistochemistry .....	110
5.3.9 Fluorescence microscopy .....	111
5.3.10 Analysis .....	111
5.3.10.1 Stereology.....	111
5.3.10.2 Minimum and maximum feret diameter.....	111
5.3.10.3 Transmission electron microscopy measurements .....	111
5.3.11 Statistics .....	111
5.4 Results.....	112
5.4.1 Contusion force.....	112
5.4.2 Locomotor scores did not change with treatment .....	113
5.4.3 Stereological analysis .....	114
5.4.3.1 Vessel number is maintained at day 5 at T11 with Ang1/VEGF treatment .....	114
5.4.3.2 Vessel surface area improves at T11 with Ang1/VEGF treatment .....	116
5.4.3.3 Vessel areal density is reduced at T10 in both Ang1/VEGF and vehicle treated groups .....	118
5.4.3.4 Surface:volume ratio is reduced with treatment at T10...	119
5.4.4 Minimum and maximum feret diameter remains constant at T11 121	
5.4.5 Microvascular structure varies across spinal cord regions with Ang1/VEGF treatment.....	124
5.5 Discussion .....	129
<b>Chapter 6 : General discussion .....</b>	<b>136</b>
6.1 Introduction .....	137
6.2 Summary of key findings.....	137
6.3 Further studies .....	143
6.4 Future perspectives and clinical relevance .....	145

6.5 Final conclusions .....	147
<b>Appendix 1: Timeline of white matter vascular changes post-SCI (Chapter 4) .....</b>	<b>149</b>
<b>Appendix 2: Macro written to automate vessel analysis in Chapter 4</b>	<b>150</b>
<b>Appendix 3: Macro written to automate vessel analysis in Chapter 5</b>	<b>152</b>
<b>Bibliography .....</b>	<b>155</b>

## Table of figures

<b>Figure 1.1: A schematic representation of an intact cord and the cord at acute and chronic timepoints following SCI. ....</b>	<b>6</b>
<b>Figure 1.2: The process of sprouting angiogenesis. ....</b>	<b>12</b>
<b>Figure 1.3: Schematic showing the relevant receptors in the blood spinal cord barrier (BSCB). ....</b>	<b>16</b>
<b>Figure 2.1: Diagram demonstrating the Infinite Horizons impactor setup and injury site. ....</b>	<b>37</b>
<b>Figure 2.2: Optimisation of stereology. ....</b>	<b>40</b>
<b>Figure 3.1: Assessment of snap frozen and fixed spinal cord tissue. ...</b>	<b>53</b>
<b>Figure 3.2: Optimisation of immunohistochemistry as demonstrated using images of the ventral grey matter. ....</b>	<b>54</b>
<b>Figure 3.3: Optimisation of dextran perfusion. ....</b>	<b>55</b>
<b>Figure 3.4: Vessel characteristics were unaltered by exercise or prazosin treatment. ....</b>	<b>59</b>
<b>Figure 3.5: The minimum feret diameter of vessels remained unchanged in all conditions. ....</b>	<b>59</b>
<b>Figure 4.1: Timeline of study following T10 contusion injury. ....</b>	<b>70</b>
<b>Figure 4.2: Actual force used for each contusion spinal cord injury. ...</b>	<b>74</b>
<b>Figure 4.3: Vessel density decreased after injury. ....</b>	<b>78</b>
<b>Figure 4.4: Vessel surface area decreased after injury and was slow to recover. ....</b>	<b>80</b>
<b>Figure 4.5: Vessel areal density increased in some segments after SCI. ....</b>	<b>83</b>
<b>Figure 4.6: Surface:volume ratio (S/V) increased acutely after injury. ...</b>	<b>84</b>
<b>Figure 4.7: Vessel minimum feret diameter at T11 remained unchanged. ....</b>	<b>86</b>
<b>Figure 4.8: Qualitative analysis of the injury epicentre at T10. ....</b>	<b>89</b>
<b>Figure 4.9: Transmission electron microscopy (TEM) revealed significant capillary damage at day 2. ....</b>	<b>91</b>
<b>Figure 5.1: Diagram showing osmotic pump and intrathecal catheter. ....</b>	<b>106</b>
<b>Figure 5.2: Modified quilting suture used to reduce seroma formation following subcutaneous osmotic pump placement. ....</b>	<b>108</b>
<b>Figure 5.3: The Basso, Beattie and Bresnahan (BBB) locomotor scoring system assessed hindlimb function in rats. ....</b>	<b>109</b>
<b>Figure 5.4: Timeline of treatment study following T10 spinal cord contusion injury. ....</b>	<b>110</b>
<b>Figure 5.5: Actual force delivered for each contusion spinal cord injury. ....</b>	<b>112</b>

<b>Figure 5.6: The Basso, Beattie and Bresnahan (BBB) locomotor scoring system assesses hindlimb function in rats.....</b>	<b>113</b>
<b>Figure 5.7: Vessel number decreased at T11 in the untreated group. ....</b>	<b>115</b>
<b>Figure 5.8: Vessel surface area per mm<sup>2</sup> was not significantly different to sham values at T11 following Ang1/VEGF treatment. ....</b>	<b>117</b>
<b>Figure 5.9: Ang1/VEGF treatment increased vessel areal density at T11 in comparison to untreated animals following spinal cord injury. ....</b>	<b>119</b>
<b>Figure 5.10: Vessel surface:volume ratio remained stable at T11.....</b>	<b>120</b>
<b>Figure 5.11: Minimum and maximum feret diameter of vessels at T11 following Ang1/VEGF or vehicle treatment. ....</b>	<b>124</b>
<b>Figure 5.12: Observational findings following Ang1/VEGF or vehicle treatment at days 5 and 15 post SCI. ....</b>	<b>126</b>
<b>Figure 5.13: Basement membrane thickness and intercellular cleft width of capillaries at the injury epicentre (T10) and T11.....</b>	<b>128</b>
<b>Figure 6.1: Representative images of semi-thin sections taken for transmission electron microscopy. ....</b>	<b>140</b>

## Table of tables

<b>Table 3.1: Antibodies optimised in rat spinal cords and their target cells/components. ....</b>	<b>50</b>
--	-----------

## List of abbreviations

**$\alpha$ -SMA** Alpha-smooth muscle actin

**$\mu$ -CT** Micro-computational tomography

**A(SP)A** Animals (Scientific Procedures) Act

**AAV** Adeno-associated virus

**Ang1** Angiopoietin 1

**Ang2** Angiopoietin 2

**ANOVA** Analysis of variance

**ARRIVE** Animals research: reporting of *in vivo* experiments

**ATP** Adenosine triphosphate

**BBB** Basso, Beattie and Bresnahan

**BDNF** Brain derived neurotrophic factor

**bFGF** Basic fibroblast growth factor

**BSCB** Blood spinal cord barrier

**CNS** Central nervous system

**CSPG** Chondroitin sulphate proteoglycan

**DAPI** 4',6-diamidino-2-phenylindole

- DGM** Dorsal grey matter
- DLL4** Delta-like ligand 4
- ECM** Extracellular matrix
- eNOS** Endothelial nitric oxide synthase
- FGF** Fibroblast growth factor
- GFAP** Glial fibrillary acidic protein
- HIF1 $\alpha$**  Hypoxia inducible factor 1 subunit  
alpha
- IP** Intraperitoneal
- MMP** Matrix metalloproteinase
- MRI** Magnetic resonance imaging
- mRNA** Messenger ribonucleic acid
- NDS** Normal donkey serum
- NMDA** N-Methyl-D-aspartate
- NO** Nitric oxide
- NP-1** Neuropilin-1
- OCT** Optimal cutting medium
- PAD** Peripheral arterial disease

- PB** Phosphate buffer
- PBS** Phosphate buffered saline
- PBST** Phosphate buffered saline Triton-X
- PDGF** Platelet derived growth factor
- PDGFR- $\beta$**  Platelet derived growth factor  
receptor beta
- PECAM-1** Platelet endothelial cell adhesion  
molecule-1
- PFA** Paraformaldehyde
- RECA-1** Rat endothelial cell antigen-1
- S/V** Surface:volume ratio
- SCI** Spinal cord injury
- SNP** Sodium nitroprusside
- TEM** Transmission electron microscopy
- TGF- $\beta$ 1** Transforming growth factor beta 1
- Tie2** Tyrosine kinase receptor with  
immunoglobulin-like and epidermal  
growth factor-like domain-2
- TNS** Tris non-saline

**UV** Ultraviolet

**VEGF** Vascular endothelial growth factor

**VEGFR2** Vascular endothelial growth factor  
receptor 2

**VGM** Ventral grey matter

**WFA** *Wisteria floribunda* agglutinin

***Chapter 1 : General introduction***

## 1.1 Spinal cord injury

Traumatic spinal cord injury (SCI) often leads to partial or complete loss of function below the injury site due to the primary mechanical injury and subsequent cascade of pathological responses within the spinal cord. This disrupts motor and sensory function, as well as autonomic functions, leading to paralysis of skeletal and smooth muscles, and sensation and pain disturbances. SCI can substantially reduce people's quality of life, with physical and psychological challenges. Traumatic SCI affects 1.5 people per 100,000 in the UK each year (NSCIB, 2012), but has a yearly global incidence of 10.5 people per 100,000 due to a higher prevalence in low/middle-income countries (Kumar et al., 2018b). There is a high male:female ratio of roughly 4:1 across the world, with the primary causes of SCI including road traffic collisions and falls (Singh et al., 2014). Treatment strategies are limited, and as many people are under the age of 40 (the mean age of traumatic SCI patients is 39.8 (Kumar et al., 2018b)), people living with SCI require long term care for the rest of their lives (Singh et al., 2014).

The primary injury of traumatic SCI involves mechanical disruption of the cord and surrounding tissues, usually by bony fragments. The secondary injury can damage previously intact cord structures due to the inflammatory response, haemorrhage, and ischaemia. Severity of the secondary injury cascade depends on the type of injury; transection, contusion, or compression; and can often be attenuated by relieving pressure on the spinal cord promptly. The most common injury type is contusion with some level of compression (Dumont et al., 2001). It has been postulated that due to the relative softness and increased capillary density of the grey matter compared to the white matter, the majority of the damage is focussed here (Wolman, 1965).

The mechanical disruption to the cord causes direct neuronal and glial cell death, and haemorrhage. Damage to the blood spinal cord barrier (BSCB) contributes to the initiation of an inflammatory response and further hypoxia-driven necrosis due to dysfunctional microvasculature, which in turn causes cord swelling and further compression (Ahuja et al., 2017) (Figure 1.1b).

Petechial or large haemorrhages in the vascular grey matter can spread and cause necrotic cavities in the surrounding tissue (Wolman, 1965). Destruction of the microvasculature exacerbates ischaemia and progressive cell death, and therefore generates a cytotoxic environment radiating from the injury epicentre.

Neurotoxicity, caused by neuronal death and high levels of the excitatory neurotransmitter glutamate in the microenvironment, contributes to additional necrosis and activation of microglia (Dumont et al., 2001; Hausmann, 2003). Hypoxia following SCI can make neurons more vulnerable to this increase in glutamate (Choi, 1987; Hausmann, 2003). In a positive feedback loop, excessive glutamate in the microenvironment released by destroyed neurons can cause direct excitotoxicity by prolonging synaptic transmission and increasing intracellular calcium ion levels (Choi, 1987; Hausmann, 2003). This influx of calcium ions can disrupt and accelerate mitochondrial metabolism, phosphorylation of cell signalling proteins, and modulation of gene transcription, leading to cell death (Ermak and Davies, 2002). Over-activation of the *N*-methyl-D-aspartate (NMDA) receptor by glutamate can also elicit intracellular sodium accumulation and generation of free radicals, contributing to Na<sup>+</sup>K<sup>+</sup> ATPase inhibition. This can cause increased intracellular sodium and water levels, inducing intracellular acidosis and oedema (Dumont et al., 2001).

Excitotoxicity leads to the generation of free radicals and nitric oxide (NO), lipid

peroxidation, and mitochondrial respiratory chain enzyme inhibition, resulting in neuronal cell death (Dumont et al., 2001; Hausmann, 2003).

As the spinal cord begins to remodel and regenerate with time, astrocytes proliferate around the injury epicentre and interact with meningeal fibroblasts to form a glial scar, which can also secrete chondroitin sulphate proteoglycans (CSPGs) and other extracellular matrix (ECM) proteins (Kundi et al., 2013) (Figure 1.1c). This biochemical and physical barrier may reduce the spread of cytotoxic products, such as by scavenging glutamate and other ions, and ameliorate the secondary injury by reducing inflammation, therefore assisting regeneration (Anderson et al., 2016; Rolls et al., 2009). However, the glial scar also paradoxically prevents axon regeneration as sprouting axons cannot penetrate the fibrous scar and so re-route around the injury epicentre (Kundi et al., 2013). The elastic modulus of the brain and spinal cord is very low ( $\sim 1$  kPa), whereas scar tissue can increase the stiffness of the tissue (Guimarães et al., 2020), causing neuronal and glial cell types to be repulsed by this physical barrier. Growth cone receptors in axons bind inhibitory factors to aid in guidance, however many of these, including CSPGs, Nogo, and ephrins, are upregulated by reactive astrocytes and fibroblasts within the scar tissue, creating a repulsive chemical barrier (Sandvig et al., 2004). Some research suggests the outskirts of the scar may provide a scaffold for recovering vasculature, however the necrotic core of the scar usually remains poorly vascularised (Rolls et al., 2009). Reducing this glial scar and enhancing blood flow to the area may help to promote a more favourable microenvironment for regeneration and repair.

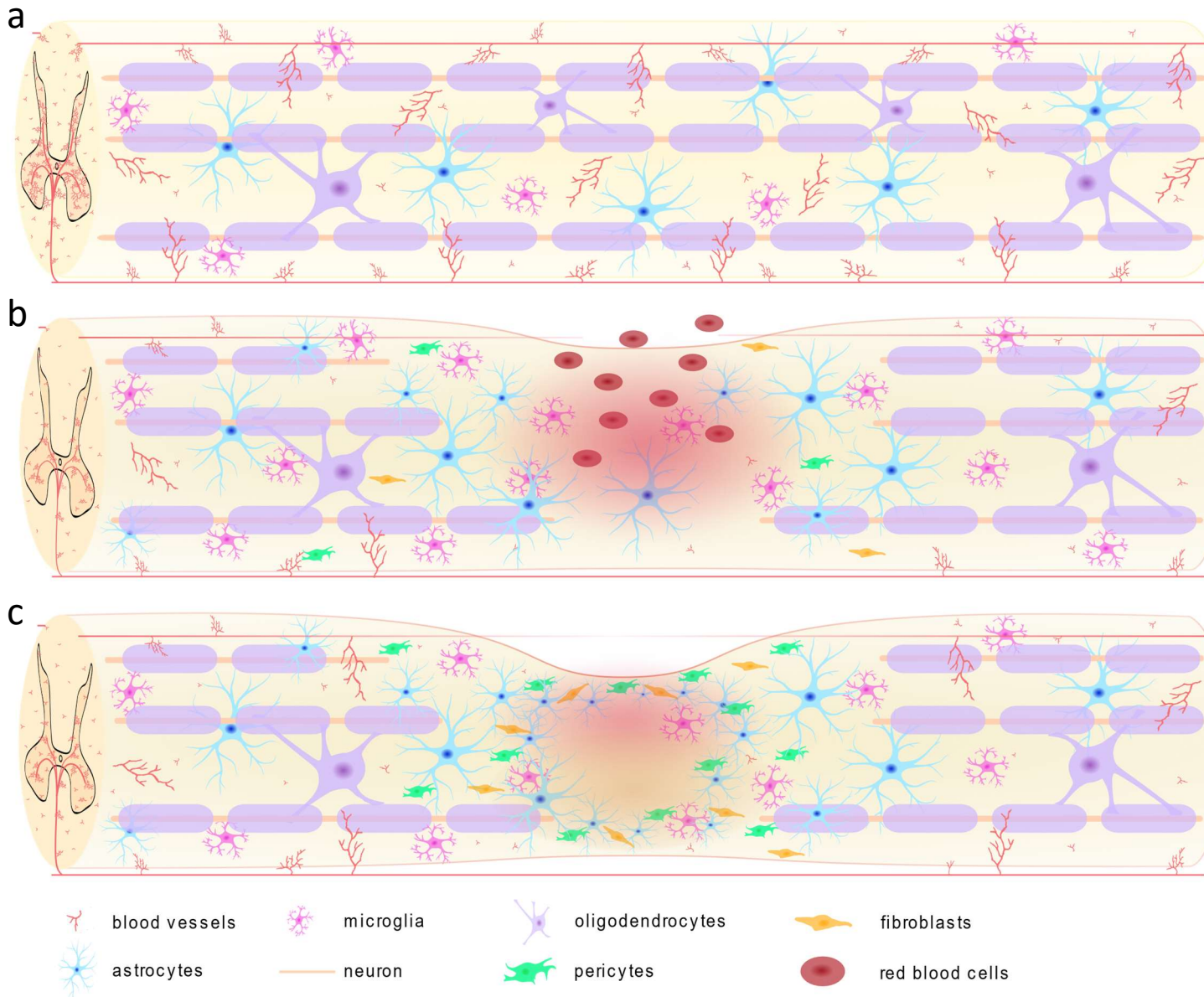


**Figure 1.1: A schematic representation of an intact cord and the cord at acute and chronic timepoints following SCI.**

An intact (a) spinal cord, the cord two days after injury (b), and 45 days post spinal cord injury (SCI) (c). Longitudinal vessels run along the ventral and dorsal aspects of the rat spinal cord, with ventral sulcal arteries branching into the grey matter. Astrocytes (blue), microglia (pink), and oligodendrocytes (purple) are distributed throughout the neural tissue (a). After SCI, haemorrhage and cell death are apparent at the injury epicentre (b). Pericytes (green) and fibroblasts (orange) migrate towards the area, along with increased numbers of astrocytes and microglia. In the chronic stages of SCI, significant tissue loss and cavity formation is notable (c). A scar composing of astrocytes, fibroblasts, and pericytes surrounds a necrotic core, blocking neuronal and capillary sprouting.

## 1.2 Angiogenesis

Angiogenesis is the formation of new blood vessels, either by intussusception (inward division) or sprouting (outward growth) from pre-existing blood vessels. Sprouting angiogenesis is a commonly observed response to pathology or a changing physiological environment, being able to invade tissues, form anastomoses, and expand the existing capillary networks. Endothelial cells are normally quiescent and require a mechanical or chemical stimulus to initiate angiogenesis by mechanotransduction or chemotransduction, for example by exposure to haemodynamic forces or growth factor gradients, respectively (Egginton, 2009).

Angiogenesis was first described by John Hunter in 1787; however, the modern study of angiogenesis is generally accepted to have begun with Judah Folkman in 1971 (Adair and Montani, 2011). Folkman identified the first angiogenic factor, tumour angiogenic factor, later renamed vascular endothelial growth factor (VEGF). Following this research, various other pro- and anti-angiogenic factors were identified. There are over 20 pro-angiogenic factors with good specificity; other non-mitogenic and oncogenic factors have also been implicated, but likely involve second order effects rather than endothelial-

specific responses (Zakrzewicz et al., 2002). These specific pro-angiogenic factors include VEGF (particularly important is VEGF-A) and fibroblast growth factors (FGFs) (especially FGF-2) to direct growth, matrix metalloproteinases (MMPs) (such as MMP2 or MMP9) to disrupt the basement membrane and help endothelial cell migration through the ECM, and angiopoietins to mobilise perivascular cells such as pericytes or modify VEGF activity (Kundi et al., 2013). This plethora of factors interact to initiate, control, and halt angiogenic growth; this tightly regulated system also involves a range of VEGF isoforms, promiscuous binding of growth factors to a variety of receptors, modulating co-receptors such as neuropilins to regulate growth factor activity, and anti-angiogenic factors such as thrombospondins (Olfert and Birot, 2011).

This complex cascade of initiating and regulatory factors means that angiogenesis is very tightly controlled and follows a common sequence.

Angiogenesis is commonly induced by environmental factors such as hypoxia or increased vascular shear stress during physiological adaptation, wound healing, or tissue growth. Once stimulated, the basement membrane surrounding an existing capillary is first degraded by proteolytic enzymes (Egginton, 2009; Levick, 2010). This is followed by detachment and migration of the surrounding pericytes (Adair and Montani, 2011). The normally quiescent endothelial cell exposed to the highest concentration of VEGF becomes a tip cell, characterised by searching filopodia (Adair and Montani, 2011) (Figure 1.2). This tip cell guides the capillary sprout along the highest angiogenic factor concentration gradient. Vessel size and endothelial cell identification is regulated by the stimulation of delta-like ligand 4 (DLL4) in tip cells by VEGF. DLL4 binds to Notch-1 on neighbouring endothelial cells, known as stalk cells, reducing expression of the VEGF receptor 2 (VEGFR2) (Adair and Montani, 2011). This

ensures that the tip cell expresses the most VEGFR2 and only one tip cell guides the forming sprout, reducing excessive branching. The tip cell can secrete proteases and MMPs to digest the ECM, thereby enhancing adhesion molecule interaction of the new capillary sprout (van Hinsbergh and Koolwijk, 2008). The following endothelial stalk cells elongate and proliferate to create the new sprout. Vacuoles develop within endothelial cells and fuse in the sprout, generating a lumen. This new sprout then fuses to an existing capillary or tip cell of another capillary sprout, generating a new anastomosis and increasing the capillary network length (increasing erythrocyte transit time) and surface area (enhancing diffusive capacity) (Adair and Montani, 2011; Egginton, 2009; Levick, 2010).

New capillaries are initially hyperpermeable until a new basement membrane is formed and inter-endothelial junctions mature. This hyperpermeability is thought to be advantageous in most tissues as it can allow fibrinogen into the ECM, generating a fibrin-rich vascular matrix (granulation tissue), which can be a favourable environment for cell growth (Levick, 2010). However, in the central nervous system (CNS) this increased permeability may be disadvantageous as blood products, including haemoglobin and haem, are toxic to neural tissue. Perivascular cells, such as pericytes, and astrocytes in the CNS, are recruited to the abluminal surface to complete maturation of the capillary (Adair and Montani, 2011; Egginton, 2009) (Figure 1.2). *In vitro* studies have demonstrated that pericytes are critical for formation of the new basement membrane, deposited by both the pericytes and endothelial cells, as endothelial cell-only capillaries do not form basement membranes (Davis et al., 2015; Stratman et al., 2009). Alignment of endothelial cells and recruitment of pericytes to stabilise

capillaries are controlled by factors such as platelet-derived growth factor (PDGF) and angiopoietins (Egginton, 2009; Kundi et al., 2013).

Angiopoietin-1 (Ang1) is a Tie2 (tyrosine kinase receptor with immunoglobulin-like and epidermal growth factor-like domain-2) ligand which acts to mature and stabilise newly formed vessels partly by attracting pericytes. Whereas, angiopoietin-2 (Ang2) acts as a Tie2 antagonistic factor contributing to the regression of blood vessels in the absence of mitotic stimuli, or to destabilisation of the endothelial cell tube which enables endothelial cells to respond to growth stimuli (Zakrzewicz et al., 2002). Both factors can be considered pro- and anti-angiogenic in different situations; Ang1 can stabilise neovasculature by preventing phosphorylation of key tight junction proteins such as VE-cadherin (Figure 1.3), however this increased stability in mature vessels can mean a higher concentration of growth factors is needed to elicit growth. Likewise, Ang2 stimulates endothelial cell destabilisation, required for the mitotic growth factor to have an effect, however this same effect can also lead to regression. Among other factors, the balance of Ang1:Ang2 is important in controlling blood vessel growth, as vessels often overgrow and then are pruned to match the changing requirements of the tissues (Zakrzewicz et al., 2002).

The interactions between pro- and anti-angiogenic factors in a spatiotemporal manner is important to consider. Hypoxia can induce expression of VEGF and Ang2 to stimulate sprouting angiogenesis, and once pre-existing capillaries are connected, Ang1 and Tie2 interact to stabilise vessels. Any redundant vessels are then pruned by the action of Ang2 (Zakrzewicz et al., 2002). VEGF contributes to the regulation of differentiation, proliferation, and migration of

endothelial cells in angiogenesis, with its effects determined in part by receptor type/density and co-factor expression; it is essential, but alone not sufficient, for angiogenesis.

Many pro-angiogenic factors, such as VEGF, FGF, semaphorins, Ang1, and Ang2, also recruit immature neurons and promote neurogenesis, the formation of new neurons (Serini and Bussolino, 2004). It has been speculated that neurons grow, migrate, and sprout axons to follow new blood vessels as the arborisation patterns are closely aligned *in situ* (Carmeliet and Tessier-Lavigne, 2005; Herrera et al., 2010; Kundi et al., 2013; Yu et al., 2016). For example, innate upregulation of Ang1 by blood vessels after stroke can act to recruit immature neurons to the infarct site, but blocking the Tie2 receptor has been shown to limit this neural migration (Ohab et al., 2006). Indeed, the presence of endothelial cells in *in vitro* cultures is enough to promote neural stem cell proliferation and neural differentiation, potentially partially through the action of FGF2 (Shen et al., 2004). It has also been postulated that neurons themselves may stimulate angiogenesis through the release of noradrenaline (Hayakawa and Wang, 2017) and VEGF (Carmeliet and Tessier-Lavigne, 2005; Mukoyama et al., 2002). It is therefore hypothesised that targeting these factors after SCI may promote both angiogenesis and neurogenesis concurrently.

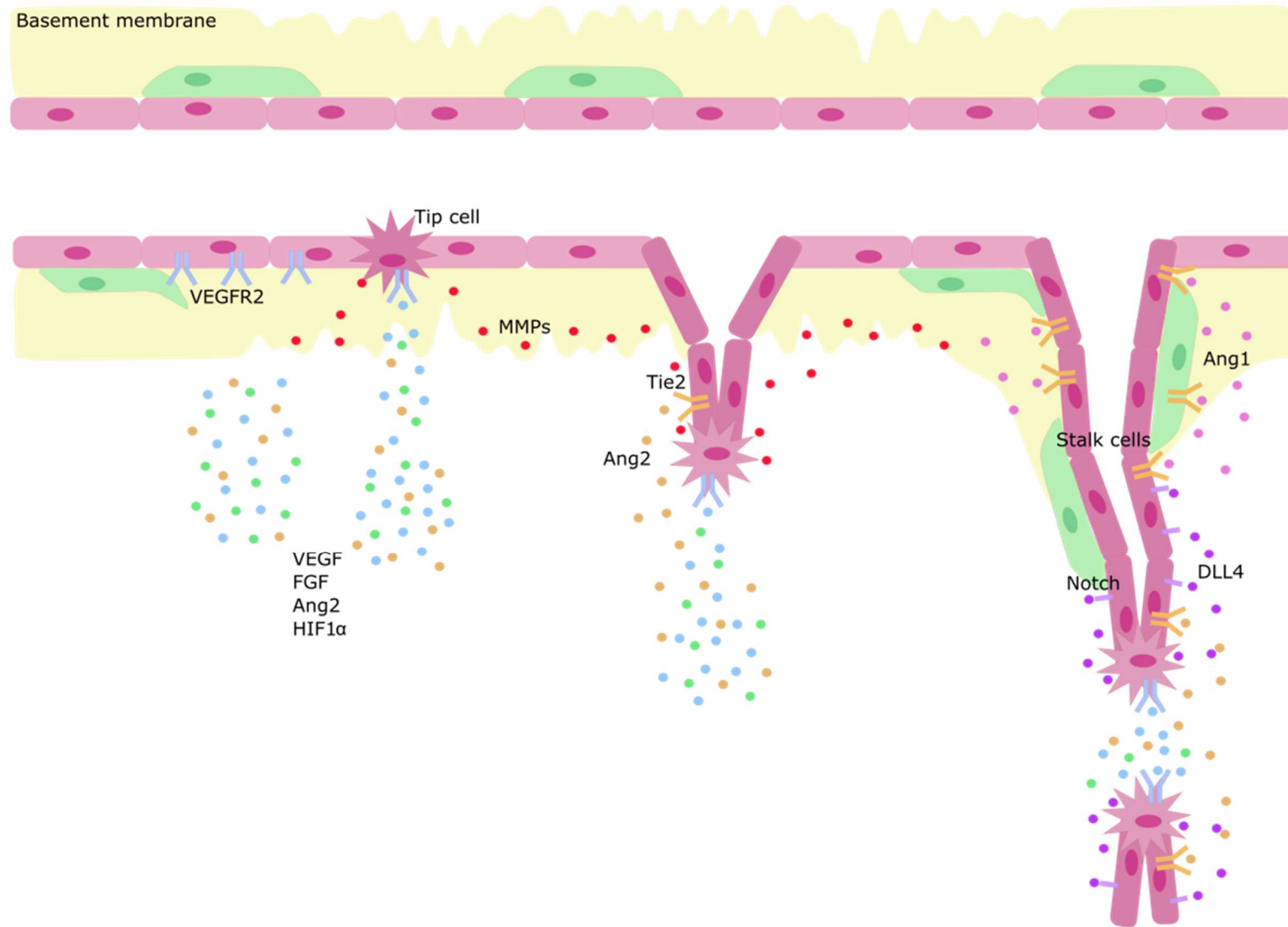


**Figure 1.2: The process of sprouting angiogenesis.**

Angiogenesis is initiated commonly by hypoxia, generating a growth factor gradient including VEGF, FGF, Ang2, and HIF1 $\alpha$ . Pericytes (green cells) begin detaching from the capillary wall. VEGFR2 (blue) is expressed on endothelial cells (pink cells), and the cell exposed to the highest concentration of VEGF becomes a tip cell. Tip cells release MMPs (red) to digest the basement membrane. Stalk cells proliferate and grow to generate a new sprout, and express Tie2 (orange) to bind Ang2 (orange) leading to decreased stability of tight junctions. As the neovessel grows, tip cells release DLL4 (purple) which binds to Notch (purple) on neighbouring stalk cells to reduce growth. Ang1 (pink) binds to Tie2 to stabilise the tight junctions and attract pericytes as the sprout matures. Sprouts from neighbouring vessels also growing towards the increased concentration of growth factors join to increase the capillary bed size. Abbreviations: VEGF: vascular endothelial growth factor; FGF: fibroblast growth factor; Ang: angiopoietin; HIF1 $\alpha$ : hypoxia inducible factor 1 $\alpha$ ; VEGFR2: VEGF receptor 2; MMP: matrix metalloproteinase; DLL4: delta-like ligand 4.

### 1.3 The blood spinal cord barrier

The BSCB is a continuation of the blood brain barrier, controlling movement of molecules and cells into and out of the delicate CNS. The neurovascular unit, vital in maintaining homeostasis in the CNS, is a specialised structure comprising of endothelial cells, pericytes, astrocytes, neurons, and the ECM (Muio et al., 2014). Capillaries are composed of an endothelial cell monolayer; cells connected to each other by tight and adherens junctions (Figure 1.3). These junctions are narrower in the CNS at around 15 nm (Peters et al., 1976), compared to 20 nm in peripheral vessels (Levick, 2010), and are formed when endothelial cells abut directly or overlap. A continuous basal lamina, containing laminin, type IV collagen, perlecan, and nidogen, surrounds the endothelial cells (Figure 1.3). This basement membrane is 30-40 nm thick in the CNS (Peters et al., 1976), and splits to also surround pericytes in the perivascular space within a common structure. Pericytes are phenotypically different in various tissues, but can be identified by their morphology and position. Vascular compliance and tone in capillaries is maintained in part by pericytes, and in the spinal cord these cells help to form the BSCB. Pericytes cover 23-30% of the endothelium, and

any loss of these cells can lead to an increase in BSCB permeability (Xu et al., 2017). Astrocyte endfeet contact pericytes and endothelial cells, increasing the physical barrier functions of the BSCB. Astrocytes convey electrical communication between neurons and capillaries to mediate vascular tone by detecting glutamate and gabaergic levels released from nearby neuronal synapses and converting this into calcium ion signals which spread to the astrocytic endfeet in contact with the capillary. This is converted into vasomotor commands by the release of vasoactive factors from astrocytes (Muoio et al., 2014; Zonta et al., 2003).

Both astrocytes and endothelial cells can propagate signals through calcium waves via gap junctions, thereby coordinating vascular tone of precapillary arterioles over large areas in feedback regulation responsive to spatially differentiated cellular activity (Giaume et al., 2010; Levick, 2010; Muoio et al., 2014). Vascular tone can be altered by release of vasodilators such as NO and prostacyclin, balanced against vasoconstrictors such as prostaglandin and endothelin (Levick, 2010; Sandoo et al., 2010). NO production can be stimulated by increased shear stress and inflammatory mediators. Acetylcholine can release calcium ions from endoplasmic reticulum stores, which in turn detach and activate endothelial nitric oxide synthase (eNOS) stored in the caveoli of endothelial cells, thereby increasing production of NO (Sandoo et al., 2010). As mentioned earlier, NO is also released by dying neurons (Dumont et al., 2001; Hausmann, 2003) at and around the injury site. This may contribute to vasodilation in the surviving blood vessels following injury, in turn causing further petechial haemorrhages and inflammation in the area.

The BSCB has not been as extensively studied as the blood brain barrier, but importantly, there appear to be some differences in permeability (Bartanusz et al., 2011; Jin et al., 2021). The barrier permeability is tightly regulated by specialised transporters to allow selective molecular exchanges whilst limiting immune cell infiltration (Jin et al., 2021; Spampinato et al., 2019). Some studies have demonstrated a greater permeability to pharmacological agents and cytokines in the spinal cord compared to the brain under physiological conditions (Bartanusz et al., 2011; Bernacki et al., 2008; Prockop et al., 1995). Unusually, the endothelial cells in the BSCB possess glycogen deposits, likely acting as an energy storage mechanism; this potentially mitigates against short term limitations in perfusion, offering a degree of glycolytic potential. Although poorly researched, this does not seem to be present in the blood brain barrier (Bartanusz et al., 2011; Jin et al., 2021; Sharma, 2005).

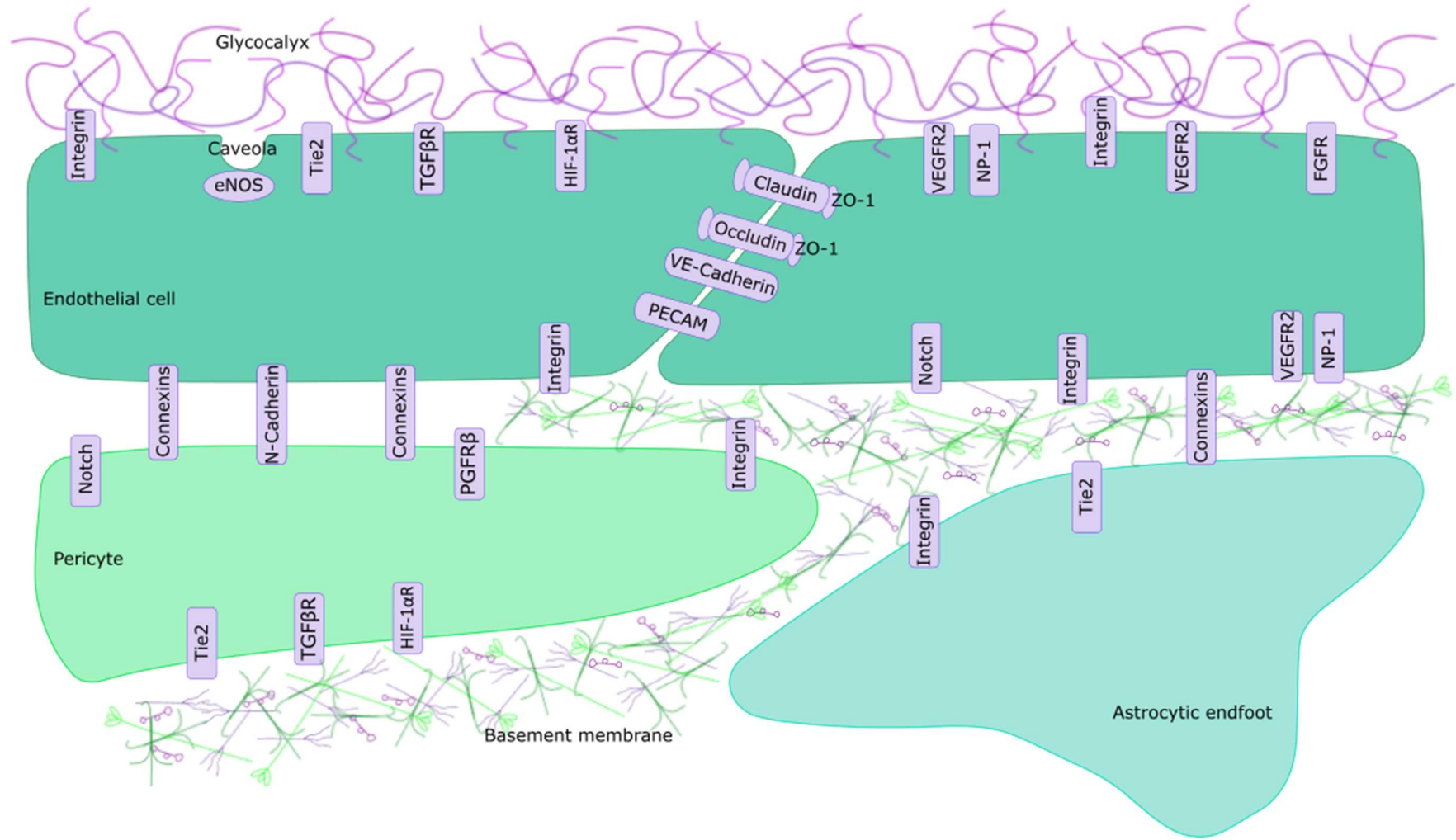


**Figure 1.3: Schematic showing the relevant receptors in the blood spinal cord barrier (BSCB).**

Endothelial cells are covered with glycocalyx containing syndecan, hyaluronan, and sialoglycoprotein on the luminal side, and joined via tight junctions with claudin, occludin, and VE-cadherin. The basement membrane, containing laminin and type IV collagen, surrounds endothelial cells and pericytes. Astrocytic endfeet complete the BSCB external to the basement membrane. Connexins and N-Cadherin join cells, and integrins bind glycocalyx and basement membrane components. All three cell types display the Tie2 receptor for angiopoietins 1 and 2. NP-1 is a co-receptor to VEGFR2, helping to guide ligand binding. Abbreviations: VEGFR2: vascular endothelial growth factor receptor 2; eNOS: endothelial nitric oxide synthase; TGF $\beta$ R: transforming growth factor beta receptor; HIF-1 $\alpha$ R: hypoxia inducible factor 1 alpha receptor; ZO-1: zonula occludens 1; NP-1: neuropilin 1; FGFR: fibroblast growth factor receptor; PGFR $\beta$ : platelet growth factor receptor beta; PECAM: platelet endothelial cell adhesion molecule.

## **1.4 Vascular response to SCI**

When the spinal cord is injured, the BSCB ceases to act as an effective barrier, and instead, the increased permeability causes further endothelial cell damage, development of perivascular spaces, and extravasation of blood products and cells. These changes in turn contribute to haemorrhage, ischaemia, and inflammation (Loy et al., 2002). The initially small haemorrhagic lesion in the central grey matter is followed by progressive capillary collapse, leading to many petechial haemorrhages within the first 24 hours (Balentine, 1978; Simard et al., 2007). These haemorrhagic areas eventually combine to form a fusiform shaped lesion, developing a necrotic core. Whilst the majority of post-traumatic haemorrhages are observed in the grey matter, the nearby white matter also demonstrates disrupted myelin and neuronal swelling. This post-traumatic haemorrhagic necrosis can spread, causing further loss of capillaries, and spreading into the dorsal white columns (Noble and Wrathall, 1989; Simard et al., 2007; Tator and Koyanagi, 1997). The cavity formed at later time points correlates with the early intraparenchymal haemorrhage distribution (Mautes et al., 2000; Noble and Wrathall, 1989).

Inflammation can cause the breakdown of junctional actin, thereby weakening the tight junctions between endothelial cells (Levick, 2010). Ang1 normally helps to stabilise the BSCB by tightening endothelial cell junctions. However, after SCI Ang1 is downregulated, thus contributing to the increased permeability of the BSCB (Herrera et al., 2010). Hypoxia induces upregulation of Ang2 after SCI in oligodendrocyte precursors and astrocytes, destabilising endothelial cell integrity and further increasing BSCB permeability. Paradoxically, higher levels of Ang2, which promotes endothelial cell apoptosis and vessel regression, correlates with improved locomotor recovery (Durham-Lee et al., 2012) and suggests that remodelling of the microvasculature is important for functional restoration.

Following contusive SCI, cytokines, proteases, and MMPs are upregulated, with a large increase in MMP9 in the spinal cord within 24 hours of injury augmenting inflammation and vessel permeability (Noble et al., 2002). Within the first 24 hours, collagen type IV and laminin are also upregulated close to the capillaries, forming 'streamers' (Loy et al., 2002). These may be indicative of future growth paths, and therefore of neovascularisation (Loy et al., 2002), or may be evidence of remnants of the basement membrane of apoptotic capillaries, which may offer guidance paths for regrowth. Current research suggests angiogenesis begins from day 3 after injury, increasing vessel density mostly in the grey matter by day 14 (Cao et al., 2017; Casella et al., 2002). Sprouting angiogenesis has been observed after day 4, with new capillaries growing into the injury site from surrounding intact vessels (Casella et al., 2002). Endothelial cells start generating new basal lamina by day 7, which is gradually associated with fibroblast-like cells and blood vessels by day 14 (Loy et al., 2002). The collapsed microvasculature has been shown to continue

remodelling at the injury epicentre, and caudal and rostral to the injury (Loy et al., 2002; Popovich et al., 1996), involving two periods of angiogenic activity following SCI; the primary wave within 3-7 days after injury, and a secondary wave 14-60 days later (Durham-Lee et al., 2012; Loy et al., 2002; Popovich et al., 1996). The secondary wave of angiogenesis has been shown to coincide with upregulated Ang2 expression predominantly in the white matter (Durham-Lee et al., 2012). As expected, there is a correlation between the increase in blood vessel density and an improved recovery following SCI (Rauch et al., 2009).

Unfortunately, angiogenesis following injury has been shown to be transient and incomplete (Cao et al., 2017; Ng et al., 2011). This may be due to a lack of observed pericytes or astrocytes associated with new vessels 14 days after injury, preventing stabilisation of the neovasculature, along with a reduced number of glucose transporters present, suggesting metabolic dysregulation (Ng et al., 2011; Whetstone et al., 2003). Significant BSCB leakage of injected luciferase has been shown to decrease after the first 24 hours and then increase again after day 3 until day 14, indicating barrier dysfunction and ongoing vascular remodelling (Whetstone et al., 2003). These vessels are unable to effectively contribute to the BSCB or function appropriately, and excessive pruning of vessels is observed, presumably in consequence (Ng et al., 2011).

Capillary regression leads to apoptosis of endothelial cells and vascular support cells. An increase in cytokines and MMPs following SCI can therefore contribute to rarefaction of capillaries. This apoptosis combined with the migration of pericytes away from capillaries further destabilises the BSCB. Goritz *et al*

discovered a new class (type A) of pericyte, which can help to form the fibroblast component of the glial scar tissue in the spinal cord (Goritz et al., 2011). A transgenic mouse model has been used to knockdown these type A pericytes. This knockdown lead to a reduced level of PDGF receptor  $\beta$  (PDGFR $\beta$ ) positive cells within the scar, and this reduction in pericyte migration resulted in a larger cavity (Dias et al., 2018). Despite the larger defect size in knockdown mice, this group performed better in the horizontal ladder test, implying that reducing pericyte incorporation into the scar may promote axonal sprouting across the lesion (Dias et al., 2018). Unfortunately, this study did not assess how pericyte detachment effected capillary and BSCB function, although we can assume that this breakdown of the neurovascular unit would lead to increased BSCB permeability.

As the microvessels adaptively remodel and potentially recover some function, arteriole number increases significantly (Cao et al., 2017) as far away as 15 mm from the injury epicentre (Loy et al., 2002), suggesting a potential target linking macro- and microvascular elements. Such a coordinated expansion of the vasculature is known in other tissues, where it is thought to be essential for maintenance of haemodynamic control (Hansen-Smith et al., 2001).

Unfortunately, an increased large vessel number or diameter does not necessarily mean an increase in perfusion of the cord (Streijger et al., 2017), instead offering reduced peripheral resistance, hence potentially increased bulk blood flow. As the microvasculature is severely damaged and angiogenesis is limited following SCI, hypoxia and ischaemia continues for many months; while this may contribute to a feedback dilatation, tissue perfusion is only realised if the microvasculature is capable of accepting such flow. Hypoxia is not exclusive to the injury epicentre and has been shown to extend down the cord caudal to

the site of injury (Li et al., 2017). Chronic vasoconstriction promotes inflammation, hypoxia, and necrosis regardless of any increased blood flow in the macrovasculature.

## **1.5 Current vascular treatment strategies**

The aim of many SCI treatments is to improve functional movements without contributing to secondary injury or inducing maladaptive remodelling. Due to the complex nature of SCI, a combinatorial treatment approach is more likely to have a positive impact on recovery of locomotor function. As the spinal cord remodels after injury, connections can be formed between different spinal pathways, often leading to allodynia and spasticity (Beuparlant et al., 2013), and therefore treatments should aim to assist in controlled remodelling to avoid incorrect neural connections. Another challenge to overcome is maintaining any improvements after the treatment period. Collectively, these aims are most likely to be achieved by enhancing intrinsic, integrated mechanisms of tissue remodelling.

Locomotor training, spinal stimulation, or implantation or injection of substances to aid recovery after SCI have been researched with limited success in patients (Angeli et al., 2014; Harkema et al., 2011; Lima et al., 2006; Willison et al., 2020; Wirz et al., 2005). An in depth understanding of the spatial and temporal changes following SCI is needed to identify potential treatment targets that could be manipulated in combination to improve the quality of life of people with SCI.

### **1.5.1 Vasodilators**

As discussed previously, neurogenesis appears to follow angiogenesis, both temporally and spatially, with neurofilaments often coupled with new blood

vessel walls (Loy et al., 2002). As a result, stimulating angiogenesis may promote or be permissive for axonal sprouting, while at the same time reducing ischaemia around the injury site. Vasodilators such as prazosin, an  $\alpha_1$  adrenoreceptor antagonist, have been used to initiate angiogenesis via capillary splitting in skeletal muscle (Egginton et al., 2001). Vasodilators function by increasing shear stress in capillaries, inducing endothelial mechanotransduction leading to rapid and energy-efficient angiogenesis (Egginton et al., 2016). This angiogenesis is temporary and vessels regress when the vasodilatory stimulus is removed, with VEGF expression returning to control levels within six weeks (Egginton et al., 2016). This may be exploited to target microvascular growth within a defined therapeutic window.

After SCI, pro-angiogenic factors to initiate vascular remodelling begin to be upregulated within 24 hours, and neovessels become established by day 7. Therefore, in order to maintain this response and mitigate against the excessive vessel pruning observed (Ng et al., 2011), studies have recommended angiogenic treatments are targeted during days 3-7 following SCI (Casella et al., 2002; Loy et al., 2002). However, increasing blood flow to the spinal cord via vasodilators may not improve perfusion of the tissue if the microvasculature is dysfunctional, and could contribute to haemorrhage and inflammation. Studies using a porcine model of SCI have shown that despite an increase in local blood pressure, the oxygen tension at the injury epicentre remains low for at least 7 days after SCI (Streijger et al., 2017). Similar, albeit less dramatic, results were obtained for an area 2.2 cm caudal to the injury (Streijger et al., 2017). As return of sufficient blood flow to the injury site has been correlated with improved somato-sensory evoked potential function in SCI (Carlson et al., 2000), the conclusion that increased blood flow to the spinal cord for at least 7

days would lead to improved locomotion could be drawn. However, with ischaemia and hypoxia showing no improvement for 7 days, it is unlikely that increased macrovascular blood flow would contribute to recovery unless coupled with an effective microvasculature. Due to the collapse of the microvasculature, increasing vasodilation and therefore blood flow to the cord may not be a suitable treatment option.

### **1.5.2 Exercise**

Currently, treatment strategies focussing on, or incorporating, exercise have shown the most promising functional outcomes in people living with SCI. Many studies focus on functional or skeletal muscle outcomes to assess the efficacy of exercise training following SCI in both rodent (Kissane et al., 2019; Smith et al., 2009; Ward et al., 2016) and human studies (Dietz et al., 1995; Dobkin et al., 2006). Exercise in healthy participants is known to have many health benefits, including improved cardiovascular health, reduced inflammation, and enhanced plasticity in the CNS (Cotman and Berchtold, 2002; Gibala and Little, 2020; Warburton et al., 2006). Angiogenesis in the brain has been demonstrated in rats following treadmill training or free wheel running for a month (Isaacs et al., 1992; Swain et al., 2003). By contrast, disuse atrophy, as commonly seen below the injury level in SCI, may reduce overall health as skeletal muscles act as endocrine organs that can regulate other bodily functions through secretion of myokines (Iizuka et al., 2014). It is difficult to find studies which have directly analysed the effect of exercise on spinal vasculature following SCI, however some research has shown indirect effects post-SCI.

Exercise modalities in rodent SCI studies commonly include treadmill training (with or without weight support), free wheel running, or swimming. Ying *et al*

used an underwater treadmill to provide weight support during exercise training of rats with a T10 contusion injury. Evans blue dye was infused intravenously to show that 7 or 14 days of training improved BSCB functionality by reducing oedema and extravasation at the injury site (Ying et al., 2020). Transmission electron microscopy showed that tight junctions between endothelial cells in exercise trained rats were closer to control range (~ 10 nm) at 15-20 nm compared to ~ 25 nm in untreated rats at day 14 post SCI (Ying et al., 2020). A 16 week treadmill training programme following a T9 contusion injury demonstrated improved locomotor scores from 9 weeks onwards (Wang et al., 2015). Grid walking, as a more specific test of locomotor capacity, also showed significant improvements in exercise trained rats at 17 weeks. However, sensory perception and thermoreception, assessed using the von Frey and Hargreaves test, respectively, showed no significant difference between groups (Wang et al., 2015).

Exercise has been shown to increase brain derived neurotrophic factor (BDNF) and neurotrophin-3 levels within the lumbar spinal cord and soleus muscle after just 5 days of treadmill training in intact rats (Gómez-Pinilla et al., 2001). When this was followed up with a BDNF inhibited rat model of hemisection SCI, injured animals with lower BDNF levels scored significantly lower on locomotor tests than injured animals with unchanged BDNF levels (Ying et al., 2008). As the exercise trained rats also had higher levels of BDNF within the cord than sedentary controls (both with no BDNF inhibition), this may imply a potential mechanism of action for exercise improving locomotor outcomes following SCI (Ying et al., 2008). BDNF is well known for its neuroprotective role, however the growth factor may also promote angiogenesis and endothelial cell survival

following ischaemic insult (Kermani and Hempstead, 2007). Linking studies like these may expand the scope for vascular targets following SCI.

Human studies using patients with T6-T12 injuries and able bodied individuals demonstrated that upper limb exercise can increase circulating angiogenic markers (Vasiliadis et al., 2014). VEGF, VEGFR2, MMP-2, and endostatin levels increased in both groups immediately post-exercise, demonstrating that exercising unaffected limbs after SCI could have beneficial systemic effects (Vasiliadis et al., 2014). Further research is required to understand how long these effects may last post-exercise and if the levels of circulating growth factors has a direct effect on the microvasculature around the injury site.

Many studies use a combination of the above treatment strategies in an attempt to address different aspects of the injury, such as neurogenesis, gliogenesis, angiogenesis, apoptosis, scar tissue formation, and synaptogenesis. The most common modality is epidural stimulation coupled with exercise training (Courtine et al., 2009; Harkema et al., 2011; Ichiyama et al., 2008). As epidural stimulation can promote plasticity in the spinal cord, it is important to direct any new growth to avoid complications such as allodynia. Exercise provides sensory feedback and can therefore help to avoid allodynia in recovering patients or animals (Ichiyama et al., 2008). Studies have demonstrated that forced epidural-stimulated stepping, as on a treadmill, may engage fewer cortical neurons than active training with sensory cues on treadmills, as active training ensures any locomotor movement is voluntary and traverses the injury site (van den Brand et al., 2012; Wernig and Müller, 1992; Wirz et al., 2005). Therefore voluntary exercise with sensory feedback is likely the most effective form of exercise when used alone or in combination with other treatments.

### 1.5.3 Growth factors

Promoting angiogenesis directly may overcome many of the problems identified above, but could also exacerbate secondary damage as newly formed capillaries are highly permeable. Reforming the BSCB quickly is imperative to reduce inflammation and preserve as much neural tissue as possible. However, the history of manipulating angiogenesis in patients is complex. When growth factors such as VEGF were initially discovered, the potential to use antagonisms or blockades to kill tumours or enhanced generation to promote blood flow in ischaemic cardiac or skeletal muscle was recognised.

Unfortunately, little was known about how these factors affected the vasculature in humans, and even less about possible side effects. This led to patients developing tumours (oncogenic side effects of growth factors), needing amputations (transient relief of ischaemia during treatment, but microvascular collapse following treatment), and even dying (growth factors acting as vasodilators and inducing shock) (Ready, 2001; Ylä-Herttuala et al., 2017).

Further research showed these factors are often not limited to acting only on vascular cells. Whilst this means that greater care and consideration is required when using pharmaceutical manipulation, it also offers an opportunity to promote more cohesive and holistic healing. For example, VEGF induces dilatation and vascular permeability, while promoting endothelial survival and antagonising apoptotic signals; it can promote endothelial cell proliferation, migration, and differentiation (Prior et al., 2004), and also neuronal migration and survival, and protect neurons from oxidative stress and excitotoxicity (Lladó et al., 2013).

VEGF administration may promote angiogenesis and neurogenesis simultaneously, whilst also being neuroprotective (Kundi et al., 2013).

Nevertheless, allodynia has been demonstrated in rodents treated with VEGF (Sundberg et al., 2011), and VEGF stimulated neovessels often regress after administration ceases (Kundi et al., 2013). Biomaterials or controlled release mechanisms may be able to facilitate long-term release of growth factors to establish angiogenesis and neurogenesis, and prevent vessel regression.

To counter the increased permeability of new capillaries, Ang1 has been combined with VEGF<sub>165</sub> to promote and stabilise new vessels, and has been associated with improved locomotor function (Herrera et al., 2010). This study used an AAV intraspinal delivery to prolong VEGF<sub>165</sub> and Ang1 expression in a mild/moderate contusion injury rat model. Whilst a vascular treatment strategy was developed, Herrera *et al* did not directly assess vascular outcomes; instead using magnetic resonance imaging (MRI) to measure oedema and necrosis by measuring lesion volume (Herrera et al., 2010). Nonetheless, this treatment did lead to improved function in the chronic phase following SCI (56 days post-injury). This study indicates that a combination of Ang1 and VEGF delivery following SCI may have beneficial effects, however more research is required to understand how these growth factors affect the vasculature specifically.

A combination of VEGF and FGF-2 can also act to preserve neural tissue, reduce excitotoxicity, and stimulate angiogenesis (De Laporte et al., 2011). This study utilised an implantation of a scaffold containing VEGF and FGF-2 microspheres into a lateral hemisection rat injury model. Micro-computational tomography ( $\mu$ -CT) and immunohistochemistry were used to assess vascular recovery. Unfortunately, the majority of vascular analysis was completed using  $\mu$ -CT which does not have the resolution to visualise capillaries. Nevertheless, De Laporte *et al* demonstrated increased blood vessel number within the lesion

epicentre following 6 weeks of VEGF and FGF-2 delivery (De Laporte et al., 2011).

Angiogenic factors, including VEGF, FGF-2, and Ang1, loaded into biodegradable microspheres have also been used to maintain growth factor release for 48 hours (Yu et al., 2016). This study demonstrated increased angiogenesis and neurogenesis, and importantly, improved motor function 10 weeks later (Basso, Beattie, and Bresnahan (BBB) scores of  $15.3 \pm 0.83$  with treatment vs  $7.7 \pm 0.72$  in vehicle treated) (Yu et al., 2016). Bioengineered implants loaded with angiogenic growth factors may be able to structurally support the growth of new capillaries, and biochemically encourage and guide growth simultaneously. Yu *et al* used an intravenous infusion of isolectin B4 to count the number of vessels at the injury site at weeks 4 and 8 post contusion injury in a rat model, showing significant increases in animals receiving the pro-angiogenic treatment ( $P < 0.01$ ), however no change between timepoints (Yu et al., 2016). This is one of the few studies targeting the microvasculature that directly assessed the changes to the microvasculature following treatment. Whilst the methods used would provide accurate and reliable information, this group did not distinguish between vascular changes in the grey and white matter, and only included two timepoints post-SCI. Further information is needed at the acute stages after injury as this is when the vasculature is likely to be the most vulnerable.

As demonstrated in the studies outlined, some progress has been made into developing a pro-angiogenic treatment strategy using growth factors following SCI. It is widely agreed that a combinatorial therapy would be the most effective at achieving integrated vascular, neural, and functional recovery following SCI.

Finding the right balance of these growth factors that does not further contribute to secondary injury is a major challenge. Whilst current research has made a little headway into understanding how these growth factors may impact recovery following SCI, much more research focussing on the vascular changes is required. In depth analysis of microvascular alterations with various treatment strategies could allow adjustments to be made to treatments to optimise vascular, and therefore potentially neural and functional, outcomes following SCI.

## **1.6 Aims and objectives**

### **1.6.1 Overall objectives**

Accurate and reliable methods to assess microvascular changes need to be developed and optimised, before using these to build an in-depth understanding of vascular changes at various timepoints across the spinal cord following injury. Assessing spinal vasculature following common angiogenic treatments before injury and combining this data with a spatiotemporal analysis of the microvasculature following SCI may identify an appropriate vascular target. It is hypothesised that by improving the quality and/or quantity of the spinal cord microvasculature after injury, a more favourable local environment will be created for neuronal recovery. This may lead to improved functional recovery after SCI.

### **1.6.2 Promoting spinal cord angiogenesis via systemic stimulation**

Angiogenesis can be stimulated in peripheral tissues following exercise protocols or drug treatments. Some studies have investigated the effects of exercise on the vasculature of the brain (Isaacs et al., 1992), however, the effects of these well-known treatments in the spinal cord is unclear. As many of the drugs are already in common use, it would be beneficial if these treatments could be used in the treatment of SCI as well.

Therefore, the first experimental chapter (Chapter 3: Spinal cord microcirculation and angiogenic stimuli) aims to establish whether an exercise protocol or delivery of a well-used  $\alpha_1$  adrenoreceptor antagonist can stimulate spinal cord angiogenesis in intact spinal cords by:

1. Identifying the optimal marker for capillaries in the rat spinal cord
2. Investigating capillary characteristics after treatment

It is expected that, as the spinal cord is a highly vascularised tissue, these treatments options may cause modest angiogenesis in the intact spinal cord, but may still be worth investigating further as SCI may sensitise the microcirculation to such stimuli.

### **1.6.3 Characterising vasculature after SCI**

Details of the changes to the spinal cord vasculature following SCI are sparse. Some studies have investigated the rarefaction and growth of capillaries after SCI, however differences in methods, experimental models, and analysis means these data need to be corroborated before an angiogenic target can be identified. Experimental Chapter 4: Timeline of vascular changes following SCI therefore aims to provide a detailed timeline of vascular changes following a contusive SCI by:

1. Investigating gross capillary morphology before and after SCI at various timepoints
2. Investigating capillary microstructure before and after SCI

### **1.6.4 Stabilising capillaries after SCI using Ang1 and VEGF**

Ang1 has been shown in a large variety of settings to stabilise capillaries after angiogenesis, promoting homeostasis. VEGF is well known to promote angiogenesis in a range of conditions and tissues. Previous studies have used Ang1 and/or VEGF in combination with other therapies and shown favourable improvements in locomotor recovery following SCI (Herrera et al., 2010; Yu et al., 2016). However, these studies do not assess the direct impact of these treatments on the vasculature of the spinal cord. Additionally, early delivery of Ang1 and VEGF may reduce the severity of the damage caused by the secondary injury by stabilising the BSCB and reducing hypoxia. Further insight

into detailed vascular changes following locally delivered Ang1 and VEGF treatment would enable the efficacy and safety of this treatment to be assessed, and for any further angiogenic targets to be identified. The aims of Chapter 5: Stabilising capillaries and promoting angiogenesis after SCI are therefore:

1. Investigate the safety of localised intrathecal delivery of Ang1 and VEGF using an implanted osmotic pump
2. Characterise capillary characteristics at various timepoints after treatment
3. Assess functional recovery following Ang1/VEGF treatment by studying locomotor function

***Chapter 2 : General materials and methods***

## 2.1 Ethics

All work involving animals has been conducted under the Animals (Scientific Procedures) Act 1986 (A(SP)A). Training has been provided by animal house staff and Home Office licenced individuals as appropriate (PPL 70/8674:2 or P7DD7EE20:2; PIL I63FCF06A). In adherence to the principles of the 3Rs, tissue was obtained from animals already involved in other experiments (all animals in Chapter 3) where possible to reduce the number of animals used. Optimisations to surgical protocols were implemented (discussed in relevant sections) to refine surgical outcomes and improve animal welfare.

## 2.2 Animals

Rats were housed in pairs or groups of four in Central Biomedical Services (University of Leeds, UK) in a controlled environment at  $20 \pm 1^\circ\text{C}$  with a 12-hour light/dark cycle. Access to food and water was *ad libitum*. Adult male Wistar rats (250 – 300 g) used in Chapter 3 were obtained from Central Biomedical Services. Adult female Sprague-Dawley rats (200 – 230 g) were obtained from Charles River Laboratories (Canterbury, UK). All rats were acclimated and handled for at least one week before studies commenced. All procedures and experiments were carried out according to local and UK Home Office guidelines, in compliance with the UK A(SP)A 1986, following the 3R principles and ARRIVE guidelines.

## 2.3 Solutions

### 2.3.1 Phosphate buffer

2x phosphate buffer (PB) for perfusions was made using 0.28 M sodium phosphate monobasic (Sigma-Aldrich, Gillingham, Dorset, UK) and 0.19 M sodium hydroxide pellets (Fisher Scientific, Loughborough, Leicestershire, UK)

dissolved in distilled water. The pH was then adjusted to 7.4 using stock adjustment solutions of 2 M sodium hydroxide and 10 M hydrochloric acid following two-point calibration of the pH meter. PB was then filtered before being stored at room temperature.

### **2.3.2 Paraformaldehyde**

Paraformaldehyde (PFA) was made by dissolving 8% w/v 2.66 M PFA powder (Sigma-Aldrich) in 60°C distilled water with sodium hydroxide pellets to aid mixing (Fisher Scientific). The pH was adjusted to 7.4 at room temperature, and then diluted to 4% PFA with 2x PB and filtered before storing at 4°C.

### **2.3.3 Sucrose**

30% w/v sucrose was made by dissolving 0.88 M sucrose crystals (Sigma-Aldrich) in 1x PB, and adjusted to pH 7.4 before storing at 4°C.

### **2.3.4 Phosphate buffered saline**

60 mM phosphate buffered saline (PBS) was made using PBS tablets (Fisher Scientific) dissolved in distilled water and adjusted pH 7.4.

### **2.3.5 Tris non-saline**

0.5 M Tris Non-Saline (TNS) was made using 6% w/v Tris base (Sigma-Aldrich) dissolved in distilled water and adjusted to pH 7.4 before storing at 4°C.

### **2.3.6 Dextran**

15 mM Dextran solution was made using 0.75% w/v fluorescein isothiocyanate-conjugated dextran (MW 500,000; Sigma-Aldrich) dissolved in PB and stored at 4°C in the dark.

### **2.3.7 Heparin and sodium nitroprusside**

Two heparin and sodium nitroprusside (SNP) solutions were made. 0.02% w/v heparin (sodium salt; AppliChem, Maryland Heights, Missouri, USA) and 0.0024% w/v SNP (Sigma-Aldrich) were dissolved in PB for use in perfusions. A separate heparin only solution was made with 0.02% w/v heparin dissolved in PB for use as an intraperitoneal (IP) injection before perfusions. 0.6% w/v heparin and 0.02% w/v SNP was dissolved in PB for use in surgery. All were stored at 4°C.

## **2.4 Spinal cord preparation**

### **2.4.1 Snap freezing**

Rats were given an overdose of pentobarbital (200 mg/kg; Pentोजect; Animalcare Ltd, York, UK) by IP injection. Once a lack of paw withdrawal and blink reflex were both noted, spinal columns were dissected out and the spinal cord removed. Spinal cords were cut into three roughly 1 cm long sections, covered in Optimal Cutting Temperature (OCT) mounting medium (VWR International, Radnor, Pennsylvania, USA) and stood against a pin on a cork disc. 2-methylbutane (isopentane; Honeywell, Morris Plains, New Jersey, USA) was cooled in a beaker over liquid nitrogen. Spinal cord sections were dropped into cold 2-methylbutane for 30 seconds, and then moved to liquid nitrogen after pin removal. Spinal cords were then stored at -80°C. Tibialis anterior and extensor digitorum longus muscles were also taken to be used as control tissue and prepared and stored in the same way.

### **2.4.2 Perfuse fixation**

Rats were given an overdose of pentobarbital (200 mg/kg; Pentोजect; Animalcare Ltd) by IP injection. Once a lack of paw withdrawal and blink reflex

were both noted, transcatheter perfusion was carried out with 1x PB followed by 4% PFA at a flow rate of 9 ml/min. Spinal columns were dissected and stored in 4% PFA at 4°C for 24 hours. Spinal cords were then dissected and transferred to 30% sucrose for three days or until tissue sunk. A 0.5-1 cm long section of the upper thoracic cord (optimised in later chapters) was then cut from intact rat cords before embedding this in OCT on dry ice, and storing at -80°C for at least 24 hours. One control rat small intestine was also taken and prepared in the same way to be used as a control tissue.

## **2.5 Acute contusive spinal cord injury**

Adult female Sprague-Dawley rats (200 – 230g) were anaesthetised in a chamber with 5% isoflurane (IsoFlo; Zoetis UK Ltd, London, UK) and 2% oxygen. Rats were weighed, the dorsal thoracic region was shaved and cleaned with a betadine (National Veterinary Services Ltd, Stoke-on-trent, UK) and ethanol mix, and eye lubrication was applied. A surgical plane of anaesthesia was maintained with 2.5% isoflurane and 2% oxygen. Rats were placed on a heat pad throughout surgery and recovery from anaesthesia. A dorsal midline incision was made over T7-T12 and skin was bluntly dissected to enlarge the surgical site. The dorsal fat pad was retracted and the T9 spinous process was identified. The paravertebral muscles were cut bilaterally and retracted to expose the dorsal laminae. A T9 laminectomy was completed to expose the spinal cord (Figure 2.1b). Sham animal laminectomy sites were packed with spongostan™ (Ethicon™ #MS0002; Ethicon Inc. Johnson & Johnson, Livingston, UK) dampened with saline, the muscle layer was closed with two absorbable sutures (5.0 Ethicon™ Vicryl) and skin was sutured closed with non-absorbable sutures (5.0 Ethicon™ Ethilon). For injured animals; using the Infinite Horizons impactor (Precision Systems and Instrumentation, LLC, Fairfax

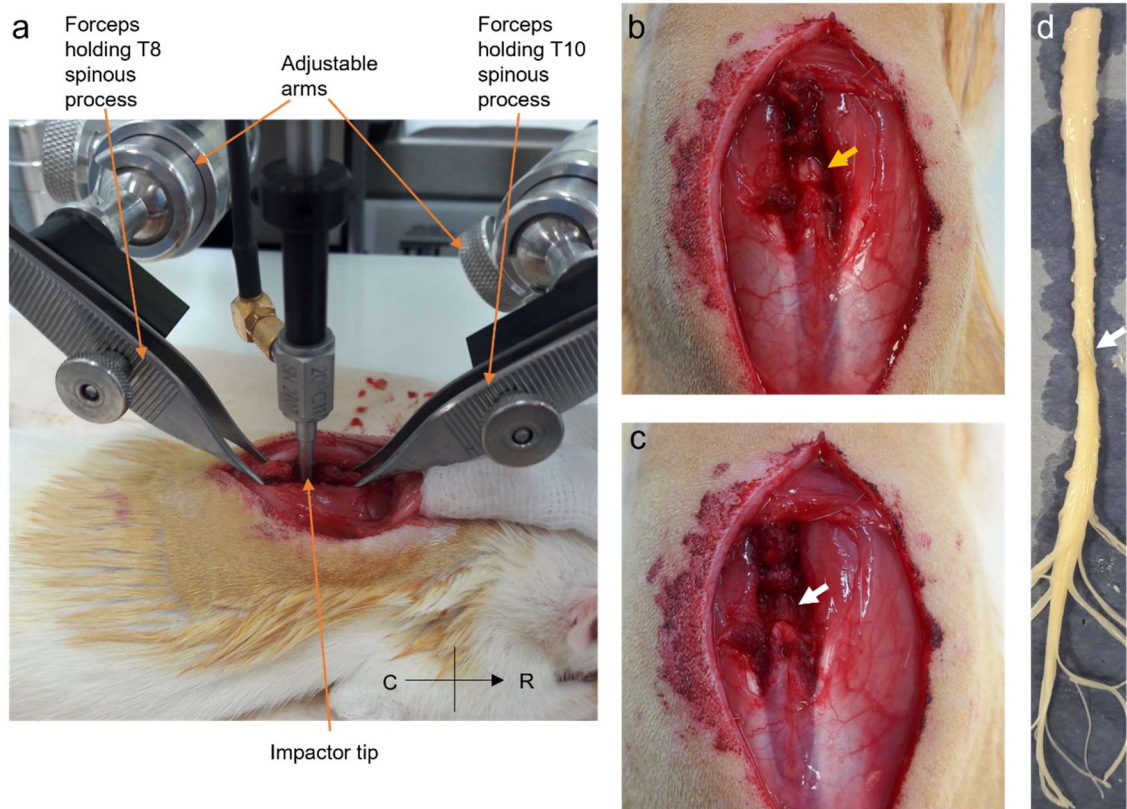


**Figure 2.1: Diagram demonstrating the Infinite Horizons impactor setup and injury site.**

Forceps on adjustable arms held the spinous processes of T8 and T10 level, and the 2.5 mm impactor tip was positioned over the cord in the T9 laminectomy site (a). The spinal cord was exposed at the T9 spinal level (b, yellow arrow), and following injury clear bruising of the cord was apparent (c, white arrow). After perfusion the cord was dissected out and the T10 injury site easily identified (d, white arrow).

Station, VA, USA) T8 and T10 vertebrae were stabilised and a 200 kDyn contusion injury was delivered with a 2.5 mm impact tip to the T10 spinal cord region exposed in the T9 laminectomy (Figure 2.1). Animals were immediately closed as above, except injured animals received Autoclips® (Stoelting Europe, Ireland) to ensure anaesthesia could be removed quickly. Before waking, all animals were given 5 ml warm sterile saline subcutaneously, and 0.015 mg/kg buprenorphine analgesia (Vetergesic; Henry Schein Animal Health, Dumfries, UK) and 2.5 mg/kg enrofloxacin antibiotics (Baytril; Henry Schein Animal Health, Dumfries, UK). Following surgery all animals were housed in pairs and received analgesic and antibiotic subcutaneous injections daily for three days

post-operatively. SCI animals had their bladders expressed twice daily until urinary reflexes recovered (roughly three weeks), at which point daily checks were completed.

## 2.6 Cryosectioning

Samples were allowed to warm to  $-21^{\circ}\text{C}$  in the cryostat chamber (Leica CM1900) before mounting for cutting. Transverse sections were cut at a chamber temperature of  $-21^{\circ}\text{C}$  and sample temperature of  $-18^{\circ}\text{C}$  at  $10\ \mu\text{m}$  or  $20\ \mu\text{m}$ . Sections were separated and picked up directly onto Polysine® adhesion slides (VWR International) to aid adhesion during staining and stored at  $-20^{\circ}\text{C}$ .

## 2.7 Immunohistochemistry

Slides were warmed to room temperature before being ringed with a PAP pen (Sigma-Aldrich). Sections were rinsed with PBS and incubated with 2% PFA for 1 minute if sections were snap frozen, or PBS if sections were fixed. Slides were then washed with PBS three times for 10 minutes. Sections were blocked with 1% normal donkey serum (NDS; Sigma-Aldrich), 1% bovine serum albumin (BSA; A-7888; Sigma-Aldrich), and 0.1% Triton-X in PBS for 1 hour at room temperature. Primary antibodies were made up in PBS with 0.1% Triton-X (PBST) after optimisation, and incubated overnight at  $4^{\circ}\text{C}$ . Optimal concentrations of primary antibodies were as follows: 1:100 platelet endothelial cell adhesion molecule-1 (PECAM-1) anti-mouse (CD31; ab182981; Abcam, Cambridge, UK), 1:100 laminin anti-rabbit (L9393; Sigma-Aldrich), 1:100 collagen IV anti-rabbit (ab19808; Abcam), 1:100 Tie2 anti-rabbit (ab218051; Abcam), 1:300 biotinylated *Wisteria floribunda* agglutinin (WFA; L1516; Sigma-Aldrich), 1:200  $\alpha$ -smooth muscle actin ( $\alpha$ -SMA) anti-mouse (ab7817; Abcam) 1:500 NeuN anti-rabbit (ABN78; Millipore), 1:200 rat endothelial cell antigen-1

(RECA-1) anti-mouse (ab9774; Abcam). Primary antibodies were removed with three washes of PBS for 10 minutes. Secondary antibodies were suspended in PBS at 1:1000, and incubated for 2 hours at room temperature in the dark. Secondary antibodies used were: Alexa-fluor 488 goat anti-mouse (A11001; Invitrogen), Alexa-fluor 546 goat anti-rabbit (A11010; Invitrogen), and Alexa-fluor 594 goat anti-rabbit (A11037; Invitrogen). Slides were then washed three times with TNS to reduce precipitates. After air drying, sections were mounted with Vectashield ( $\pm$ DAPI, Vector Laboratories, Burlingame, California, USA) and a coverslip, and sealed with nail varnish to prevent the mountant drying out.

## **2.8 Microscopy**

All sections for analysis were imaged on a Nikon Eclipse E600 microscope (Nikon, Japan). All sections were visualised with an exposure of 2 seconds under darkfield fluorescence. Images were analysed in FIJI ImageJ (National Institutes of Health, Bethesda, Maryland, USA). Some sections were imaged on a Zeiss LSM700 Inverted confocal microscope and analysed in Zen lite (Karl Zeiss).

## **2.9 Analysis**

### **2.9.1 Stereology**

In order to reduce bias and replication error, systematic random sampling was utilised. Images were taken of the ventral and dorsal grey and white areas.

Three images of each area were analysed for each spinal cord segment. In FIJI ImageJ, a grid with squares with a  $150 \mu\text{m}^2$  area was overlaid (Figure 2.2). As the first point is located randomly, all points in the lattice are as well, but in a systematic manner which reduced the number of events counted needed for a given variance (Weibel, 1980). The number of vessels in each area were

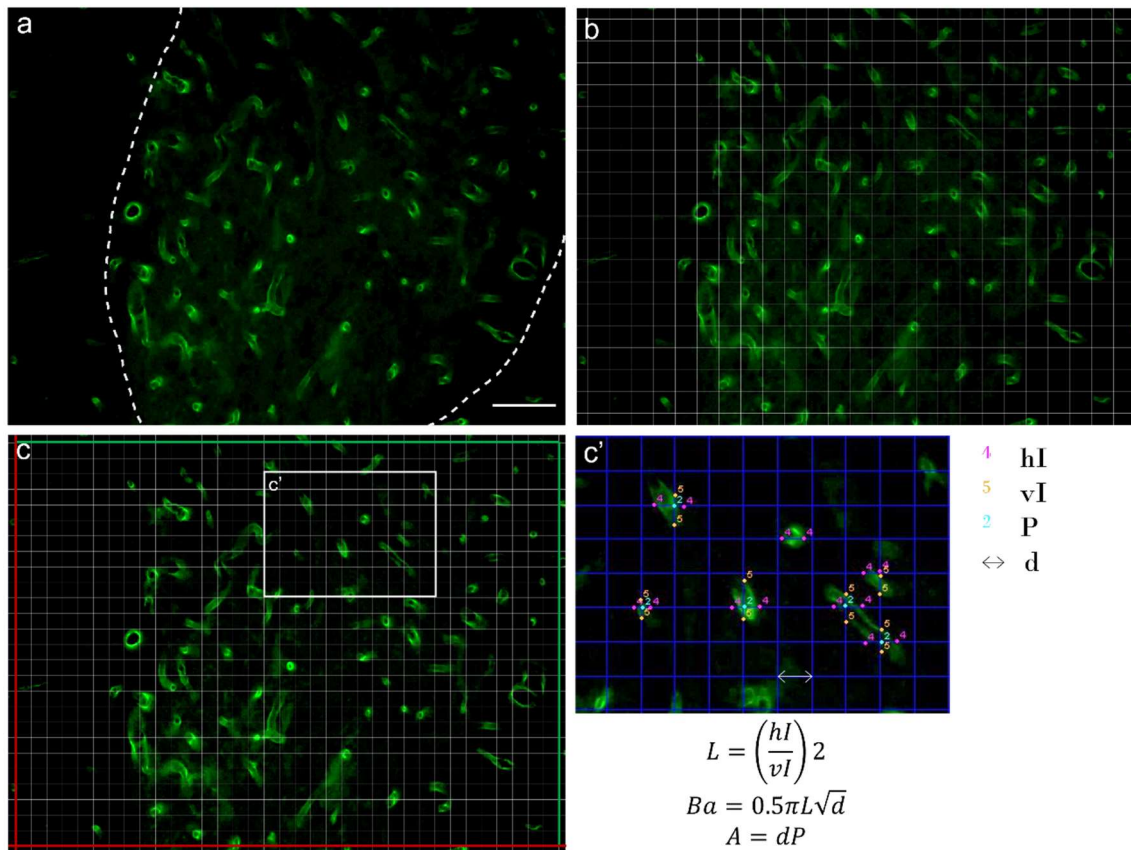


**Figure 2.2: Optimisation of stereology.**

As an example, ventral grey region of interests were identified (a), with outside areas excluded (white dotted line). Grid sizes of  $300 \mu\text{m}^2$  (b) and  $150 \mu\text{m}^2$  (c) were trialled, and grids of  $150 \mu\text{m}^2$  were then used to analyse all future images, with red borders excluded and green included as per stereology convention. Inset c' shows how measurements were taken. When vessel walls crossed horizontal (hI) or vertical lines (vI), a marker was placed. Likewise, when vessels were overlaid with grid crosses (P) a different marker was placed. These measurements were used to calculate vessel surface area (Ba) and areal density (A). Scale bar:  $50 \mu\text{m}$ .

manually counted and tallied using the 'Cell counter' FIJI plugin. Vessel surface area was calculated on the number of times a vessel perimeter crossed horizontal (hI) and vertical (vI) lines, and the stereological equation for perimeter (boundary length, Ba) was used:  $Ba=0.5\pi L\sqrt{d}$  where L is the average of hI and vI and d is the length of each grid square ( $12.25 \mu\text{m}$ ). The areal density of vessels was calculated as the number of points (P) defined by grid cross-sections lying over vessels, and the equation for area (A) was utilised:  $A=dP$ , where d is grid pitch (spacing of lines). These numbers were then normalised to the area of each region within a section, for example in dorsal grey area images

any grid square that included white matter was excluded (Figure 2.2) to calculate areal density ( $A_A$ ). Vessel count normalised for sample area allowed calculation of capillary density (CD,  $\text{mm}^{-2}$ ).

### **2.9.2 Minimum feret diameter**

Images were thresholded in FIJI ImageJ, outliers over 5 pixels removed, and the 'Fill holes' function was used to close vessel lumens (the image processing closing routine refers to dilation followed by erosion). Any vessels in excluded areas were removed. Minimum feret diameter (a measurement of an object size with respect to a specified direction) along the minimal axis for individual vessel profiles was quantified with the 'Measure' function, to provide an index of vessel diameter. Data were plotted as a frequency distribution.

### **2.9.3 Statistics**

Graphpad Prism 9 (GraphPad Software Inc., California, USA) was used for all statistical tests and graphs. All data was initially analysed with a Shapiro-Wilk test of normality. Two-way ANOVAs were conducted on stereology and transmission electron microscope (TEM) data with post hoc Tukey tests. A two-way ANOVA with post-hoc Bonferroni test was conducted on behavioural data. The Kolmogorov-Smirnov test (a non-parametric t-test of the equality of probability distributions) was used for distribution analysis as data were not normal. Contusion force data was analysed using a one-way ANOVA. The significance level was set to 0.05 for all tests. \*  $p < 0.05$ , \*\*  $p < 0.01$ , \*\*\*  $p < 0.001$ , \*\*\*\*  $p < 0.0001$ .

***Chapter 3 : Spinal cord microcirculation and  
angiogenic stimuli***

### 3.1 Introduction

Angiogenesis (growth of capillaries) can be stimulated naturally by the body through adaptive remodelling (e.g. exercise), during pathology (e.g. tumour growth), or as a reparative response (e.g. wound healing). While the growth responses to different stimuli involved may contain specific signalling pathways involving chemo- and/or mechanotransduction of signals by the endothelium, there are many common features. Various pro-angiogenic signals are involved (see Chapter 1) including, but not limited to: VEGF, angiopoietins, and PDGF (Rust et al., 2019). Many therapies have made use of these growth factors to promote angiogenesis by supplementation or regression by blockade of capillaries. Pro-angiogenic treatments have been investigated in a wide variety of conditions, including peripheral arterial disease (PAD) (Ouma et al., 2012), coronary arterial disease (Deveza et al., 2012), and stroke (Navaratna et al., 2009).

Promoting angiogenesis in these conditions characterised by vascular insufficiency or impaired microvascular supply of oxygen and nutrients may have many benefits, such as reducing hypoxia, promoting wound healing, and reducing tissue loss, but there are many associated second-order problems. In patients with PAD treated with pro-angiogenic growth factors, the majority of clinical trials demonstrated diminished clinical and patient-perceived outcomes, such as reduced peak walking time, increased ulcer size and number, and reduced quality of life (Ouma et al., 2012; Shigematsu et al., 2010). This may be linked to the inadequate angiogenic stimuli delivered by only one growth factor, such as VEGF stimulated capillary sprouting, leading to incomplete stabilisation of the expanded neovasculature. Furthermore, using VEGF chemotransduction to promote angiogenesis in the brain has been shown to increase blood brain

barrier permeability and subsequent oedema (Navaratna et al., 2009; Rust et al., 2019).

Other methods of promoting angiogenesis have also been studied. Vasodilators such as prazosin, an  $\alpha_1$ -adrenoreceptor antagonist, have been used to initiate angiogenesis via mechanotransduction, resulting in capillary splitting (Egginton et al., 2001). Vasodilators function by increasing luminal shear stress in capillaries, inducing rapid energy efficient angiogenesis (Egginton et al., 2016). Although, this form of angiogenesis is temporary and vessels regress when the stimulus is removed, with VEGF expression and capillary density returning to control levels in six weeks (Egginton et al., 2016). Prazosin is a drug approved for use in many conditions and the effects in humans have been well studied, so is worth investigating the previously unstudied effects on the spinal cord.

Exercise may promote angiogenesis through a combination of chemo- and mechanotransduction (metabolite release or hypoxia, and muscle strain or luminal shear respectively). Physical activity can lead to the increased production of growth factors such as eNOS, VEGF, VEGFR2, Ang-2, and Tie2 in rat skeletal muscle (Lloyd et al., 2003), which is linked to a subsequent increase in muscle capillarity (Bloor, 2005). Exercise has also been shown to increase levels of BDNF in the hippocampus, cerebellum, cortex, and lumbar spinal cord after 5-7 days of treadmill training or wheel running (Gómez-Pinilla et al., 2001; Neeper et al., 1996). BDNF can have pro-angiogenic actions in skeletal and cardiac muscle (Kermani and Hempstead, 2007), as well as promoting neural plasticity in the brain (Cotman and Berchtold, 2002). Whilst not directly studied, it is therefore reasonable to propose that BDNF may be able to promote angiogenesis in the CNS.

As the vasculature after SCI has not been well studied, it is important to first optimise reliable methods for investigations. Some researchers in the SCI field have reported a brief foray into microvasculature, identifying it as a problem and highlighting some interesting changes (Dias et al., 2018; Li et al., 2017; Loy et al., 2002), before ultimately returning to their primary neural research question. Due to the complex nature of the CNS, understanding the pros and cons to angiogenic treatments may be difficult. Approaching the problem of SCI vasculature from a microvascular perspective may emphasise some previously overlooked aspects. Techniques such as unbiased stereology, whilst commonplace in systemic vascular physiology, are rarely utilised in the SCI literature.

### 3.2 Aims

This study therefore aims to establish protocols to assess relevant capillary structural characteristics and to use these to determine the effects of well-known angiogenic stimuli in the intact rat spinal cord.

Aim 1: Create reliable and accurate protocols to visualise spinal cord vasculature by:

- a) Optimising tissue collection methods to ensure tissue integrity and optimal visualisation.
- b) Optimising immunohistochemistry protocols using a variety of vascular markers, including CD31, RECA-1, and laminin.
- c) Determining the optimal stereological counting method for all areas of the spinal cord.

Aim 2: Determine the angiogenic influence of common stimuli in the intact rat spinal cord by:

- a) Using RECA-1 stained vessels and stereology to characterise the microvasculature following exercise and prazosin treatment.
- b) Using RECA-1 stained vessels to determine the frequency distribution of the internal diameter of capillaries as a measure of potential change in microvascular function.

### **3.3 Methods**

#### **3.3.1 Spinal cord preparation**

##### **3.3.1.1 Snap freezing**

Rats were kindly donated after a 10 day protocol of prazosin (50 mg L<sup>-1</sup> drinking water *ad libitum*; Sigma-Aldrich) by Dr P. Tickle as a control experiment to examine the role of systemically elevated shear stress without SCI pathology. Four male Wistar rats (250 – 300 g) were sacrificed with an overdose of pentobarbital (Pentoject; Animalcare Ltd) by IP injection. Dissection and snap freezing were then carried out as described in section 2.4.1.

##### **3.3.1.2 Perfuse fixation**

Male Wistar rats (250 – 300 g) obtained from an experiment by Dr P. Tickle following a 10 day protocol of prazosin (50 mg L<sup>-1</sup> drinking water *ad libitum*) administration (n=3), or 4 weeks of free wheel running (n=3), or sedentary cage controls (n=3) were sacrificed with an overdose of pentobarbital by IP injection. Once a lack of paw withdrawal and blink reflex were both noted, transcatheterial perfusion was carried out as described in section 2.4.2.

#### **3.3.2 Optimisation of dextran labelling**

##### **3.3.2.1 Dextran perfusion**

Cage control male Wistar rats (n=2) were sacrificed with an overdose of pentobarbital by IP injection. Once a lack of paw withdrawal and blink reflex was noted, transcatheterial perfusion was carried out with 2x PB containing heparin and SNP. This was followed by slowly injecting 12 ml of dextran (MW 500,000) into the transcatheterial cannula over 1-2 minutes. PFA perfusion was then continued as described in section 2.4.2. Following dissection, the spinal cord was kept in foil to reduce light exposure.

### 3.3.2.2 Dextran surgery

Cage control male Wistar rats (n=2) (~300 g) were anaesthetised with an IP injection of 100 mg/kg ketamine (Ketavet®; Henry Schein, Kent, UK) and 3.2 mg/kg xylazine (Rompun®; Henry Schein). Two cannulae were inserted into branches of the left and right jugular veins, one to maintain anaesthesia and one for dextran infusion. 0.5 ml of heparin (to avoid microvascular clots) and SNP (to ensure maximal vasodilation) was injected IP. After 2-4 minutes to allow circulation, this was followed by 2 ml of dextran injected slowly over 2 minutes via the cannula. Laminectomies were performed to expose the lumbar and thoracic spinal cord. After an extra administration of anaesthetic, the spinal cord was carefully dissected out and placed directly into PFA in foil. An IP injection of pentobarbital was given before the brain was dissected out and placed directly into PFA in foil. The brain and spinal cord were kept in PFA at 4°C in the dark for 3 days, and then transferred to 30% sucrose.

### 3.3.3 Cyrosectioning

Cyrosectioning was carried out as described in section 2.6. Some sections were cut at 10, 12, 16, 20, and 50 µm to optimise section integrity and staining efficacy.

### 3.3.4 Lectin histology

After warming to room temperature slides were ringed with a wax PAP pen (Sigma-Aldrich). Sections were rinsed with PBS and incubated with 2% PFA for 1 minute if sections were snap frozen, or PBS if sections were fixed. Sections were further rinsed with PBS before incubation with 1:250 rhodamine conjugated *Griffonia (Bandeiraea) simplicifolia* lectin 1 (Vector Labs, Burlingame, California, USA) for 1 hour at room temperature. Slides were then

washed three times in PBS for 10 minutes and mounted with VectaShield (Vector Labs) to minimise photobleaching.

### **3.3.5 Immunohistochemistry optimisation**

Slides were warmed to room temperature before being ringed with a PAP pen (Sigma-Aldrich). This was subsequently stopped to reduce the risk of wax interfering with antibody binding, and parafilm (VWR International) was instead used to maintain liquid surface tension during incubation periods. Sections were rinsed with PBS and incubated with 2% PFA for 1 minute if sections were snap frozen, or PBS if sections were fixed. Slides were then washed with PBS three times for 10 minutes. Sections were initially blocked with 3% NDS (Sigma) in PBST (Fisher Scientific) for 30 minutes at room temperature. After optimisation, this step changed to 3% NDS, 1% bovine serum albumin (BSA; A-7888; Sigma), and PBST for 1 hour at room temperature, and then changed again to reduce the concentration of NDS to 1%. Primary antibodies were made up in this blocking solution initially, and then PBST after optimisation, and incubated overnight at 4°C. Optimal concentrations of primary antibodies (Table 3.1) are outlined in section 2.7. Primary antibodies were removed with three washes of PBS for 10 minutes. Secondary antibodies were suspended in PBS at 1:500 initially, and then subsequently 1:1000 once optimised, and incubated for 2 hours at room temperature in the dark. Secondary antibodies used are outlined in section 2.7. Occasionally 1:200 biotinylated IgG for mouse (BA-2001) or rabbit (BA-1000; Vector Labs) for 1 hour followed by 1:250 streptavidin pacific blue (S11222; Thermo Fisher) for 1 hour was used instead of a secondary antibody during optimisation. Slides were then washed three times with PBS initially, and then after optimisation, with TNS to reduce precipitates. Sections were mounted as described in section 2.7.

**Table 3.1: Antibodies optimised in rat spinal cords and their target cells/components.**

PECAM: platelet endothelial cell adhesion molecule,  $\alpha$ -SMA:  $\alpha$ -smooth muscle actin, ECM: extracellular matrix, RECA-1: rat endothelial cell antigen-1.

Antibody	Species	Cell specificity
PECAM-1/CD31	Anti-mouse	Endothelial cells, T cells
Laminin	Anti-rabbit	Basement membrane
Type IV collagen	Anti-rabbit	Basement membrane
Tie2	Anti-rabbit	Endothelial cells, haematopoietic cells
<i>Wisteria floribunda</i> lectin	Biotinylated	Perineuronal nets and ECM components
$\alpha$ -SMA	Anti-mouse	Smooth muscle cells
NeuN	Anti-rabbit	Neuronal nuclei
RECA-1	Anti-mouse	Endothelial cells

### 3.3.6 Microscopy

All sections were imaged at a magnification of 20x on a Nikon Eclipse E600 microscope. All sections were visualised with an exposure of 2.5 seconds under darkfield fluorescence. Images of the grey and white matter were analysed in FIJI ImageJ.

### 3.3.7 Analysis optimisation

#### 3.3.7.1 Co-localisation

Antibody co-localisation was assessed by counting clearly defined structures stained with either or both of the antibodies of interest. A percentage was then calculated of total structures counted stained by both antibodies.

#### 3.3.7.2 Stereology

In order to reduce bias, systematic random sampling was utilised as described in section 2.9.1. In FIJI ImageJ, a grid with squares with a 100, 150, or 200  $\mu\text{m}^2$  area was overlaid during optimisation steps. All analysis continued as in section 2.9.1 with 150  $\mu\text{m}^2$  grid squares.

### **3.3.7.3 Minimum Feret Diameter**

Images were thresholded in FIJI ImageJ analysis was carried out as in section 2.9.2.

### **3.3.7.4 Statistics**

Graphpad Prism 9 was used for all statistical tests and graphs as outlined in section 2.9.3. Two-way ANOVAs were conducted on stereology data with post hoc Tukey tests. The Kolmogorov-Smirnov test (a non-parametric t-test of the equality of probability distributions) was used for distribution analysis as data were not normal. The significance level was set to 0.05 for all tests.

## 3.4 Results

### 3.4.1 Optimising immunohistochemistry

#### 3.4.1.1 Fixed vs frozen tissue

Snap frozen or perfuse fixed sections were taken to assess staining efficacy. *Griffonia* lectin (labelling endothelial glycocalyx), CD31 (or PECAM-1), Tie2 (receptor for Ang1), laminin (basement membrane component), and WFA (labelling CSPG components in perineuronal nets) antibodies with DAPI Vectashield were used to compare tissue quality. CD31 and lectin have previously been used to stain endothelial cells in other tissues (Egginton, 2016). Lectin was found to have non-specific staining in both fixed and snap frozen spinal cord tissue after multiple optimisation steps (Figure 3.1 a, b), as denoted by high background staining and staining of non-vascular structures. CD31, Tie2, and WFA staining was more localised and reliable in fixed tissue. Laminin was equally specific to blood vessel shaped structures in fixed and frozen tissue, although a lower concentration was required in frozen tissue (Figure 3.1 c, d). Due to better staining efficacy with fixed tissue and to allow comparison to current literature, it was decided to continue with perfuse fixed spinal cords. Spinal cord sections over 20  $\mu\text{m}$  thick did not stain well on slides, with reduced efficacy and higher background staining, and so a new free-floating protocol would be required. Use of 10  $\mu\text{m}$  sections provided the most efficient staining and clearest structures.

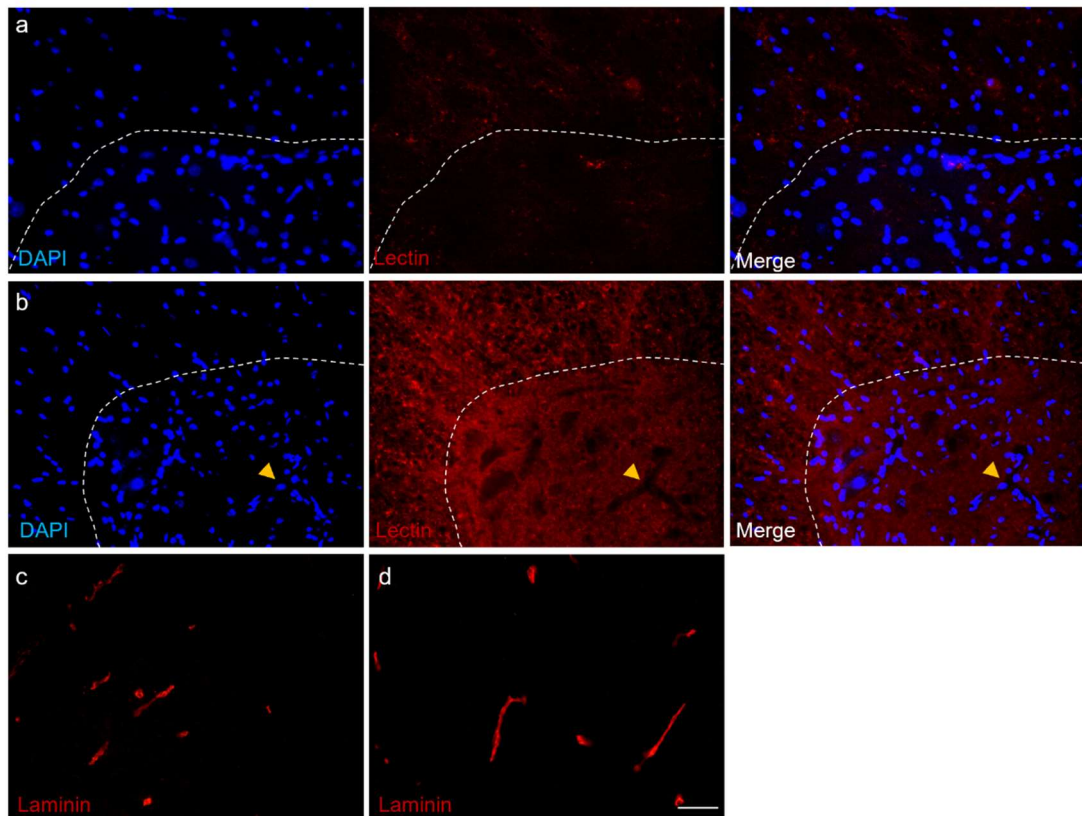


**Figure 3.1: Assessment of snap frozen and fixed spinal cord tissue.**

Lectin staining in frozen tissue (a) was very minimal. Lectin stained more tissue structures in fixed tissue (b), however it did not stain blood vessels (yellow arrowheads). Dotted white lines mark the boundary of the ventral grey and white matter. Laminin was equally specific for blood vessel shaped structures in frozen (c) and fixed (d) tissue. Scale bar: 50  $\mu\text{m}$ .

#### 3.4.1.2 Specificity and co-localisation

Some  $\alpha$ -SMA co-localised with laminin (Figure 3.2 a), however co-localisation with NeuN and WFA in the ventral grey matter indicated some of the  $\alpha$ -SMA positive structures were motor neurons. Based on the structural morphology,  $\alpha$ -SMA also appeared to stain oligodendrocytes in the white matter indicating this antibody was non-specific in the spinal cord. CD31 did not co-localise with laminin and appeared to stain mostly straight 1  $\mu\text{m}$  wide structures in the white matter with axonal morphology (Figure 3.2 b). CD31 may be unable to bind in CNS capillaries as PECAM-1 is a junctional protein between endothelial cells and these junctions are tighter in the CNS, either restricting access or reflecting lower content. RECA-1 has previously been used in rat spinal cord tissue to stain endothelial cells (Bellacen and Lewis, 2009; Kumar et al., 2018a; Loy et

al., 2002). Both laminin and collagen IV co-localised with RECA-1 90% and 95% of the time respectively (Figure 3.2 c, d), indicating these antibodies specifically and reliably stain blood vessels in the spinal cord. Laminin and collagen type IV are located in the basement membrane on the abluminal surface of vessels, so have a larger surface area in tissue sections, explaining the remaining 5-10%.

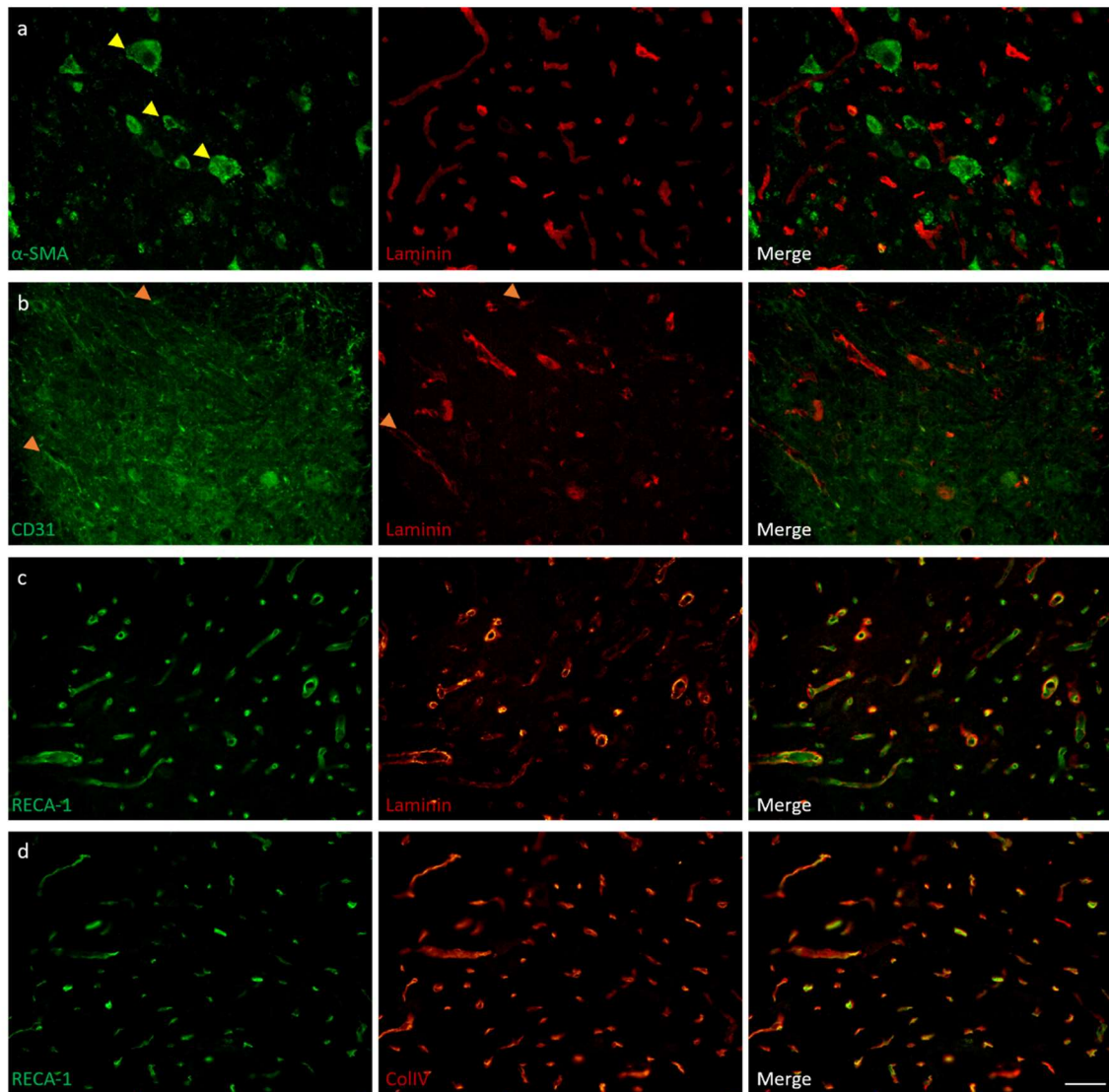


**Figure 3.2: Optimisation of immunohistochemistry as demonstrated using images of the ventral grey matter.**

$\alpha$ -smooth muscle actin ( $\alpha$ -SMA) identified  $\alpha$ -motorneurons (yellow arrowheads, a) rather than blood vessels and did not co-localise with laminin well. CD31 showed more specific staining in the white matter, however structures identified in the grey matter (b) did not appear to be blood vessels (orange arrowheads highlight two instances of co-localisation). Rat endothelial cell antigen-1 (RECA-1) co-localised well with both laminin (c) and type IV collagen (CollIV) (d) to identify blood vessels. Scale bar: 50  $\mu$ m.

### 3.4.1.3 Dextran perfusion

Perfusing with dextran before PFA fixation did stain vessels in the spinal cord, however tissue quality was dramatically reduced, and as a result co-localisation staining with RECA-1, laminin, or collagen IV was not possible (Figure 3.3 a).

Injecting dextran during surgery demonstrated clearer staining of vessels in the cord, however, tissue quality was negatively affected and again co-localisation staining could not be achieved (Figure 3.3 b).

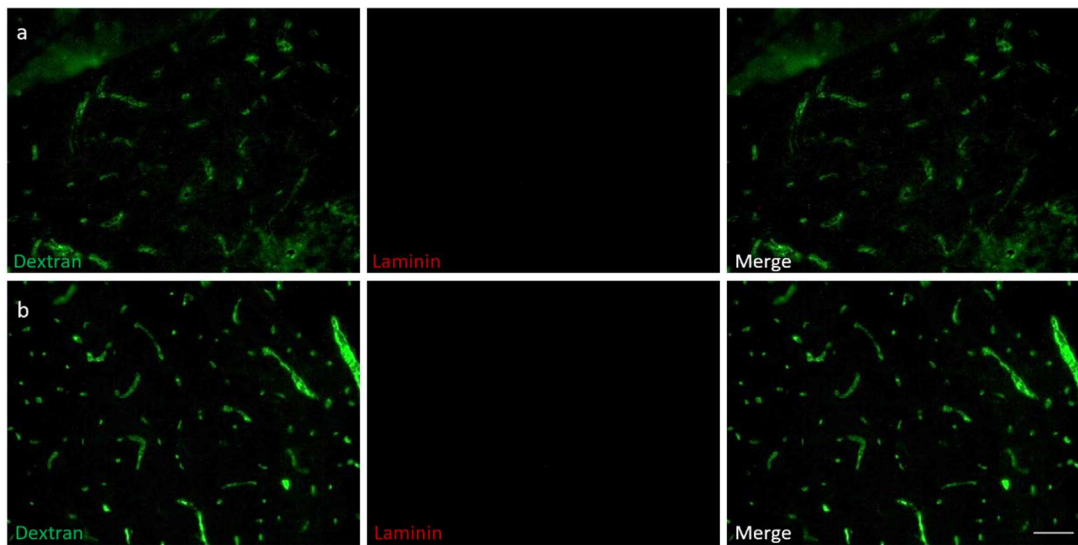


**Figure 3.3: Optimisation of dextran perfusion.**

Dextran perfusion before fixation (a) and during surgery with post-fixation (b) highlighted blood vessels in the anterior grey matter of the spinal cord. Both methods negatively affected tissue quality, so co-localisation with other markers such as laminin was not possible. Scale bar: 50  $\mu\text{m}$ .

### 3.4.2 Effects of known angiogenic promoters on microvasculature

RECA-1 and laminin staining were used to accurately identify blood vessels.

Subsequent analysis was based on RECA-1 staining to ensure capillary areal density and surface area were measured from endothelial lumen surface, and not skewed by measuring from the abluminal basement membrane. In control spinal cords, the ventral grey matter contained  $484.9 \pm 93.6$  vessels per  $\text{mm}^2$  whereas the dorsal grey matter contained  $533.1 \pm 44.4$  vessels per  $\text{mm}^2$ .

Prazosin administration or wheel running exercise, which produce either chronic

or periodic hyperaemia respectively, did not promote angiogenesis in the healthy spinal cord. The number of capillaries remained unchanged compared to control spinal cords in all areas analysed (Figure 3.4 a). Capillary areal density and surface area also remained unchanged.

Surface:volume ratio (S/V) can give an indication of angiogenesis or regression, with values closer to 0.5 indicating that vessels are round and cut transversely, while values  $> 0.5$  may indicate collapsed vessels or those sectioned obliquely. Values were slightly larger in the white matter as these capillaries are more likely to be cut longitudinally as they follow the orientation of the transverse axons. If, for example, vessel surface area increased as areal density decreased, this may indicate new capillary growth or an increased number of transverse vessels. However, as any changes in vessel surface area and areal density were equal in both measurements, such as the slight non-significant decrease in the dorsal grey matter with prazosin treatment, the S/V remained within range of the control for all measurements (Figure 3.4 d).

Minimum feret diameter is a measurement of the smallest internal diameter of a structure (or the minimum calliper diameter of the selection boundary). RECA-1 stained vessels were analysed in the ventral and dorsal grey and white matter and a probability distribution generated. This generated a geometric, rather than arithmetic, progression as the extent of diameter changes in the capillary bed would be influenced by initial values. The Kolmogorov-Smirnov test was used as it can detect differences in the shape of the distribution in geometric (non-parametric) distributions, whereas an ANOVA detects shifts in the mean of normally distributed data, so is less sensitive. Minimum feret diameter could potentially indicate if stereological data resulted from changes to larger vessels,

altered tortuosity, or oblique sections of vessels. Despite an apparent increase in the number of vessels with a minimum feret diameter between 4 and 6  $\mu\text{m}$  in the ventral white matter in the exercise group (Figure 3.5 b), no significant difference was detected. The peak vessel diameter for all areas and conditions was 4-6  $\mu\text{m}$ , apart from in the dorsal grey matter of the control group (peak diameter 6-8  $\mu\text{m}$ ). If this difference was more than a one bin centre shift or the shape of the bell curve was altered significantly, we may be able to draw conclusions on capillary changes such as angiogenesis, regression, or oedema.

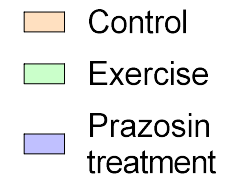
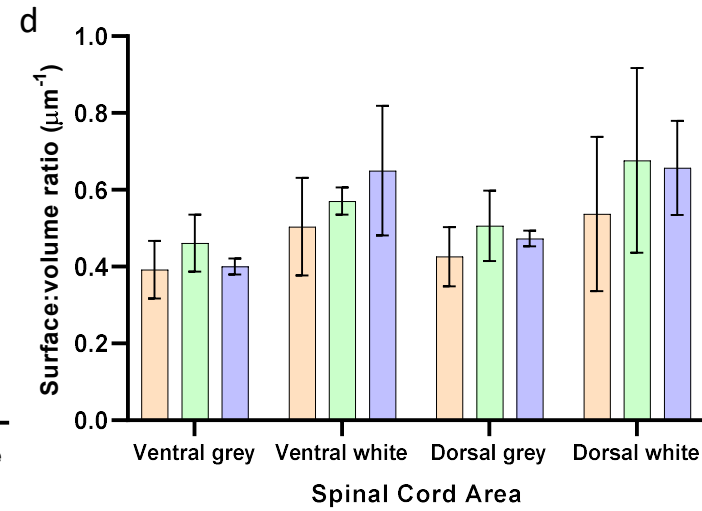
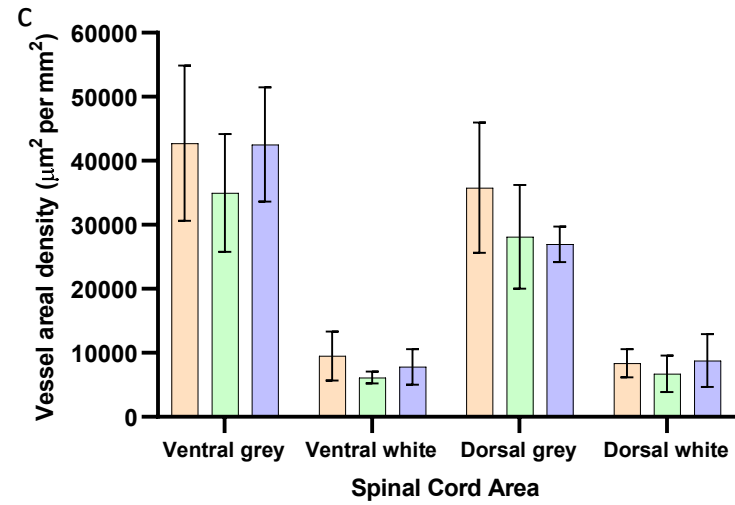
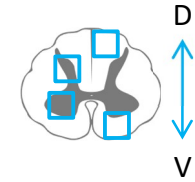
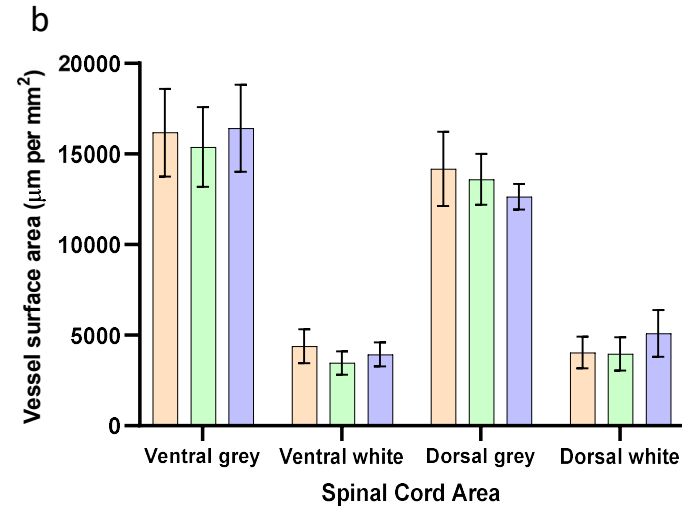
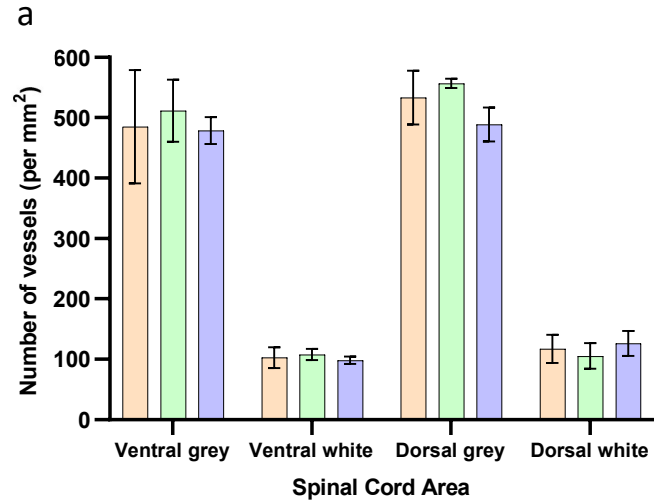


**Figure 3.4: Vessel characteristics were unaltered by exercise or prazosin treatment.**

The vessel density (a) in each spinal cord area remained unchanged in all conditions, as did vessel surface area (b), areal density (c), and surface:volume ratio (d). Error bars  $\pm$  SD. Statistics: two-way ANOVA.  $n=3$  for all groups.

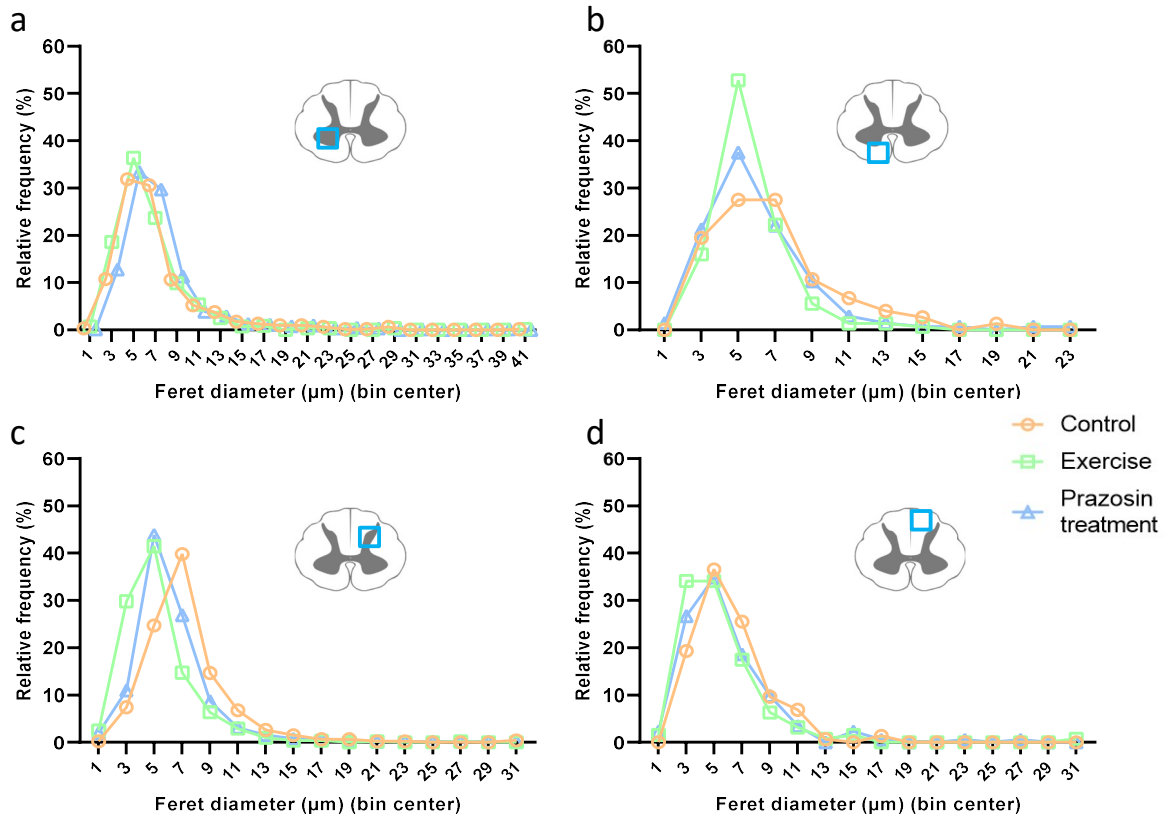


**Figure 3.5: The minimum feret diameter of vessels remained unchanged in all conditions.**

Vessel diameter in the ventral grey (a) and dorsal white (d) matter clearly demonstrated no curve shift. Minor curve shifts in the ventral white (b) and dorsal grey (c) matter were not statistically significant. Statistics: Kolmogorov-Smirnov test.  $n=3$  for all groups.

### 3.5 Discussion

This study aimed to find the most appropriate and reliable method of visualising spinal cord vasculature and use that to determine the effects of exercise and prazosin on the intact spinal cord microvasculature. Immunohistochemistry is by far the most common method used for visualising tissue components, however many markers often used to stain capillaries in peripheral tissues did not work in the spinal cord. For example, CD31, or PECAM-1, is an adhesion and signalling molecule, mostly found on endothelial cells (Figure 1.3). CD31 is used to visualise the microvascular system in many tissues, including rat muscle (Perrin et al., 2004), rat brain (Zhan et al., 2019), and mouse spinal cord (Halder et al., 2018). However, in the rat spinal cord, CD31 appears to mostly highlight axonal structures in the white matter. An alternative antibody used to visualise the rat spinal cord microvasculature is RECA-1 (Kumar et al., 2018a; Loy et al., 2002). RECA-1 binds to an endothelial cell surface antigen, and has been shown to bind to all vascular endothelium in the rat without cross-reacting with any other cell types (Duijvestijn et al., 1992). Due to the reliability of this marker, and the co-localisation with laminin and collagen type IV in the vascular basement membrane of capillary-sized objects with appropriate morphology, RECA-1 was chosen as the most appropriate antibody to continue the study with.

Visualising the vasculature by injecting a marker intravenously can also provide insight into capillary structure and functionality. Injecting the RECA-1 antibody would highlight all functional capillaries, and co-staining with laminin or collagen IV could demonstrate any non-functional capillaries present by a lack of RECA-1 staining co-localisation. However, due to the volumes required and costs associated with using this method in adult rats, an alternative method was sought. Intravenous administration of lectins, Evans blue dye, or various size

dextran molecules has been previously used for this purpose, and can also demonstrate blood brain barrier integrity as any staining outside the vasculature indicates increased permeability of capillaries (Xu et al., 2019). Dextran with a high molecular weight of 500,000 was chosen for this purpose as this size molecule would not be able to pass through the BSCB without significant vascular damage being present.

As all immunohistochemistry had been optimised for fixed tissue, as is the standard in neuroscience due to the fragility of neural tissue, dextran perfusion was first incorporated into the perfusion protocol. Dextran was slowly injected after blood was flushed out with PB and before PFA was perfused to allow dextran to bind to the endothelium before being blocked by PFA crosslinks. Due to the chance of the PFA flushing the dextran out of the vascular system, the perfusion pressure was reduced to limit this effect. Unfortunately, dextran labelling appeared to be incomplete, with some unlabelled vessels visualised by the negative spaces created in tissue sections. The altered perfusion protocol also affected tissue quality, as antibodies such as laminin and collagen IV no longer picked up any vascular structures (Figure 3.3 a).

An alternative method of infusing dextran during surgery and then post-fixing the spinal cord in PFA was also attempted. This method produced improved dextran staining (Figure 3.3 b), potentially as dextran may also bind to serum albumin within the vascular system (Vink and Duling, 1996) which had not been flushed out in this method. However, as the spinal cord was only post-fixed in PFA following removal, tissue quality was negatively affected and again, co-localisation staining was not possible. As pilot study data was not promising,

and in line with the principles of the 3Rs, it was decided to discontinue with dextran labelling.

Stereology is seldom used in SCI research, however there are many benefits to this approach, including accuracy, reduced bias, and a plethora of structural characteristics available for quantification. Unbiased stereology is commonly utilised to assess vascular changes in conditions such as diabetes (Guo et al., 2005; Noorafshan et al., 2013), cardiac disease (Egginton et al., 2016; Muhlfeld et al., 2010; Tang et al., 2009), and exercise (Jensen et al., 2020; Meinild Lundby et al., 2018). This method has the advantage of allowing the researcher to make informed decisions during data collection, eliminating the error often introduced by using automated software. Using a counting grid system and standard stereological exclusion criteria can reduce the chances of skewing the data by counting all vessels that may appear in serial sections. Three-dimensional structure geometry can be inferred from two-dimensional samples using stereological principles (Howard and Reed, 1998; West, 2012).

As expected, due to the differing metabolic requirements of different areas of the spinal cord, the white matter had significantly fewer vessels than the grey matter (around 21.6% of the vessel density of the grey matter; Figure 3.4). No significant differences were observed in any parameters measured. This may be due to the brevity of the treatment or exercise programme, however 10 days of prazosin administration has previously been shown in large group rodent studies to promote angiogenesis in peripheral tissues (Baum et al., 2004; Dunford et al., 2017; Egginton et al., 2016), as has exercise (Lloyd et al., 2003). Indeed, even a single bout of moderate to intense exercise can significantly increase mRNA levels of VEGF, basic fibroblast growth factor (bFGF), and

transforming growth factor- $\beta$ 1 (TGF- $\beta$ 1) in skeletal muscle (Breen et al., 1996). It may be that the CNS requires a longer or more intense stimulus to promote angiogenesis, or that any microvascular changes are very subtle in the spinal cord of uninjured animals. A larger study, potentially utilising other methods of measuring vascular changes such as electron microscopy or VEGF protein level analysis within the cord, may be able to elucidate if these treatments have any effect on the microvasculature of the intact spinal cord.

Another consideration is that exercise or prazosin treatment may have different effects in the injured spinal cord. As the spinal cord is actively remodelling after SCI, there may be more potential to promote angiogenesis. However, a more detailed timeline of vasculature changes following SCI is required to assess this. Exercise is not possible within the first week of SCI recovery in humans or animal models, and when attempted three days after SCI, increased extravasation around the injury site was noted (Smith et al., 2009). Prazosin, as a vasodilator, would likely cause more damage to the spinal cord if given early on by contributing to the haemorrhage and oedema. Therefore, as treatment within the first few days would likely have more favourable outcomes, such as reduction in hypoxia, oedema, inflammation, and necrosis, as well as eventual scar formation, it is probable that a more targeted approach is necessary.

Despite the importance of the microvascular system in the CNS, details on capillary structural characteristics, even in intact animals, are largely unexplored. This study provided valuable insight into the microvasculature in intact spinal cords, demonstrating that short term angiogenic stimuli may not promote angiogenesis in these conditions. Further research is required to validate these results and to look at other markers of angiogenesis, such as

VEGF levels within the cord. Protocols for tissue collection, visualisation, and analysis were established, and could now be applied to the following study assessing microvasculature changes post-SCI.

***Chapter 4 : Timeline of vascular changes following SCI***

## 4.1 Introduction

Traumatic SCI is a serious, life-changing injury with often severe long-lasting effects. The initial injury initiates a series of responses including inflammation, ischaemia, and apoptosis (Ahuja et al., 2017; Fitch et al., 1999). Mechanical disruption (the primary injury) to the cord causes neuronal, glial, and endothelial cell death. Concomitant destruction of the microvasculature perpetuates haemorrhage, ischaemia, and progressive cell death, and therefore creates a cytotoxic environment radiating from the injury epicentre (Mauter et al., 2000). Increased permeability of the damaged BSCB causes endothelial cell damage, development of perivascular spaces, and extravasation of erythrocytes and inflammatory cells, which in turn causes cord swelling and further compression (Ahuja et al., 2017; Bartanusz et al., 2011). These changes further contribute to haemorrhage, ischaemia, and inflammation in a self-perpetuating cycle (Loy et al., 2002).

The collapsed microvasculature after SCI has been shown to continue to remodel at the injury epicentre, and caudal and rostral to the injury (Loy et al., 2002; Popovich et al., 1996), involving two periods of angiogenic activity following SCI indicated by an increase in the microvasculature; the primary wave within 3-7 days after injury, and a secondary wave 14-60 days later (Durham-Lee et al., 2012; Loy et al., 2002; Popovich et al., 1996). As expected due to the microvascular functions of trophic support in the CNS to neural and glial cells (Miyamoto et al., 2014), there is a general correlation between the increase in blood vessel density and an improved neural and functional recovery following SCI (for example, vessel number predicts mouse locomotor BBB score,  $R^2=0.55$ ,  $P<0.001$  (Han et al., 2010)) (Duan et al., 2015; Han et al., 2010; Kaneko et al., 2006; Rauch et al., 2009). Unfortunately, an increased

large vessel number or diameter does not necessarily mean an increase in perfusion of the cord as larger vessels, such as arterioles or venules, are less diffusive (Streijger et al., 2017). Larger vessels may indirectly support perfusion, however if the increase in vasculature does not include an increase in the density of exchange vessels, diffusive capacity may not increase regardless of the number of larger vessels. Chronic vasoconstriction can promote hypoxia and necrosis despite increased blood flow in the macrovasculature. As the microvasculature is severely damaged and angiogenesis is limited following SCI, hypoxia and ischaemia continues for many months. This hypoxia is not exclusive to the injury epicentre and has been shown to extend down the cord caudal to the site of injury (Li et al., 2017), thereby potentially exacerbating the extent of the injury and/or recovery time.

Angiogenesis following injury has been shown to be transient and incomplete (Cao et al., 2017; Ng et al., 2011). This may be due to a lack of observed pericytes or astrocytes associated with new vessels 14 days after injury, which normally aid stabilisation of neovasculature. A reduced number of glucose transporters present in the acute stages following injury, which usually act to supply glucose across the BSCB to the neurons, can suggest metabolic dysregulation (Ng et al., 2011; Whetstone et al., 2003). Whilst the number of vessels has been shown to increase somewhat following injury, the majority of these neovessels do not appear to express glucose transporters (Whetstone et al., 2003). As these vessels are therefore unlikely to contribute to an effective BSCB or function appropriately, excessive pruning of vessels is observed (Ng et al., 2011). Investigation into the rarefaction and growth of capillaries after SCI is sparse. Details of the changes in spinal cord vasculature need to be analysed in

more detail and corroborated before a potential vascular target can be identified.

Some studies utilising MRI,  $\mu$ CT, or synchrotron radiation- $\mu$ CT have been used to assess spinal cord vasculature (Cao et al., 2017; Herrera et al., 2010; Sundberg et al., 2011). However, the resolution of images in these methods is too low to accurately visualise capillaries rather than arterioles or venules. Many papers misuse the term microvasculature to include these less-diffusive vessels (Herrera et al., 2010; Hu et al., 2012; Long et al., 2014; Moisan et al., 2014).

With immunohistochemistry we can selectively analyse only those vessels with a diameter of less than eight microns to ensure a greater selectivity. This means we can analyse only the critical microvessels for oxygen delivery, and create a more accurate picture of the spatiotemporal changes after SCI. TEM can be used at acute and chronic timepoints to confirm any structural changes, and can provide a basis for high spatial resolution analyses.

## 4.2 Aims

The primary aim of this study was therefore to develop a complete timeline of vascular changes in the acute period following traumatic SCI using immunohistochemistry. RECA-1 was chosen as the principal vascular marker as it is reliable, accurate for vascular diameter measurements, and comparable to previous literature (Kumar et al., 2018a; Liu et al., 2010; Loy et al., 2002).

Aim 1: Develop a timeline of vascular changes following SCI by:

- a) Using RECA-1 stained vessels and stereology to characterise the microvasculature at acute and chronic timepoints post-SCI.
- b) Using RECA-1 stained vessels to determine the frequency distribution of the internal diameter of capillaries as a measure of vessel changes in key spinal segments.

Aim 2: Assess microstructural changes to the neurovascular unit by:

- a) Utilising TEM to measure basement membrane thickness as a gauge of vascular integrity.
- b) Utilising TEM to measure intercellular cleft thickness to infer tight junction integrity.

## 4.3 Methods

### 4.3.1 Surgery

All procedures were carried out according to local and Home Office guidelines, in compliance with A(SP)A 1986. All surgical procedures were carried out as outlined in section 2.5.

### 4.3.2 Spinal cord preparation

SCI rats were perfuse-fixed at days 2, 5, 15, and 45, (n=4 for all groups) with sham animals (n=6) being perfused at day 5 (Figure 4.1). Spinal cords were prepared as in sections 2.4.2. An additional step of an IP injection of heparin was added between the IP injection of pentobarbital and perfusion with PB and PFA to prevent microvascular occlusion. Before freezing in OCT, spinal cord segments were identified under a dissection microscope, and the injury epicentre (T10) and three segments rostral and caudal were dissected and frozen separately.



**Figure 4.1: Timeline of study following T10 contusion injury.**

Animals were perfused on days 2, 5, 15, and 45 following injury. Cx: contusion injury.

### 4.3.3 Transmission electron microscopy

#### 4.3.3.1 Fixative solution

To make the 2% glutaraldehyde and 2% PFA w/v combined fixative, the appropriate volume of 25% glutaraldehyde solution (Sigma-Aldrich) was mixed with 8% PFA (Sigma-Aldrich) and 1x PB. The solution was made up to pH 7.4

and filtered, before being used within 24 hours to minimise aldehyde polymerisation.

#### **4.3.3.2 Tissue preparation**

Animals from day 2 post SCI (n=2) and sham (n=2) groups were perfused as described in section 4.3.2. with some refinements. Briefly, rats were given an overdose of pentobarbital, followed by an IP injection of heparin. Perfusion was carried out with 1x PB followed by 2% glutaraldehyde 2% PFA at a slower flow rate of 6 ml/min. Spinal columns were post-fixed in the glutaraldehyde PFA mix for 24 hours at 4°C, after which the spinal cord was dissected out. Cords were cut into segments (injury epicentre and one segment rostral and caudal) with a double-edged razor.

#### **4.3.3.3 Transmission electron microscopy**

All further tissue preparation steps were kindly carried out by Martin Fuller in the University of Leeds Electron Microscopy Facility. Briefly, samples were embedded in resin and semi-thin 0.5 µm sections were cut using an ultramicrotome (Reichert-Jung Ultracut E). Sections were stained with 1% toluidine blue on a hot plate for 25 seconds and assessed under a light microscope to identify orientation. Ultra-thin sections for electron microscopy were cut using a diamond knife at 100 nm and stained with uranyl acetate (Saturated/8% aqueous) and lead citrate (Reynolds Lead Citrate). Images were taken using a Thermo Fisher (FEI) Tecnai T12 transmission electron microscope at an accelerating voltage of 120 kV. A systematic search of microvessels present in regions of interest was used to image capillaries at a magnification of 5,000x and then 10,000x.

#### **4.3.4 Cyrosectioning**

Samples from seven spinal cord segments were cut at 20  $\mu\text{m}$  as described in section 2.6. Due to tissue friability after SCI, 20  $\mu\text{m}$  sections were used rather than 10  $\mu\text{m}$  to ensure section integrity.

#### **4.3.5 Immunohistochemistry**

Tissue sections were stained as outlined in section 2.7. Optimal concentrations of primary antibodies were as follows: 1:200 Laminin anti-rabbit (L9393; Sigma), 1:200 RECA-1 anti-mouse (ab9774, Abcam), 1:100 Collagen IV anti-rabbit (ab19808; Abcam). Secondary antibodies used were: Alexa-fluor 488 goat anti-mouse (A11001; Invitrogen) and Alexa-fluor 546 goat anti-rabbit (A11010; Invitrogen) and the concentration was increased to 1:500 for SCI tissue.

#### **4.3.6 Fluorescence microscopy**

All sections were imaged on a Nikon Eclipse E600 microscope at a magnification of 20x with an exposure of 2 seconds. Images of the ventral and dorsal grey and white matter from T7 to T13 were analysed in FIJI ImageJ.

#### **4.3.7 Analysis**

##### **4.3.7.1 Stereology**

Analysis of vessel number, surface area, and areal density continued as in section 2.9.1.

##### **4.3.7.2 Minimum feret diameter**

A macro was written in FIJI ImageJ to analyse minimum feret diameter for a large data set (Appendix 2). Image contrast was enhanced (using histogram stretch) and the background was subtracted before images were thresholded using 'Moments'. Minimum feret diameter was then assessed as in section 2.9.2. Data was exported to Excel using the 'Read and write Excel' plugin.

Based on extensive manual counts and distribution analysis, outliers over 50  $\mu\text{m}$  and under 2  $\mu\text{m}$  were removed from data sets. Due to the level of background staining and artefacts at day 2, this timepoint was excluded from automated analysis.

#### **4.3.7.3 Transmission electron microscopy measurements**

TEM images at 10,000x were used to measure basement membrane and intercellular cleft width using the measurement tool in FIJI ImageJ to generate orthogonal lines to endothelial cell membrane. To validate analysis steps, repeat measurements were taken two weeks after initial analysis, confirming measurements were reliable.

#### **4.3.7.4 Statistics**

Graphpad Prism 9 was used for all statistical tests and graphs as outlined in section 2.9.3. Two-way ANOVAs were conducted on stereology and TEM data with post hoc Tukey tests. The Kolmogorov-Smirnov test (a non-parametric t-test of the equality of probability distributions) was used for distribution analysis as data were not normal. Contusion force data was analysed using a one-way ANOVA. The significance level was set to 0.05 for all tests.

## 4.4 Results

The following results demonstrate various aspects of microvasculature changes after a T10 moderate/severe contusion SCI. Immunohistochemistry coupled with unbiased stereology was utilised to collect data on the number, surface area, and areal density of capillaries up to 12 mm (or three spinal segments) rostral and caudal to the injury epicentre. Feret diameter was calculated in ImageJ to assess the relative diameter of capillary profiles in the grey matter. These results inferred some rarefaction or oedema of vessels until day 5, so tissue was collected for TEM in order to confirm this.

### 4.4.1 Contusion force

All SCI animals received a T10 ~200 kDyn contusion injury following a T9 laminectomy. The Infinite Horizons impactor was used as it accurately controlled the amount of force used and gave a read out of the actual force delivered. The spinal column was stabilised by forcep arms on the impactor to avoid displacement. The small diameter (2.5 mm) of the metal impactor allowed precise injury location. An average contusion of  $204 \pm 4$  kDyn was delivered, and there was no significant difference between groups ( $P=0.77$ ) (Figure 4.2).

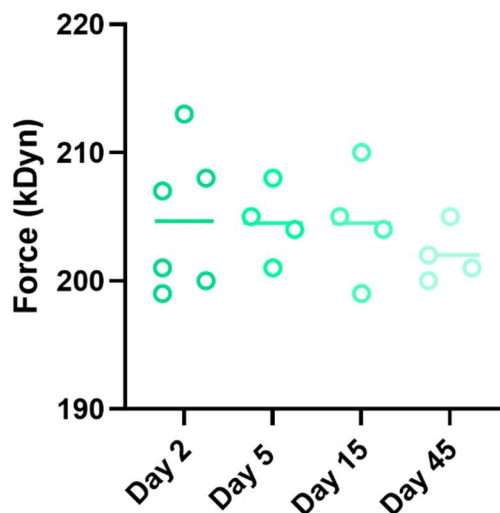


**Figure 4.2: Actual force used for each contusion spinal cord injury.** Average contusion force was 204 kDyn, with no significant difference between groups.  $n=4$  for all groups, except day 2 animals ( $n=6$ ).

#### **4.4.2 Stereological analysis**

Previous literature has demonstrated that damage can spread up to three spinal segments rostrally and caudally from the injury site (Loy et al., 2002). Thus, seven spinal segments in total were analysed: the injury epicentre and three segments rostrally and caudally. As the injury site is a rapidly changing environment, multiple early timepoints were required. Behavioural data following a 200 kDyn moderate/severe contusion injury demonstrates recovery plateaus around week 6 post SCI, so a later time point of day 45 was also included to assess how the vasculature had changed in the scar tissue and surrounding more stable environment.

##### **4.4.2.1 Vessel number decreases after injury**

Assessing vessel number in a standardised area gives an insight into the oxygen supply in tissue, and potential for development of hypoxia. The spinal cord, and specifically the grey matter, has a high oxygen demand in normal conditions. Understanding how this changes after SCI in the necrotic epicentre and following scar tissue could expose new avenues of treatment options.

Unsurprisingly, the most intense damage was seen at earlier timepoints closest to the injury site and at the injury epicentre (Figure 4.3). In intact spinal cords, the thoracic ventral grey matter contained roughly 570 vessels per mm<sup>2</sup>, whereas the thoracic dorsal grey matter contained approximately 480 vessels per mm<sup>2</sup>. Vessels in the white matter remained unchanged in most segments, although some increases in parameters were seen at day 45 (Appendix 1). In comparison to sham operated animals at each segment, a significant reduction of vessel density (vessel number per mm<sup>2</sup>) was seen at day 2 in both the ventral and dorsal grey matter at T9 (P<0.0001 ventral, P=0.0038 dorsal), T10, (P<0.0001 ventral and dorsal), T11 (P<0.0001 ventral and dorsal), and T12

( $P=0.0004$  ventral,  $P<0.0001$  dorsal). Vessel number also significantly decreased by 29% at day 45 at T8 in the dorsal grey matter ( $488.1 \pm 38.1$  vessels per  $\text{mm}^2$  in sham animals vs  $347.0 \pm 45.9$  vessels per  $\text{mm}^2$  at day 45).

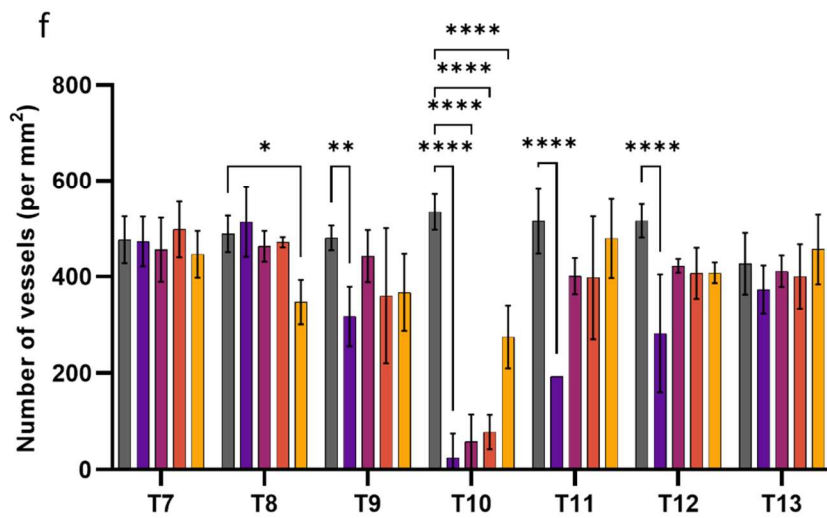
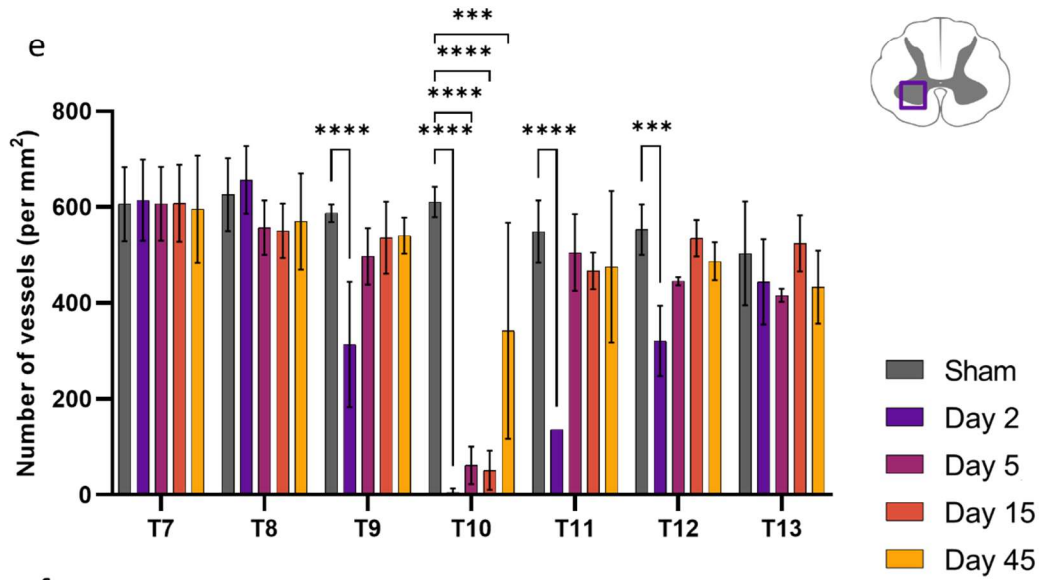
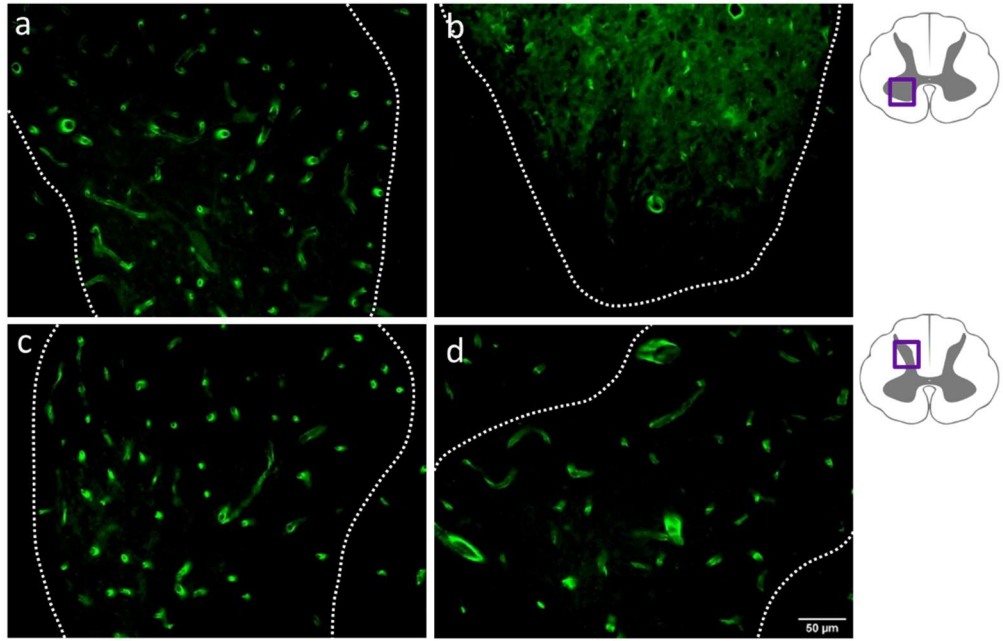


**Figure 4.3: Vessel density decreased after injury.**

Sham (a) vessels stained well with RECA-1, however day 2 vessels close to the injury site, such as at T9 (b), demonstrated more background staining and fewer vessels. Vessel density (number per mm<sup>2</sup>) was significantly lower by day 45 in the dorsal grey matter at T8 (d) compared to sham (c). Spatiotemporal changes in both the ventral (e) and dorsal (f) grey matter were widespread. Statistics: two-way ANOVA; \* P<0.05, \*\* P<0.01, \*\*\* P<0.001, \*\*\*\* P<0.0001. Error bars  $\pm$  SD. Scale bar: 50  $\mu$ m. n=4 for all injured groups, n=6 for sham group.

**4.4.2.2 SCI compromises vessel surface area**

Vessel surface area is a measurement of the anatomical boundary, and therefore diffusive capacity, of capillaries. This measurement gives useful insight into the functionality of blood vessels; a larger surface area may be found on small vessels due to the surface:volume ratio, inferring a larger diffusive capacity than larger members of the microcirculation, such as arterioles, that regulate the extent of perfused tissue. Vessel surface area (normalised to sample area) significantly decreased by 35% at day 2 following injury (P<0.0001), and remained lower for at least 15 days in the ventral grey matter at T9 (P=0.03 at day 5, P=0.035 at day 15) (Figure 4.4). This trend was also present at T11 in the ventral grey matter (P=0.35 at day 15) and at both T9 and T11 in the dorsal grey matter (P=0.15 and P=0.46 at day 15 respectively). Vessel surface area at the injury epicentre (T10) remained significantly decreased at all time points in both the ventral and dorsal grey matter. At T13 in the ventral and dorsal grey matter, there was an increasing trend towards a larger vessel surface area at day 45 (21,357.51  $\pm$  5,357.264  $\mu$ m per mm<sup>2</sup> in sham animals vs 27,824.54  $\pm$  4,349.84  $\mu$ m per mm<sup>2</sup> in the ventral grey matter at day 45 (P=0.04), 16,420.33  $\pm$  2,668.73  $\mu$ m per mm<sup>2</sup> in sham animals vs 22,429.37  $\pm$  2,390.13  $\mu$ m per mm<sup>2</sup> in the dorsal grey matter at day 45 (P=0.064)). Reduced vessel surface area was significant as far away as 8 mm

caudal (T12) to the injury site at day 2 post SCI ( $P < 0.0001$  in both the ventral and dorsal grey matter).

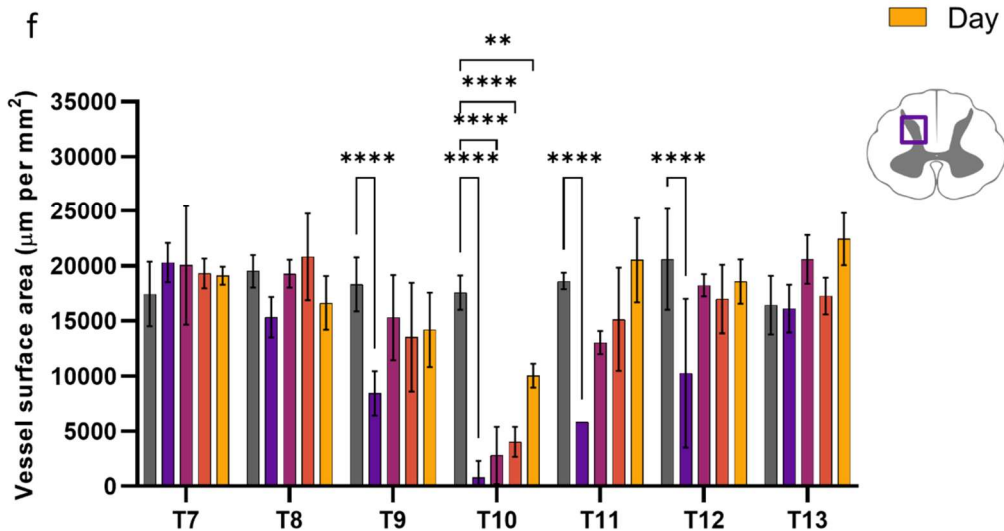
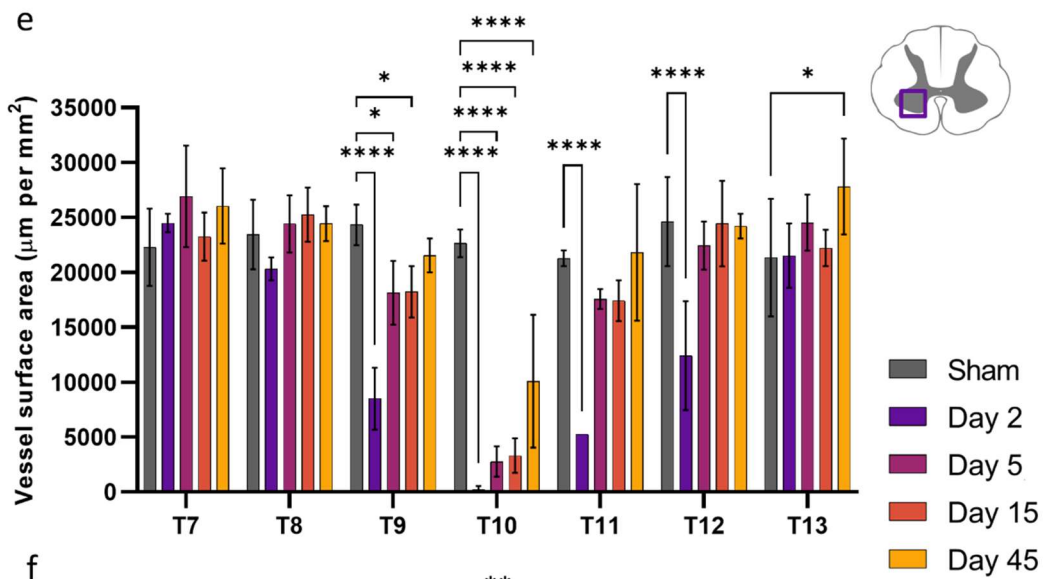
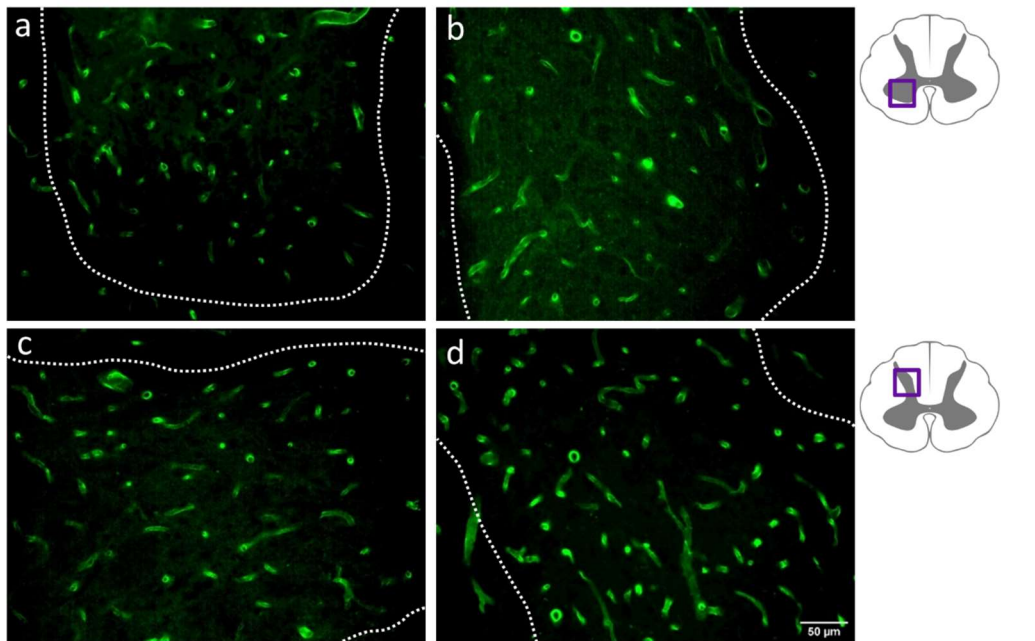


**Figure 4.4: Vessel surface area decreased after injury and was slow to recover.**

Vessel surface area significantly decreased at T9 in the ventral grey matter from day 2 to day 15 (b) when compared to sham (a). Vessel surface area showed an increasing trend at day 45 at T13 (d) in the dorsal grey matter compared to sham (c). Long term spatiotemporal changes in both the ventral (e) and dorsal (f) grey matter were observed. Statistics: two-way ANOVA; \*  $P < 0.05$ , \*\*  $P < 0.01$ , \*\*\*  $P < 0.001$ , \*\*\*\*  $P < 0.0001$ . Error bars  $\pm$  SD. Scale bar: 50  $\mu\text{m}$ .  $n=4$  for all injured groups,  $n=6$  for sham group.

**4.4.2.3 Vessel areal density is more variable following SCI**

Analysing total vessel areal density in comparison to sham controls can show how capillary functionality may have changed, providing an index of instantaneous volumetric capacity of the microcirculation. The area of vessels relative to sample area provides an estimate of areal density. A reduced overall areal density may indicate vessels have collapsed, or be undergoing regression or angiogenesis. An increased vessel areal density may indicate a larger proportion of non-diffusive vessels, arterioles or venules, or oedematous or swollen dysfunctional capillaries. However, an increase in areal density alongside increased number of capillaries may demonstrate successful angiogenesis leading to a larger number of functioning diffusive vessels.

Vessel areal density at T7 in day 5 animals increased significantly in the ventral grey matter ( $56,311.8 \pm 7,332.4 \mu\text{m}^2$  per  $\text{mm}^2$  in sham animals vs  $78,411.0 \pm 12,711.1 \mu\text{m}^2$  per  $\text{mm}^2$  at day 5), however dropped to within sham range by day 15 ( $65,813.2 \pm 7,491.6 \mu\text{m}^2$  per  $\text{mm}^2$ ) (Figure 4.5). As this change did not correlate with a concurrent increase in vessel number, this transient areal density increase may therefore be a demonstration of capillary swelling, or a change in vessel orientation as more tortuosity will increase the proportion of oblique profiles. Likewise, the greater vessel areal density at day 45 at T13 in the ventral grey matter is likely indicative of an increased number of arterioles or

venules as vessel number at this time decreased slightly. Vessel areal density was significantly lower on day 2 in both the ventral and dorsal grey matter at T9, T11, and T12, possibly indicating vessel collapse as areal density increased by day 5. A significant reduction in vessel areal density was observed at the injury epicentre (T10) at all time points except at day 45 in the dorsal grey matter ( $P=0.095$ ), indicating rarefaction at acute timepoints.

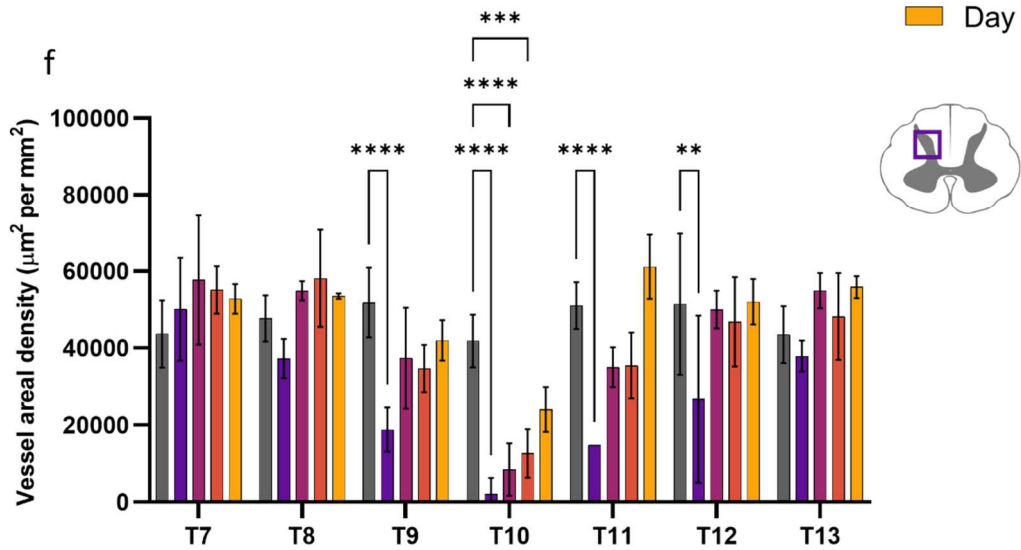
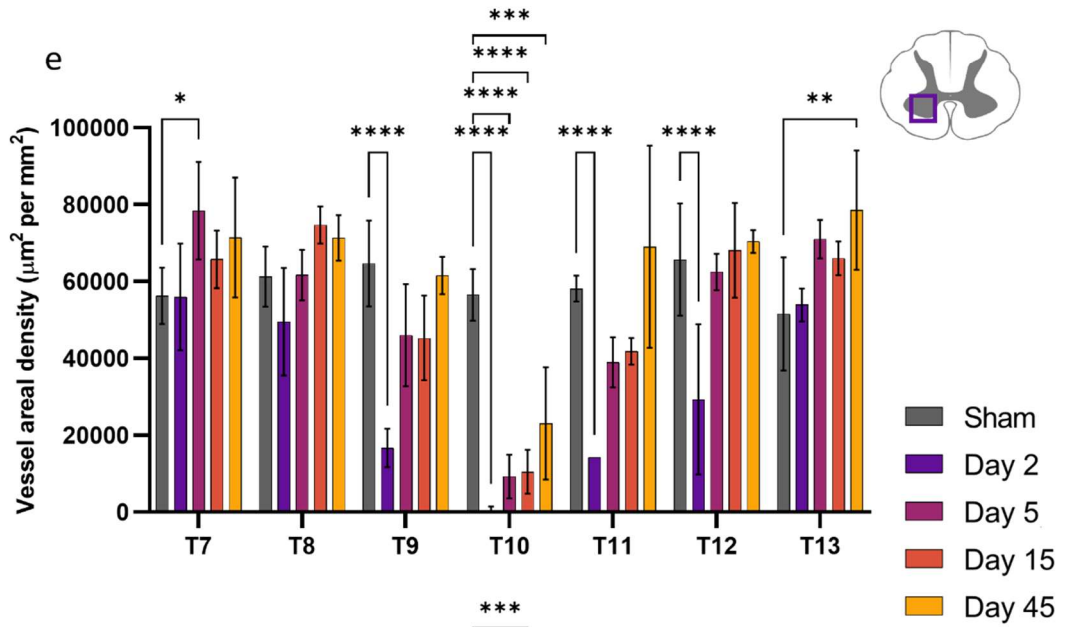
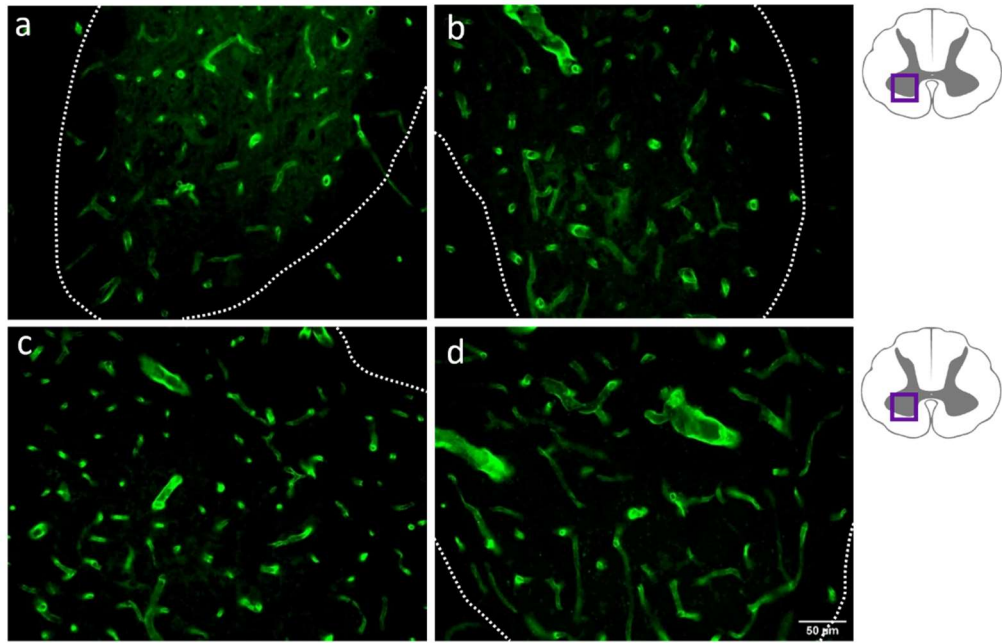


**Figure 4.5: Vessel areal density increased in some segments after SCI.**

In the ventral grey matter at T7 (a), areal density increased at day 5 (b). A similar significant change was seen at day 45 in the ventral grey matter at T13 (d) when compared to sham (c). Vessel areal density decreased at acute timepoints in multiple segments in both the ventral (e) and dorsal (f) grey matter. Statistics: two-way ANOVA; \*  $P < 0.05$ , \*\*  $P < 0.01$ , \*\*\*  $P < 0.001$ , \*\*\*\*  $P < 0.0001$ . Error bars  $\pm$  SD. Scale bar: 50  $\mu\text{m}$ .  $n=4$  for all injured groups,  $n=6$  for sham group.

#### 4.4.2.4 Surface:volume ratio decreases acutely post-SCI at the injury epicentre

Vessel perimeter and area measurements can both be skewed by the tortuosity and orientation of vessels. Calculating the S/V can reduce the effect of this, making the results a more reliable indicator of vessel functionality. Values close to 0.5 indicate vessels are well rounded and cut transversely within the plane of the section, as typically seen in muscle sections. Higher values indicate a larger profile boundary length relative to cross sectional area (equivalent to area relative to volume in stereological terms), meaning vessels are more likely to be capillaries, but also may represent collapsed vessels or vessels cut obliquely. Lower values indicate larger vessels, which may be non-diffusive such as arterioles, or oedematous microvessels after injury. This measurement can be used to assess if vessel recovery is isotropic.

In the ventral grey matter, mean vessel S/V was higher at T9 and T12 at day 2 post SCI ( $P=0.006$  and  $P=0.008$  respectively) (Figure 4.6); as this appeared to recover by day 5, this may be due to vessel collapse immediately following injury. Mean S/V was significantly lower at the injury epicentre (T10) at day 2 in the ventral grey matter ( $0.41 \pm 0.03 \mu\text{m}^{-1}$  in sham animals vs  $0.09 \pm 0.12 \mu\text{m}^{-1}$  in day 2 animals,  $P < 0.0001$ ), and at days 2 and 5 in the dorsal grey matter ( $P < 0.0001$  and  $P=0.005$ ), indicating an increase in vessel areal density relative

to surface area. As vessel number decreased significantly in the epicentre (T10) (Figure 4.3), it may be that only larger vessels survive at the injury site.

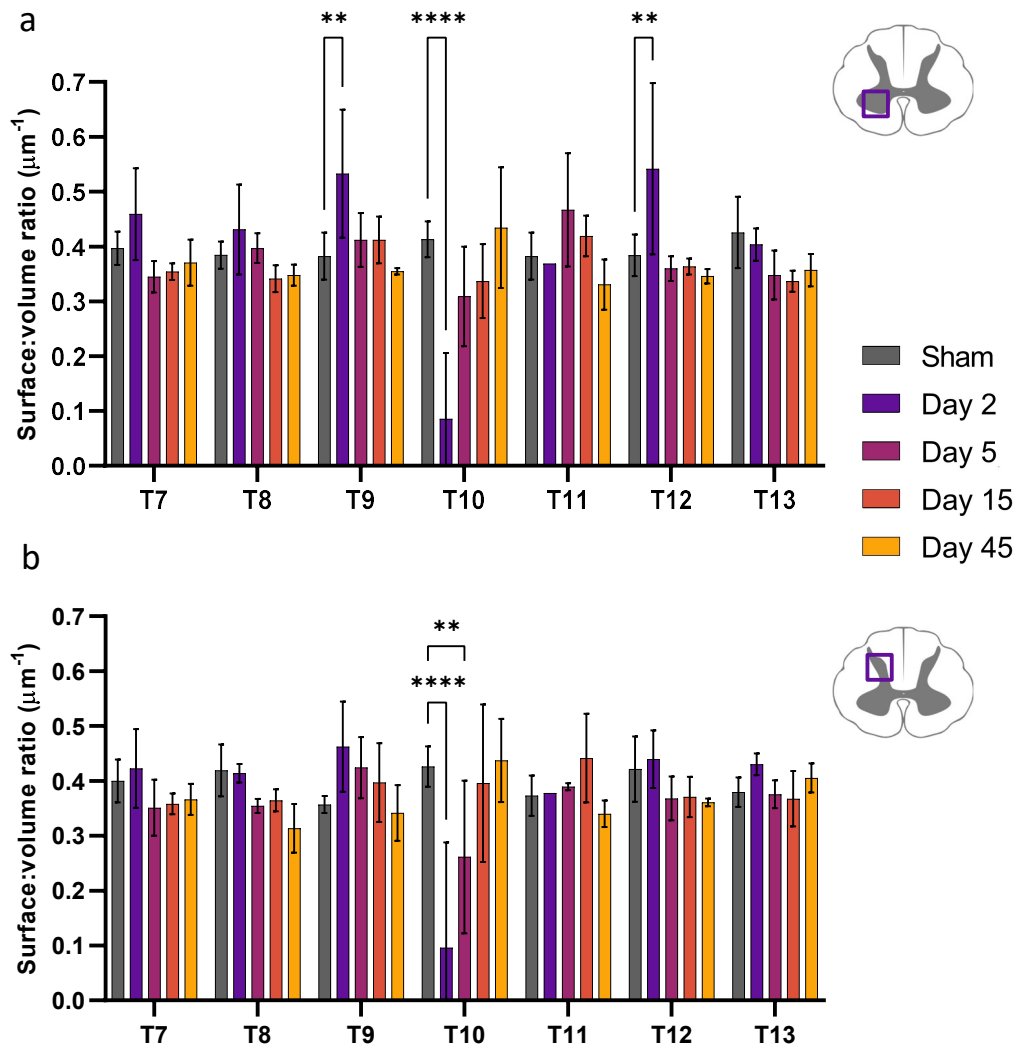


**Figure 4.6: Surface:volume ratio (S/V) increased acutely after injury.**

Mean vessel S/V was higher at day 2 in the ventral grey matter at T9 and T12 (a). S/V also showed an increasing trend at day 2 in the dorsal grey matter at T9 (b), however the most significant changes were at T10 in both regions.

Statistics: two-way ANOVA; \*  $P < 0.05$ , \*\*  $P < 0.01$ , \*\*\*  $P < 0.001$ , \*\*\*\*  $P < 0.0001$ .

Error bars  $\pm$  SD.  $n=4$  for all injured groups,  $n=6$  for sham group.

**4.4.3 Minimum feret diameter remains unchanged following SCI**

The minimum feret diameter is calculated as the minimum distance between two parallel tangential lines to the vessel wall, or the minimum calliper diameter.

This is a useful measurement of diameter when the object is not uniformly

sectioned relative to the longitudinal axis, such as occurs with a tortuous capillary network. As with any tubular structure, oblique sectioning will tend to over-estimate vessel size while the minimum feret diameter provides an objective readout of true diameter. Comparing these values can help to interpret changes in vessel size or surface relative to differences in tortuosity or vessel collapse. As vessels at T11 showed the greatest change and variability in the stereological analysis, minimum feret diameter analysis was focussed on this region. T10 epicentre and day 2 images showed increased background, non-specific staining, and artefacts, so it was not possible to analyse these images accurately with an automated macro.

In both the ventral and dorsal grey matter, no significant difference was detected between the sham animals and at any point following SCI at T11 (Figure 4.7). The peak minimum feret diameter in sham animals shifted from 4-6  $\mu\text{m}$  (bin centre 5  $\mu\text{m}$ ) in the ventral grey matter (Figure 4.7 a) to 6-8  $\mu\text{m}$  (bin centre 7  $\mu\text{m}$ ) in the dorsal grey matter (Figure 4.7 b), as seen in the previous chapter (Figure 3.5). Whilst the peak relative frequency shifted left slightly (to 2-4  $\mu\text{m}$ ) from sham values in both areas analysed at days 5, 15 and 45, the curve shape remained consistent and so no significant difference was detected.

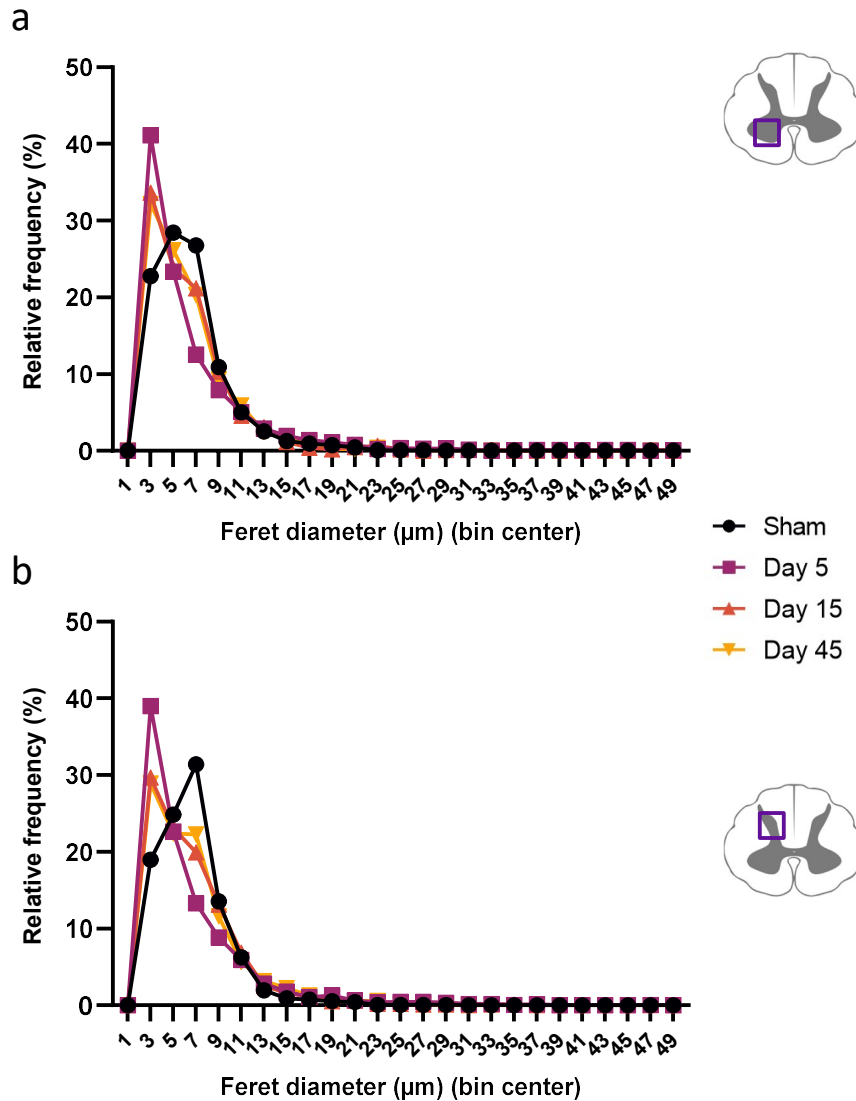


**Figure 4.7: Vessel minimum feret diameter at T11 remained unchanged.** The relative frequency of vessel minimum feret diameter ( $\mu\text{m}$ ) in the ventral (a) and dorsal (b) grey matter at T11. No significant curve shifts were detected between sham values and any timepoint post SCI. Statistics: Kolmogorov-Smirnov test.  $n=4$  for all injured groups,  $n=6$  for sham group.

#### 4.4.4 Injury epicentre is highly variable following SCI

Quantitatively analysing the injury epicentre is challenging due to the extent of tissue damage. Background staining was increased due to tissue necrosis and oedema, as well as extravasated blood products within the neural tissue.

Necrotic cavities also make accurately assessing spinal cord regions difficult, and reduced tissue integrity meant more air bubbles and artefacts were unavoidably introduced during the immunohistochemistry protocol. Reduced

RECA-1 staining, as seen close to the epicentre particularly at day 2 (Figure 4.3.), was also present at most timepoints at the epicentre. Some staining was possible, however there were many inconsistencies between animals that are de-emphasised by averaging when quantifying images (Figure 4.8). Some animals developed large cavities or many smaller cavities, whereas others appeared to have a much larger number of smaller vessels.

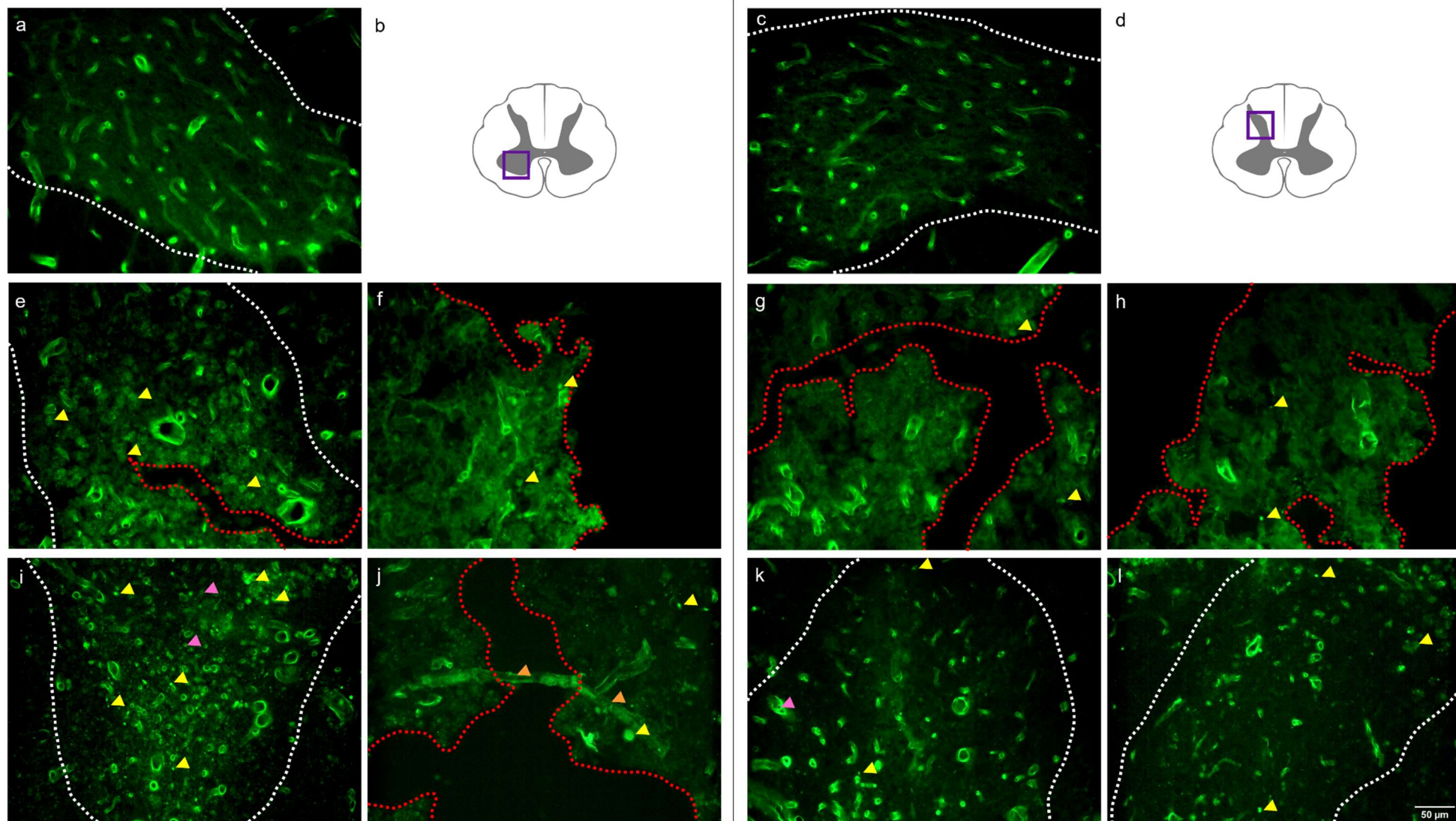


**Figure 4.8: Qualitative analysis of the injury epicentre at T10.**

All ventral grey areas (left panel) (b) were compared to sham T10 (a), and all dorsal grey areas (right panel) (d) were compared to sham T10 (c) of that region. White lines describe the borders of the ventral or dorsal grey areas respectively, whilst red lines delineate tissue cavities. More cavities were observed at earlier timepoints, such as day 5 (e-h) in both the ventral and dorsal regions. Considerable variation occurred between animals, particularly at day 45 (i-l). Artefacts (yellow arrowheads), air bubbles (pink arrowheads), and dura mater (orange arrowheads) often infiltrated tissue sections. Scale bar: 50  $\mu$ m.

**4.4.5 Transmission electron microscopy demonstrates significant ultrastructural changes to microvasculature following SCI**

In order to assess what ultrastructural vessel changes may be causing the reduced immunohistochemical staining, TEM was utilised. We hypothesised that endothelial oedema and dysfunction may be causing an increase in endothelial cell thickness, possibly obscuring receptors. Previous studies in chronic SCI have demonstrated neurovascular unit disruption using TEM (Xu et al., 2017), however there are currently no comparable studies in acute SCI.

Basement membrane width was significantly greater in the injury epicentre (T10) two days after SCI, increasing from  $34.28 \pm 6.65$  nm in sham animals to  $91.08 \pm 24.34$  nm in day 2 animals in the ventral grey matter (Figure 4.9 k), and  $29.71 \pm 7.99$  nm in sham animals to  $71.21 \pm 34.22$  nm at day 2 in the dorsal grey matter (Figure 4.9 l). The same effect was seen at T11 in both the ventral and dorsal grey matter ( $P < 0.0001$ ). Intercellular cleft width was used to infer tight junction diameter and therefore functionality, which increased significantly at T10 in the ventral and dorsal grey matter, and at T11 in the dorsal grey matter by day 2 post SCI ( $P < 0.0001$ ). In the ventral grey matter at T11, intercellular cleft thickness increased from  $15.98 \pm 2.99$  in sham animals to  $19.05 \pm 3.41$  at day 2 post-injury, however this was not significant ( $P = 0.051$ ).

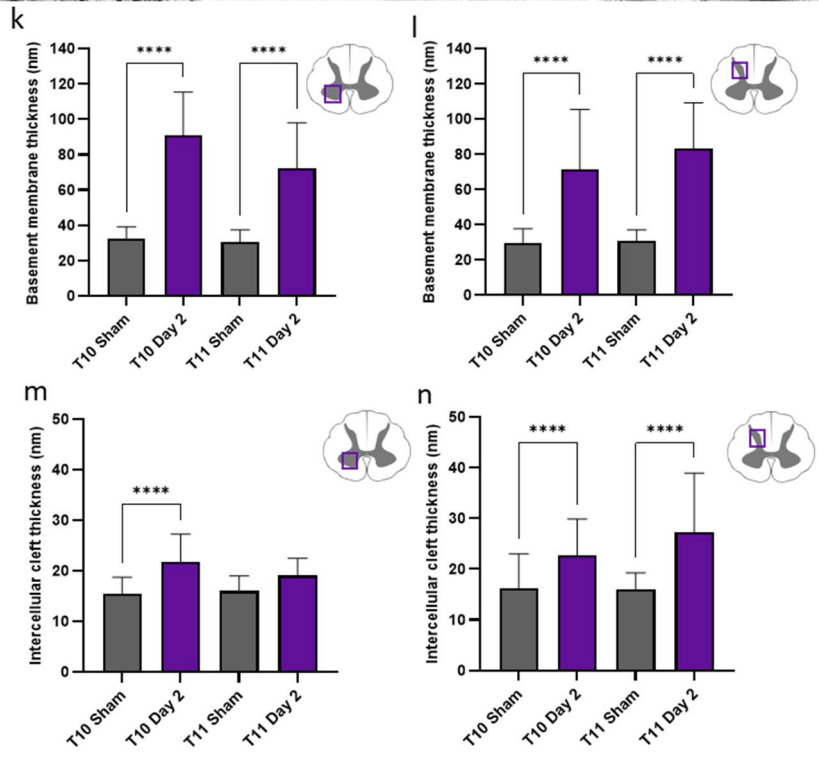
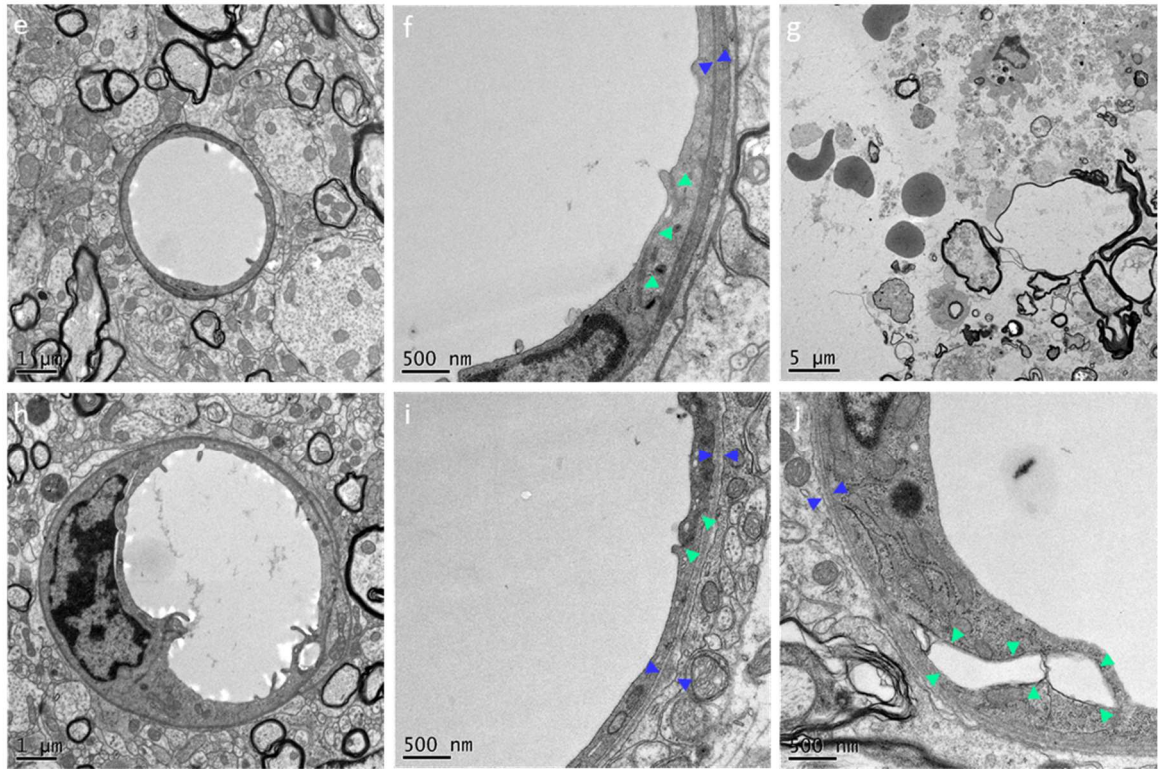
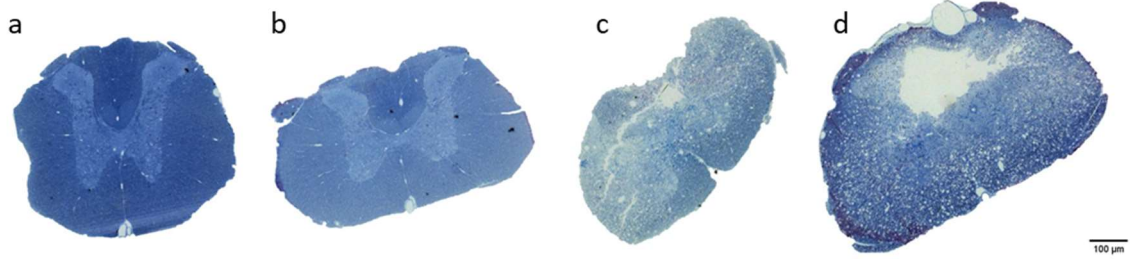


**Figure 4.9: Transmission electron microscopy (TEM) revealed significant capillary damage at day 2.**

Semi-thin sections show the extent of the injury damage at day 2 at T10 (c) and T11 (d) compared to sham cords at T10 (a) and T11 (b). Capillaries were identified (e, h), and close-up images taken of endothelial structures of interest (f, i, j), including the basement membrane (blue arrowheads) and intercellular clefts (green arrowheads). The ventral grey matter of day 2 spinal cords (g-j) demonstrated features of vascular damage including vacuolation (h), nuclear detachment (h), increased basement membrane thickness (i, j) in the ventral (k) and dorsal (l) grey matter, and increased intercellular junction width (i, j) in the ventral (m) and dorsal (n) grey matter when compared to shams (e, f). Significant parenchyma damage in the dorsal region was demonstrated by cavity formation, demyelination, and presence of extravasated red blood cells (g). Statistics: two-way ANOVA; \*\*\*\* P<0.0001. Error bars  $\pm$  SD. n=2 for all groups.

## 4.5 Discussion

This study aimed to generate an accurate timeline of microvascular changes following SCI, including acute effects on capillary fine structure. Using a combination of immunohistochemistry and TEM, we have shown that there are drastic alterations to the capillary bed at acute timepoints that are likely to impact functionality. Increases in basement membrane thickness, with observed reduced diffusivity, and intercellular cleft width both imply increased BSCB permeability, and this, coupled with the reduced number, surface area, and areal density per  $\text{mm}^2$  of vessels may promote hypoxia, extravasation, oedema, and inflammation within the spinal cord.

A vascular approach to SCI has many advantages. The majority of vascular research in the field of SCI is carried out by neuroscience-focused groups, and as such they appear largely unaware of standard vascular physiology approaches. Unbiased stereology is commonly used to assess vascular changes in other conditions as discussed previous (Section 3.5). With such an approach, comparisons can be drawn with other vascular conditions, for example, vessel morphology during sepsis or other inflammatory disorders. This may give new insight into which aspects of capillary changes may be useful to investigate further as a potential therapeutic target. The stereology data (Section 4.4.2) indicates vessel oedema and damage at day 2, which partially recovers by day 5. This oedema or regression appears to spread as much as 8 mm, or two spinal segments, caudally from the injury epicentre at acute timepoints. Generalised vessel disruption, however, can travel as much as 12 mm both rostrally and caudally (Figure 4.4 e and Figure 4.5 e). This could be due to the systemic vascular effects thoracic SCI can have, such as impaired resting haemodynamics (systolic blood pressure, mean arterial pressure, and

heart rate) and autonomic dysreflexia, however these effects are lessened the more caudal the injury is (Squair et al., 2017; West et al., 2012). Widespread vessel disruption could also be due to damage to the posterior spinal arteries and veins caused by the compression injury, leading to constriction and consequent downstream ischaemia. These data alone are insufficient to comment on the origin of waves of angiogenesis following SCI proposed (Loy et al., 2002). Combining this data with minimum feret diameter analysis, qualitative analysis of the injury epicentre, and TEM measurements can give a more accurate picture of any potential waves of angiogenesis and regression.

The white matter remained largely stable in all areas. This could be because there are many fewer capillaries per mm<sup>2</sup> in both ventral and dorsal white matter due to the lower metabolic requirements in the parenchyma. The white matter may possess a greater degree of hypoxia tolerance or suffer from less disruption in perfusion caused by larger vessel compression. However, there was a significant increase in vessel areal density in the ventral white matter at T9 at day 45 and a similar increase at day 45 at T11 in both the ventral and dorsal white matter corresponding with an increase in vessel number and surface area (Appendix 1). This could indicate angiogenesis within the white matter during the chronic phases of recovery. Previous literature has linked white matter sparing with improved locomotor recovery (Slomnicki et al., 2020), however the potential causes of this have not been investigated thoroughly.

These measurements are good indicators of vascular change after SCI, however, a more holistic approach is necessary to understand the potential reasons behind these variations. Alone, a decrease in vessel number could mean regression, collapse, a larger cavity, or fewer capillaries but more non-

diffusive vessels. When combined with vessel areal density and surface area measurements, we can start to build up a more accurate picture. At earlier timepoints, capillary collapse and regression occurs, as indicated by a reduction in all measurements. The increase in vessel areal density at day 5 in the T7 ventral grey matter, without concurrent increases vessel surface area or number suggests either swollen capillaries or more non-diffusive vessels. Likewise, the increasing trend at day 45 in all measurements implies later-stage angiogenesis as there are more vessels with a larger surface area. It is difficult to draw conclusions from a single quantitative analysis method, as vital insight into other aspects of capillary health are necessarily excluded. Images give an overall impression of vascular and neural health and qualitatively showed that there was more severe damage limited to the edges of the grey matter, particularly in the ventral horn. Cavities often formed along the border of the ventral and dorsal grey matter, potentially caused by spreading of the injury longitudinally rather than transversely due to longitudinally arranged white matter tracts (Wolman, 1965).

The injury epicentre at all time points was difficult to reliably stain due to the extent of tissue damage. Epicentre sections were often not structurally intact, with cystic cavities in all areas leading to section lifting. Other sections 4 mm rostral or caudal to the epicentre, especially at earlier time points were equally challenging to stain. High levels of background fluorescence and reduced antibody uptake made analysis impossible in some day 2 sections. This could be due to increased blood products within the parenchyma, necrosis of the cord, altered pH, or oedema (Akino et al., 1997; Erschbamer et al., 2011). Using stereology in this situation was beneficial as an experienced researcher will be

able to exclude any artefacts, and thus obtain more accurate data, relative to, for example, automated image analysis.

As mentioned above, many sections included cavities. These areas were excluded from analysis, however if the area to be excluded was large, the raw data could be artificially skewed when standardised by sample area. Images were often taken to try to exclude cavities where possible, without introducing sample bias, although this was not feasible all of the time. Where it was not possible to avoid cavities, more images were taken of serial sections to limit any possible skewing effect.

Due to the large amount of tissue collected, it was not feasible to carry out all data analysis methods manually. For this reason, minimum feret diameter analysis was automated and key areas prioritised. Automated analysis of minimum feret diameter is possible within FIJI ImageJ, however as discussed previously, software cannot always correctly identify structures of interest where either staining was inconsistent or indistinct from background, or pathological changes generated irregular shapes. This was a particular problem in the SCI sections due to the increased amount of background staining and artefacts in all segments analysed, but especially closest to the injury epicentre; a problem previously highlighted in the literature (Loy et al., 2002). A macro was written which worked well for sham cords, however this had to be altered to reliably work for injured cords. It was not feasible to obtain error-free measurements in the most damaged areas, and therefore it was decided to exclude day 2 cords from analysis, as well as T10 epicentre sections, despite the fact that stereological data indicated significant vascular changes occurred in these sections. After comparing individual images and outputs analysed by both the

automated macro and an assessor, values below 2  $\mu\text{m}$  and above 50  $\mu\text{m}$  were excluded as the majority of these values were due to artefacts or high background staining. Whilst likely not as accurate as manual assessment for individual vessels, due to the vast number analysed (1000-2500 per group), and assuming a two-tailed probability of error, we can assume a good standard of overall reliability.

Vessel surface area and areal density at T11 was decreased compared to sham values at both day 5 and 15 post SCI, albeit not significantly. This correlates with the slight left shift of the minimum feret diameter distribution analysis. It is interesting that the peak minimum feret diameter of vessels at day 45 also decreased when vessel areal density in the ventral and dorsal grey matter at T11 was significantly higher compared to both days 5 and 15 ( $P < 0.01$ ). This may be explained by stereological analyses often demonstrating the highest variability in all measurements at day 45. No significant change in the minimum feret diameter may indicate that there is no major gross remodelling of vessel architecture, with limited angiogenesis or regression. The potential preservation of the existing network structure could offer the possibility of therapeutic intervention to ensure this architecture is functional. The slightly decreased minimum feret diameter peak may suggest vessel regression, angiogenesis, or collapse, so TEM analysis can be used to give further insight into these possibilities.

TEM analysis of sham and day 2 capillaries at the injury epicentre revealed some key signs of vascular damage. Some areas were too damaged to be analysed effectively, particularly on the dorsal aspect of the cord, where indistinct structures indicated widespread apoptosis or necrosis. Grey matter

capillaries were assessed as the stereology data suggested the most significant changes occurred in the more vascularised areas, and hence likely most sensitive to hypoxic challenge. Previous data has shown the basement membrane of capillaries in the CNS to be 30-40 nm thick (Peters et al., 1976); results which were corroborated with the sham spinal cords here. The increased basement membrane thickness may be indicative of capillary oedema, with increasing wall strain inducing a corresponding gain in structural support. However, the thickened basement membrane was observed to have decreased density (increased electron translucency), indicative of degradation prior to capillary regression. Such increases have similarly been observed in models of chronic SCI (Xu et al., 2017) and cerebral ischaemia (Nahirney et al., 2016). This has also been well described in diabetes (Tsilibary, 2003) and peripheral arterial disease (Baum et al., 2016), so may have a metabolic as well as a haemodynamic factor. Capillaries demonstrated endothelial cell oedema, tight junction gapping, and nuclear detachment; signs of potentially non-recoverable damage. These results, combined with the stereology analysis, indicate severe microvascular damage in the acute period following SCI. Angiogenesis may occur in the more chronic period between days 15 and 45, however more research is required to assess the functionality of these microvessels.

#### **4.5.1 Summary**

Overall, this study has shown that significant vascular damage occurs at the acute stages after SCI as far as three spinal segments away from the injury epicentre, with potential angiogenesis at later timepoints. However, whilst some vascular recovery has been observed, vascular dysfunction is prevalent for many weeks following injury. This may be due to ongoing capillary instability leading to decreased BSCB functionality. Further TEM analysis could be

conducted at acute timepoints, with added measurements on vesicular number, and pericyte and astrocytic endfoot coverage of the neurovascular unit. By combining the stereology data and TEM analysis of these images, these insights could be used to design a vascular treatment strategy for SCI.

Promoting angiogenesis and vascular stability may improve the microenvironment around the injury site and thereby enhance the potential for functional recovery after SCI.

***Chapter 5 : Stabilising capillaries and promoting  
angiogenesis following SCI***

## 5.1 Introduction

SCI currently has no cure and very limited treatments. Due to the immense complexity of the spinal cord, it is recognised that effective treatments will need to be multifactorial. Targeting the vasculature is not a new idea (Goldsmith, 1994; Imperato-Kalmar et al., 1997; Noble and Wrathall, 1989; Popovich et al., 1996), as improved perfusion helps any tissue heal via removal of toxins, metabolites, and inflammatory mediators, and delivery of oxygen, other nutrients, and mobilised anabolic precursors. Despite this, it is surprising how little detailed research there is into the vasculature following SCI. Improving perfusion to the damaged spinal cord may not only improve the microenvironment by providing oxygen and removing neurotoxic by-products such as glutamate, but may also directly promote axonal sprouting due to the similarity between some neurogenic and angiogenic growth factor families (Dumont et al., 2001; Hausmann, 2003). It has previously been shown that neovasculature either promotes or is promoted by axonal growth (Mukouyama et al., 2002; Serini and Bussolino, 2004), and so by encouraging angiogenesis, axonal sprouts may be able to follow the new vessels through the injury site and scar tissue (Rolls et al., 2009).

The previous study (Chapter 4), showed that the microcirculation is severely damaged at and around the injury site following SCI. This damage can spread as far as three spinal segments (12 mm) rostrally and caudally, and severe abnormalities are apparent even 45 days after injury. Vessels appear to collapse at acute timepoints, and TEM has shown that many of these collapsed capillaries have significant, potentially non-recoverable, damage, including nuclear detachment, tight junction gaping, and oedema with cytosolic inclusions. If some of these capillaries could be rescued, it may be possible to

reduce the levels of hypoxia at acute timepoints and therefore limit the spread of necrotic tissue, cystic cavities, and scar tissue formation. Angiogenesis may help to replace any capillaries that are too severely damaged and undergoing apoptosis, with the additional benefit of potentially promoting axonal sprouting.

VEGF promotes endothelial cell proliferation, differentiation, and vascular permeability in the early stages of angiogenesis. Following contusive SCI, overall VEGF protein (isoforms 121, 165, and 189) levels have been shown to decrease at the injury site at day 1 (Herrera et al., 2009). VEGF<sub>165</sub> (usually the most potent angiogenic isoform) levels remain significantly reduced up to 28 days post SCI one segment rostral and caudal to the injury site (Herrera et al., 2009). This implies that there may be a reduced potential for innate angiogenesis post injury. Interestingly, VEGF receptor mRNA showed a staggered upregulation following partial unilateral hemisection injury; VEGFR1 was upregulated from days 1-3, VEGFR2 days 1-5, and neuropilin-1 5-21 days post SCI (Sköld et al., 2000). The increased neuropilin-1 mRNA has potential ramifications for both angiogenesis and neurite growth as the receptor can act as a co-receptor to VEGFR2 and binds inhibitory neuronal growth cues such as semaphorins (Sköld et al., 2000). VEGF can also have a neuroprotective role; promoting neural survival as well as angiogenesis (Sun et al., 2003). A similar study using a contusion SCI model confirmed VEGFR1 mRNA upregulation from days 1-3 and VEGFR2 upregulation from days 1-7 post SCI (Choi et al., 2007). As the VEGF receptors are not downregulated following this model of SCI, signal transduction is likely intact, so artificially increasing levels of VEGF in the cord may therefore have a positive effect, potentially leading to increased angiogenesis.

Ang1 protein levels also decrease following contusive SCI from 6 hours to 56 days post injury (Durham-Lee et al., 2012; Herrera et al., 2010). As the protein levels of Ang2 increase concomitantly, the ratio of Ang1:Ang2 is significantly reduced (Durham-Lee et al., 2012). Ang1 acts to promote tight junction integrity, whereas Ang2 acts to destabilise endothelial cell junctions prior to capillary growth or rarefaction (Zakrzewicz et al., 2002). The balance of Ang1 and Ang2 is critical for maintaining vascular quiescence and angiogenesis, so this reduction in Ang1 may imply reduced vascular integrity. Importantly, increased Ang2 levels are required to allow VEGF-induced angiogenesis (Hanahan, 1997), so there may be a fine balance between pathological microvascular instability and tissue repair involving microvascular growth.

VEGF gene therapy following a compression model of SCI has previously been shown to improve BBB (Basso, Beattie, and Bresnahan) locomotor scores in comparison to untreated animals, as well as enhancing tissue preservation at the injury epicentre (Liu et al., 2010). This study also demonstrated increased number of vessels 4 mm from the injury site compared to untreated animals at 10 days and 6 weeks following SCI (Liu et al., 2010), however no further analysis of vessel characteristics was carried out. Ang1 promotes endothelial cell adhesion, vessel maturation and stability, and recruits perivascular cells. Ang1 has been shown to decrease blood brain barrier leakage, thereby reducing lesion volume, following middle cerebral artery occlusion in the brain (Zhang et al., 2002). Microspheres containing VEGF, Ang1, and bFGF can increase vessel number at the injury site 4 and 8 weeks post SCI (Yu et al., 2016). Although it is unknown whether these vessels showed normal morphology or function, BBB scores for this treatment group were significantly higher than the control group from day 14 onwards (Yu et al., 2016). Delivery of

VEGF and Ang1 via a viral vector following traumatic SCI has also shown reduced lesion volume and improved BBB scores at day 56 (Herrera et al., 2010). However, this study did not assess the direct effects this treatment combination had on the microcirculation. As demonstrated, some research has been conducted into the effects of vascular growth factors following SCI, although direct assessment of the microvasculature following these treatments is sparse. Further research is needed to understand the full effects and potential of these growth factors on vascular recovery following SCI.

## 5.2 Aims

The primary aim of this study was to characterise the effects of Ang1 and VEGF delivery on the spinal cord microvasculature during the acute phases of a traumatic contusion SCI. Using methods optimised in the previous two studies, unbiased stereology was utilised to quantify microvascular changes, and microstructural changes were assessed with TEM.

Aim 1: Characterise vascular changes at acute timepoints following SCI and delivery of Ang1/VEGF by:

- a) Using RECA-1 stained vessels and stereology to assess capillary remodelling following Ang1/VEGF delivery.
- b) Using TEM to quantitatively measure basement membrane and intercellular cleft width, and qualitatively observe alterations to the parenchyma following Ang1/VEGF treatment.

Aim 2: Assess functional locomotor recovery following Ang1/VEGF treatment by using the BBB hindlimb locomotor scoring system for rats to assess movement and stepping ability.

## 5.3 Methods

### 5.3.1 Growth factor preparation

Under sterile conditions, recombinant human VEGF<sub>165</sub> protein (293-VE-010/CF; R&D systems, Abingdon, UK) and recombinant human Ang1 protein (130-06; Peprotech, London, UK) were reconstituted to a stock concentration of 100 µg/ml with sterile PBS or sterile distilled water, respectively. These were then diluted in sterile saline to 1 µg/ml Ang1 and 0.83 µg/ml VEGF. Aliquots were stored at 4°C until loaded into the osmotic pumps the day before surgery. Sterile saline was used as the vehicle solution.

Concentrations of Ang1 and VEGF growth factors were chosen based on previous research involving administration of these factors to the spinal cord, and modified for osmotic pump delivery. Yin *et al* 2019 used a single intrathecal injection of Ang1 at a concentration of 800 ng/kg and demonstrated improved BBB scores following an ischaemic spinal cord injury (Yin *et al.*, 2019). Dale-Nagle *et al* 2011 delivered 10 µl of VEGF<sub>165</sub> at a concentration of 100 ng as a single intrathecal injection (Dale-Nagle *et al.*, 2011). Yu *et al* 2016 used microspheres releasing roughly 70 ng/ml of Ang1, 80 ng/ml of VEGF, and 90 ng/ml bFGF at each timepoint tested delivered intraspinally to the injury epicentre (Yu *et al.*, 2016). The concentrations taken from these slow release and single dose studies were modified to a concentration of Ang1 and VEGF hypothesised to be appropriate for the novel intrathecal delivery via an osmotic pump used in this study. As such, a final concentration of 142.9 ng/day and 118.6 ng/day of Ang1 and VEGF, respectively, was utilised.

### 5.3.2 Osmotic pump preparation

Custom-made intrathecal catheters were built using 6 cm of intrathecal tubing (0.108 mm internal diameter; 0041, ReCathCo, Allison Park, USA) connected to 6 cm of silicone tubing (0.702 mm internal diameter; 00702, Detakta, Norderstedt, Germany) using liquid silicone to create a silicone bubble (Figure 5.1). This silicone tubing was attached to the flow moderator (Alzet, 2ML2, Durect Co., Cupertino, USA) again using liquid silicone. Catheters were sterilised with a 90 minute UV cycle. Under sterile conditions, osmotic pumps were loaded with 2 ml of the Ang1/VEGF solution or 2 ml saline. These solutions were relabelled to enable the researchers to be blinded to study conditions. Flow moderators were inserted and the pumps were placed in sterile saline at 37°C overnight before surgery.

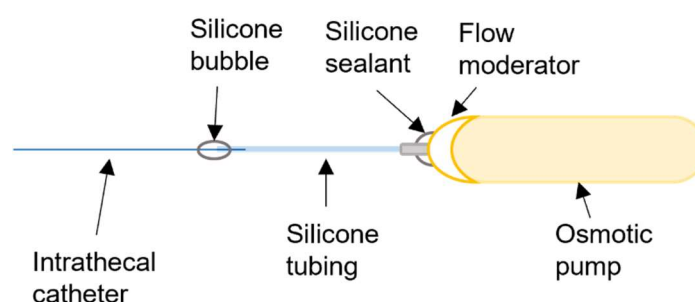


**Figure 5.1: Diagram showing osmotic pump and intrathecal catheter.**

The intrathecal catheter tubing was inserted a short way into the silicone tubing and sealed with a silicone bubble. The silicone tubing was attached to the flow moderator of the osmotic pump using liquid silicone. Osmotic pumps delivered the drug or vehicle at 5  $\mu\text{l/hr}$ .

### 5.3.3 Surgery

#### 5.3.3.1 Osmotic pump implantation

All procedures were carried out according to local and Home Office guidelines, in compliance with A(SP)A 1986. All surgical procedures were carried out as outlined in section 2.5 with some modifications. After a T9 laminectomy, a

separate L2 laminectomy was performed. The 200 kDyn contusion injury was then delivered as described in section 2.5 (n=32), with sham animals receiving no contusion and closure as performed in section 2.5 (n=6). For injured animals, the catheter was passed through a passage in the paravertebral muscles lateral to the L2 laminectomy and the silicone bubble anchored to the muscles with a suture. The intrathecal catheter was carefully inserted through a small hole in the dura at L2. The paravertebral muscles were closed over both laminectomy sites. The osmotic pump was implanted subcutaneously and left in place for the duration of the experiment, delivering 5  $\mu$ l/hr for 14 days. The drug and vehicle pumps were implanted in a random sequence to ensure researchers were blinded (n=12 for each group).

#### **5.3.3.2 Osmotic pump implantation optimisation**

Following the development of post-surgical seromas in roughly 50% of animals in the first cohort, osmotic pump implantation was optimised to improve surgical outcomes. A modified quilting suture was developed to reduce dead space around the osmotic pump (Figure 5.2.). This had an additional benefit of keeping the pump in place under the skin and enabling easier assessment of hip movement during behavioural/locomotor testing. Following this optimisation, no rats developed post-surgical seromas.

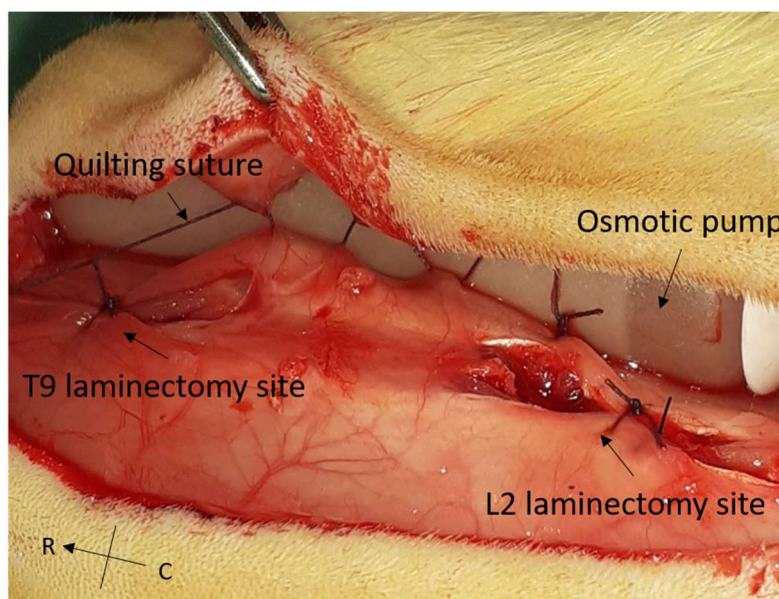


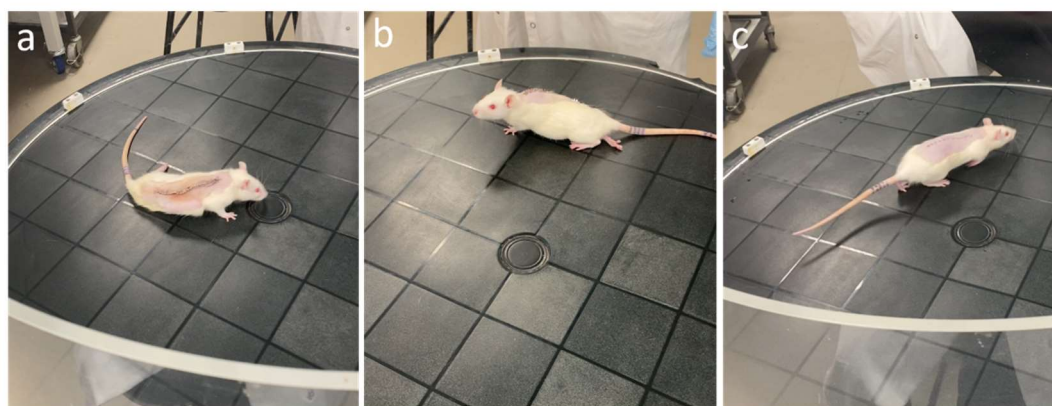
**Figure 5.2: Modified quilting suture used to reduce seroma formation following subcutaneous osmotic pump placement.**

The paravertebral muscles around the T9 laminectomy site were sutured closed, as was the L2 laminectomy site after securing the intrathecal catheter. The osmotic pump was placed subcutaneously and then a modified quilting suture was used to approximate the skin and muscle layers. The image shows the suture before approximating the edges further and securing the suture. Rostral and caudal aspects are indicated.

#### 5.3.4 Locomotor testing

The BBB locomotor rating scale (Basso et al., 1995) was used to assess hindlimb locomotor movement of all animals on days 2, 5, 10, and 15. Briefly, animals were individually placed in an open field arena (custom-built Perspex O-ring: diameter 80 cm, height 30 cm) (Figure 5.3). Movements were observed for four minutes by two independent blinded observers to minimise subjectivity, and scores were then averaged. Animals were scored on aspects such as range of movement in individual hind limb joints, trunk position, and coordination. A full score of 21 indicates movement of an intact animal. Three categories can be determined using the BBB score: early stage of little to no hindlimb movement (score of 0-7), intermediate stage of some uncoordinated stepping (score of 8-13), and late stage of forelimb and hindlimb coordination with stability (score of 14-21). Injured animals at day 5 commonly dragged their

hindlimbs (Figure 5.3 a). Some could sweep their hindlimbs in an attempt at walking by day 5, and a couple could push their weight backwards into a semi-weight bearing position (Figure 5.3 b). Sham animals walked easily, with no trunk instability and their tails elevated (Figure 5.3 c).



d

Rat #: \_\_\_\_\_ Date: \_\_\_\_\_ DPO: \_\_\_\_\_ Rater: \_\_\_\_\_ Score: L \_\_\_\_\_ R \_\_\_\_\_

Limb Movement						Trunk Position				Abdomen	Paw Placement				Stepping				Coordination	Toe Clear		Predominant Paw Position				Trunk Instability	Tail			
Hip		Knee		Ankle		Side		Prop			Drag	Plantar Pl.		Dorsal		Plantar		L		R	Initial Contact		Lift Off							
L	R	L	R	L	R	L	R	L	R			Sweep	W/O Supp.	W Supp.	L	R	L				R	L	R	L	R			L	R	
Ø	Ø	Ø	Ø	Ø	Ø	L	R	L	R	Drag	L	R	L	R	L	R	L	R	Ø	Ø	Ø	Ø	Ø	Ø	I	I	I	I		
S	S	S	S	S	S					Parallel					O	O	O	O	O	O	E	E	E	E						
E	E	E	E	E	E	Mid				High					F	F	F†	F†	F	F	P	P	P	P						
															C	C	C	C	C	C										

Comments: \_\_\_\_\_

**Figure 5.3: The Basso, Beattie and Bresnahan (BBB) locomotor scoring system assessed hindlimb function in rats.**

Injured animals dragged (a) or swept (b) limbs, whereas sham operated animals could walk normally (c). The score sheet for BBB scoring shows what movements and functions are assessed over the four minute test (d).

### 5.3.5 Spinal cord preparation

SCI rats were perfuse fixed at days 5 (n=6 for each treatment group) and 15 (n=6 for each treatment group) with sham animals (n=6) being perfused at day 5 (Figure 5.4) as in the timeline study (Chapter 4). Spinal cords were prepared as in sections 2.4.2 and 2.6. An additional step of an IP injection of heparin was added between the IP injection of pentobarbital and perfuse fixation. Before freezing in OCT, spinal cord segments were identified under a dissection

microscope, and the injury epicentre (T10) and one segment rostral and caudal were dissected and frozen separately.

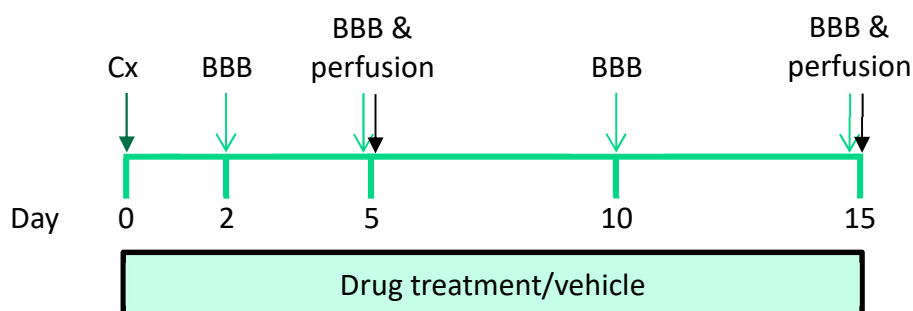


**Figure 5.4: Timeline of treatment study following T10 spinal cord contusion injury.**

Animals were assessed using the Basso, Beattie and Bresnahan (BBB) locomotor rating scale on days 2, 5, 10, and 15 post injury. Perfusions were carried out on days 5 and 15. Cx: contusion injury.

### 5.3.6 Transmission electron microscopy

Spinal cords were taken from sham (n=2), day 5 (n=2 for each treatment group), and day 15 (n=2 for each treatment group) rats, and prepared and imaged as described in section 4.3.3.

### 5.3.7 Cyrosectioning

Samples from three spinal cord segments (T9, T10, T11) were transversely cut at 20  $\mu$ m as described in section 2.6.

### 5.3.8 Immunohistochemistry

Sections were stained as outlined in section 2.7. Optimal concentrations of primary antibodies were as follows: 1:200 Laminin anti-rabbit (L9393; Sigma), 1:200 RECA-1 anti-mouse (ab9774, Abcam). Secondary antibodies used were: Alexa-fluor 488 goat anti-mouse (A11001; Invitrogen) and Alexa-fluor 546 goat anti-rabbit (A11010; Invitrogen) at 1:500.

### **5.3.9 Fluorescence microscopy**

All sections were imaged on a Nikon Eclipse E600 microscope with an exposure of 2 seconds at 20x magnification. Images of the dorsal and ventral grey matter at T9, T10, and T11 were analysed in FIJI ImageJ as in section 2.9.

### **5.3.10 Analysis**

#### **5.3.10.1 Stereology**

Analysis of vessel number, surface area, and areal density continued as in section 2.9.1.

#### **5.3.10.2 Minimum and maximum feret diameter**

The macro used in section 4.3.7.2 was edited due to higher levels of background staining in this cohort (Appendix 3). Briefly, an erosion dilation loop was included and a higher radius for outlier exclusion was used to reduce the amount of background structures included incorrectly in analysis.

#### **5.3.10.3 Transmission electron microscopy measurements**

TEM images at 10,000x were used to measure basement membrane and intercellular cleft width using the measurement tool in FIJI ImageJ.

### **5.3.11 Statistics**

Graphpad Prism 9 was used for all statistical tests and graphs as outlined in section 2.9.3. Two-way ANOVAs were conducted on stereology and TEM data with post hoc Tukey tests. A two-way ANOVA with post-hoc Bonferroni test was conducted on behavioural data. The Kolmogorov-Smirnov test (a non-parametric t-test of the equality of probability distributions) was used for distribution analysis as data were not normal. Contusion force data was analysed using a one-way ANOVA. The significance level was set to 0.05 for all tests.

## 5.4 Results

The following results demonstrate microvascular changes in the spinal cord following a T10 contusion injury and intrathecal delivery of Ang1/VEGF or a vehicle. Methods optimised in the previous chapters (immunohistochemistry with stereology, and TEM) were utilised to assess the effects of these growth factors at days 5 and 15 post SCI. As the majority of vascular changes following SCI were seen in the injury epicentre (T10) and adjacent sections (Chapter 4), all analysis was carried out in T9, T10, T11.

### 5.4.1 Contusion force

All animals received a T10 ~200 kDyn contusion injury as in the previous study. This was delivered before the subcutaneous osmotic pump with intrathecal catheter was implanted to ensure the catheter did not alter the injury force or distribution. Animals were allocated to groups randomly and the experimenter was blind to treatment groups. An average contusion force for this study of  $206 \pm 10$  kDyn was delivered and there was no significant difference between groups ( $P=0.81$ ) (Figure 5.5).

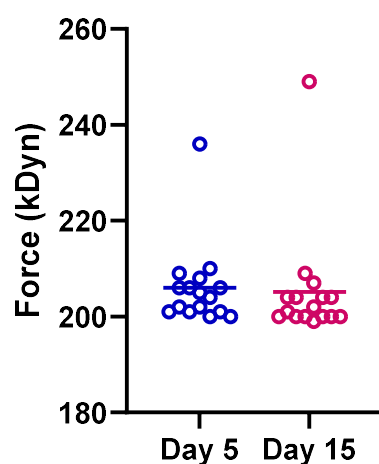


**Figure 5.5: Actual force delivered for each contusion spinal cord injury.** The average contusion force was 206 kDyn, with no significant difference between groups.  $n=16$  for each group.

### 5.4.2 Locomotor scores did not change with treatment

The BBB locomotor scoring system was used to assess the hindlimb function of animals following SCI. Animals were tested on days 2, 5, 10, and 15 post injury. Sham animals received a perfect score of 21, indicating normal walking function of an uninjured animal. There was a significant difference between the BBB scores of treated and untreated animals at day 10 post injury ( $P=0.018$ ), however no difference at day 15 ( $P=0.84$ ) (Figure 5.6). Rats in the treatment group scored lower than the vehicle group at day 10;  $4.78 \pm 3.82$  vs  $8.41 \pm 3.45$  respectively; the difference between slight movement of all three hindlimb joints, and extensive movement of all three joints with sweeping and no weight support.

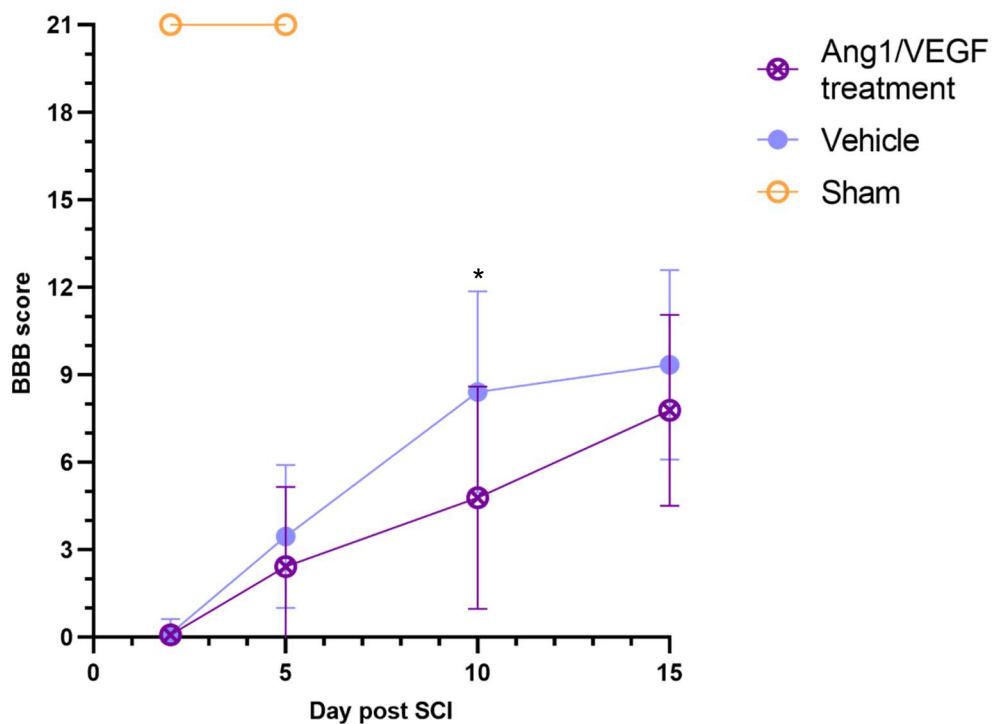


**Figure 5.6: The Basso, Beattie and Bresnahan (BBB) locomotor scoring system assesses hindlimb function in rats.**

Sham animals received a perfect score of 21, whereas injured animals showed only occasional weight support (score of 10) by day 15. At day 10 post injury, vehicle treated animals had a significantly higher score than Ang1/VEGF treated animals ( $P<0.05$ ). Error bars  $\pm$  SD. Statistics: two-way ANOVA; \*  $P<0.05$ .  $n=16$  for each group at days 2 and 5,  $n=8$  for each group at days 10 and 15,  $n=2$  for sham group.

### **5.4.3 Stereological analysis**

The previous study (Chapter 4) demonstrated the most significant changes both in stereological analysis and TEM data in the injury epicentre and one segment either side. Therefore, it was decided to focus on these segments for all analysis following treatment. The majority of significant vascular changes were seen at acute timepoints, however, day 2 may be too early to see any differences in the microvasculature with or without treatment. As the aim was to rescue damaged vasculature and promote new growth, days 5 and 15 were chosen as the most relevant timepoints. Osmotic pumps can deliver treatment for up to 14 days, so these timepoints also meant that the treatment was delivered continuously for almost the whole duration of the study.

#### **5.4.3.1 Vessel number is maintained at day 5 at T11 with Ang1/VEGF treatment**

The number of vessels in the ventral and dorsal grey matter was assessed at T9, T10 (injury epicentre), and T11 at days 5 and 15 following SCI. Vessel density (number per mm<sup>2</sup>) remained unchanged at T9 at both timepoints in treated and untreated animals (Figure 5.7.) Unsurprisingly, vessel numbers were significantly reduced at the injury epicentre in all groups compared to sham values ( $P < 0.0001$ ). At T11 in the ventral grey matter, the number of vessels significantly reduced in the vehicle group at both day 5 ( $P = 0.016$ ) and day 15 ( $P = 0.002$ ). The number of vessels (per mm<sup>2</sup>) in the ventral grey matter at days 5 and 15 in the Ang1/VEGF treatment group was not significantly different to sham animals ( $546.7 \pm 50.1$  vessels per mm<sup>2</sup> in sham animals vs  $452.9 \pm 140.8$  vessels per mm<sup>2</sup> at day 5 and  $410.7 \pm 98.6$  vessels per mm<sup>2</sup> at day 15). A similar pattern was observed in the dorsal grey matter at T11 in the untreated group ( $P = 0.017$  at day 5 and  $P = 0.001$  at day 15), however vessel

number was also reduced in the Ang1/VEGF treatment group at day 15 (P=0.025).

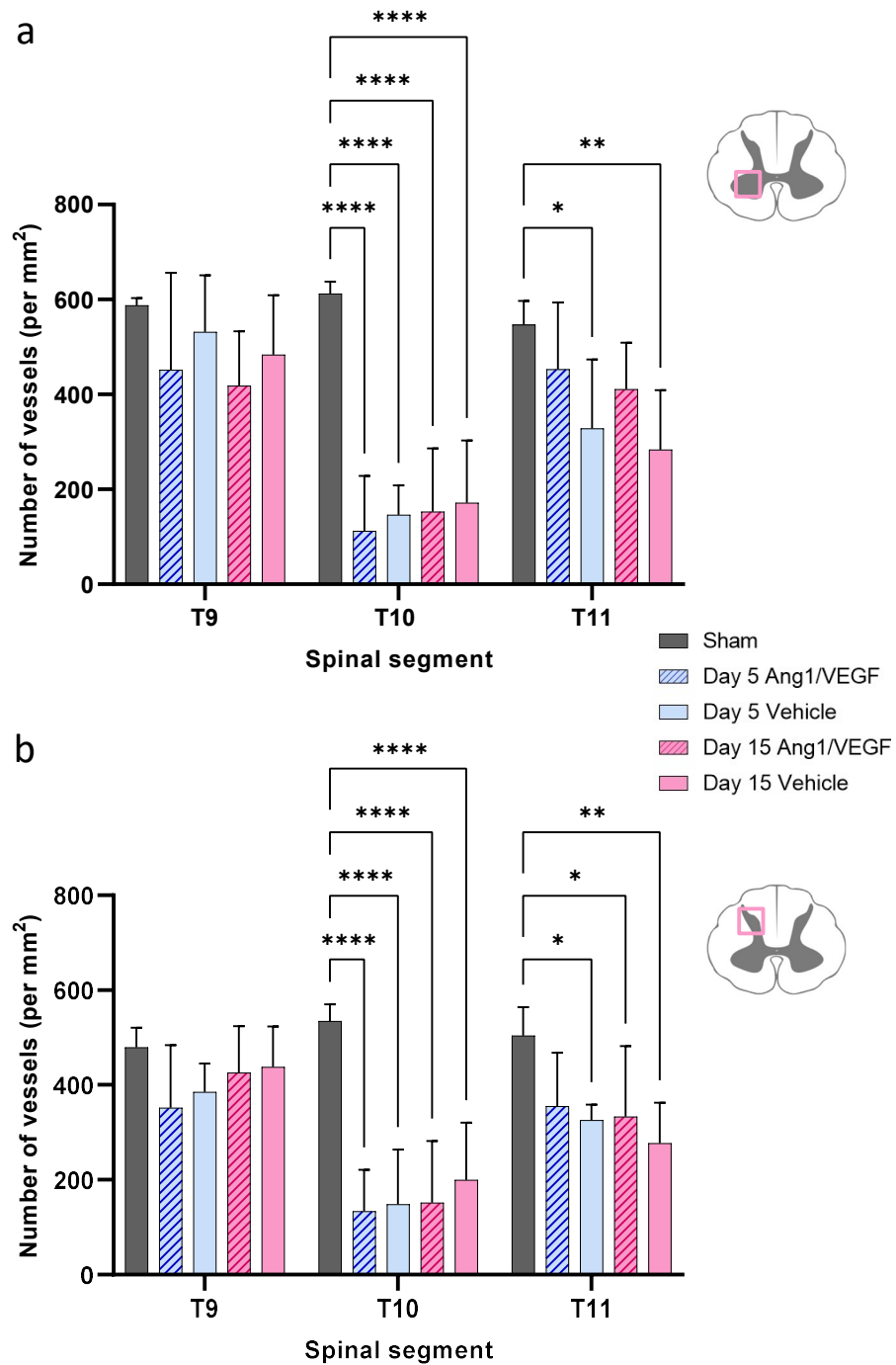


**Figure 5.7: Vessel number decreased at T11 in the untreated group.**

The number of vessels was significantly lower in the vehicle group in the ventral (a) and dorsal (b) grey matter at both timepoints compared to sham operated animals at T11. The injury epicentre at T10 demonstrated significantly reduced number of vessels in all groups. Statistics: two-way ANOVA; \* P<0.05, \*\* P<0.01, \*\*\* P<0.001, \*\*\*\* P<0.0001. Error bars  $\pm$  SD. n=6 for each group.

#### **5.4.3.2 Vessel surface area improves at T11 with Ang1/VEGF treatment**

The surface area of vessels per mm<sup>2</sup> (microvascular surface density) was significantly reduced at the injury epicentre (T10) in both the ventral and dorsal grey matter in all groups ( $P < 0.0001$ ) (Figure 5.8). At T9, the vessel surface area was lower in all groups compared to sham animals in the ventral grey matter (Figure 5.8 a), however in the dorsal grey matter vessel surface area recovered by day 15 in both treated ( $18,232.1 \pm 1,912.4 \mu\text{m per mm}^2$  in sham animals vs  $15,080.3 \pm 3,492.7 \mu\text{m per mm}^2$  at day 15,  $P = 0.57$ ) and untreated groups ( $13,858.2 \pm 2,274.5 \mu\text{m per mm}^2$ ,  $P = 0.24$ ) (Figure 5.7 b). In both the ventral and dorsal grey matter at T11, vessel surface area was not significantly different to sham values in the Ang1/VEGF treated groups at both days 5 and 15. Conversely, vessel surface area was significantly reduced at both timepoints in the vehicle treated group in the ventral and dorsal grey matter at T11.

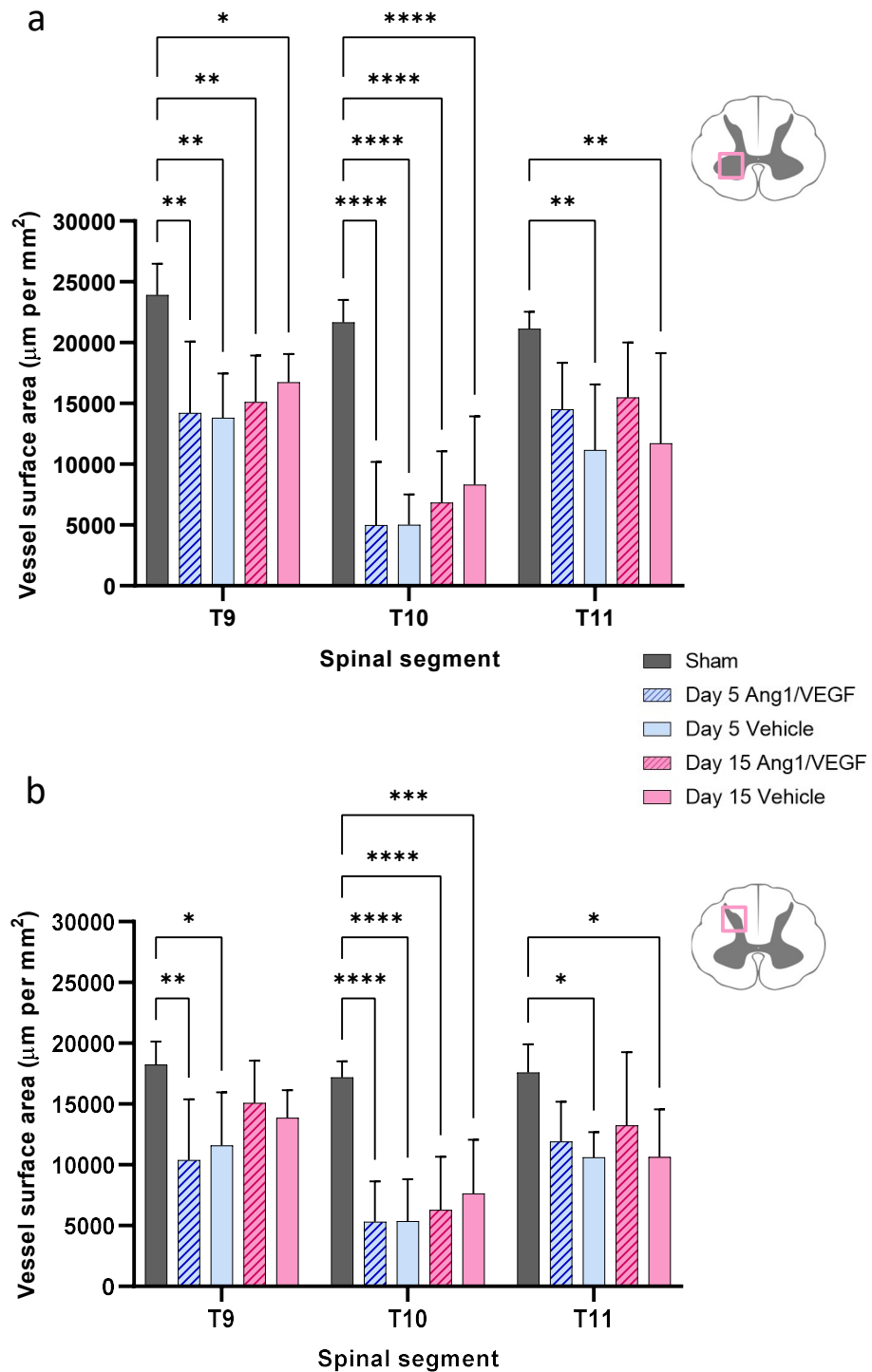


**Figure 5.8: Vessel surface area per  $\text{mm}^2$  was not significantly different to sham values at T11 following Ang1/VEGF treatment.**

Surface area of vessels per  $\text{mm}^2$  was significantly decreased in the ventral grey matter at T9 at all timepoints in both groups (a), but only at day 5 in the dorsal grey matter (b). In both the ventral and dorsal grey matter, vessel surface area was significantly reduced in the vehicle group compared to sham operated animals at T11. Statistics: two-way ANOVA; \*  $P<0.05$ , \*\*  $P<0.01$ , \*\*\*  $P<0.001$ , \*\*\*\*  $P<0.0001$ . Error bars  $\pm$  SD.  $n=6$  for each group.

#### **5.4.3.3 Vessel areal density is reduced at T10 in both Ang1/VEGF and vehicle treated groups**

Vessel areal density significantly decreased in all groups in the ventral grey matter at T9 and T10 (Figure 5.9 a). In the dorsal grey matter at T9, only the Ang1/VEGF treatment group at day 5 post injury had a significantly reduced vessel areal density ( $64,049.9 \pm 14,169.5 \mu\text{m}^2$  per  $\text{mm}^2$  in sham animals vs  $32,121.0 \pm 10,037.4 \mu\text{m}^2$  per  $\text{mm}^2$  at day 5,  $P=0.003$ ); the vehicle group at both timepoints was not significantly different to the sham operated group (Figure 5.9 b). As with the vessel number and surface area measurements, the trend at T11 in the ventral and dorsal grey matter showed a positive effect with Ang1/VEGF treatment. Vessel areal density was significantly lower than sham values in the untreated vehicle group at days 5 and 15 in the ventral grey matter ( $P=0.0002$  and  $P=0.01$  respectively) and at day 5 in the dorsal grey matter ( $P=0.024$ ). Areal density of vessels was also significantly reduced in in the ventral grey matter at T11 in the treatment group at day 5 ( $55,547.8 \pm 5,517.0 \mu\text{m}^2$  per  $\text{mm}^2$  in sham animals vs  $33,932.6 \pm 10,590.9 \mu\text{m}^2$  per  $\text{mm}^2$  at day 5,  $P=0.025$ ), however this recovered by day 15 ( $41,064.6 \pm 17,664.1 \mu\text{m}^2$  per  $\text{mm}^2$ ,  $P=0.25$ ).

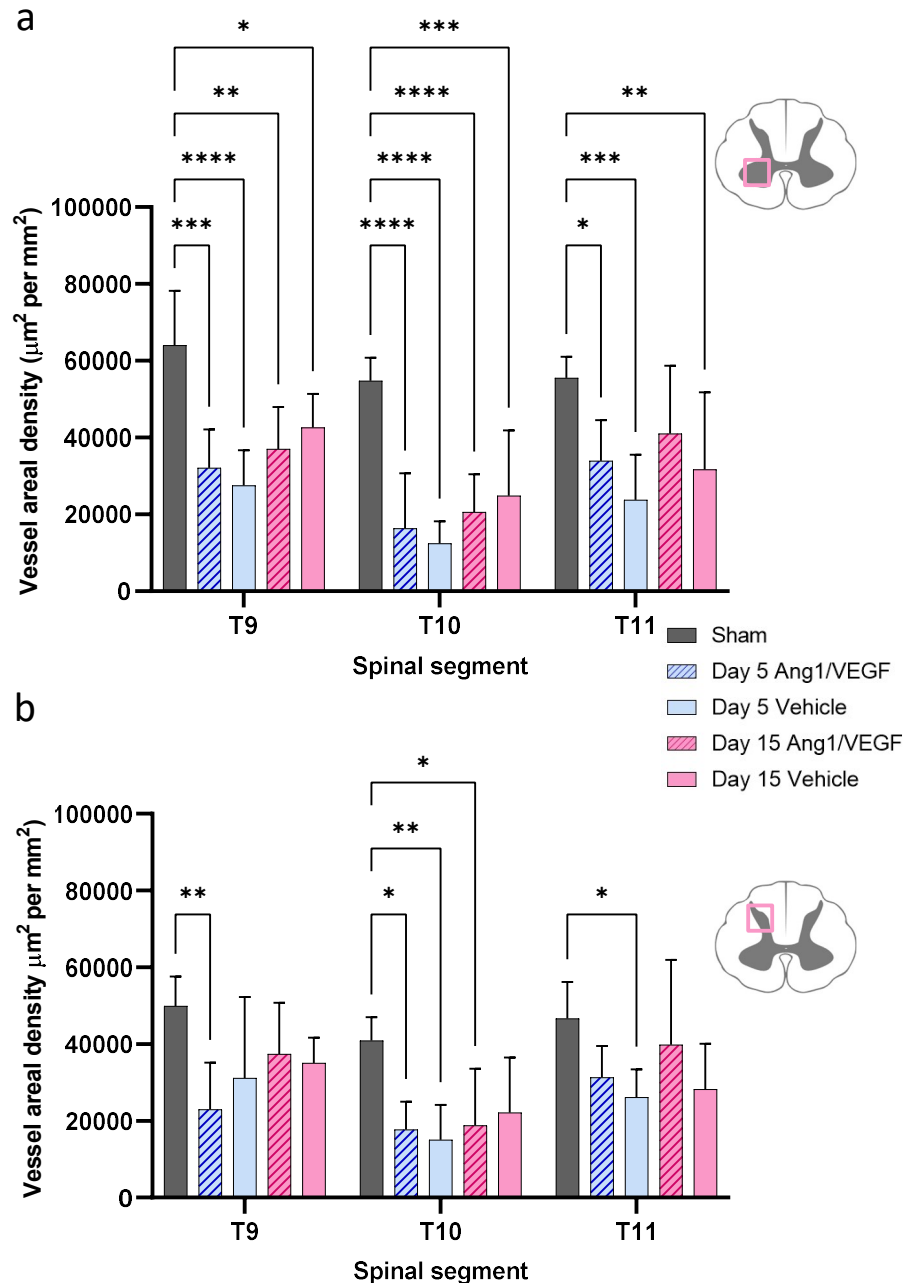


**Figure 5.9: Ang1/VEGF treatment increased vessel areal density at T11 in comparison to untreated animals following spinal cord injury.**

At T11, there was no significant difference between the vessel areal density per  $\text{mm}^2$  in the sham operated animals and treated animals at day 15 in the ventral (a) and dorsal (b) grey matter. In the dorsal grey matter at T9, Ang1/VEGF treatment significantly reduced vessel areal density at day 5, however this returned to within normal sham range by day 15. Statistics: two-way ANOVA; \*  $P < 0.05$ , \*\*  $P < 0.01$ , \*\*\*  $P < 0.001$ , \*\*\*\*  $P < 0.0001$ . Error bars  $\pm$  SD.  $n=6$  for each group.

#### 5.4.3.4 Surface:volume ratio is reduced with treatment at T10

As the changes in total vessel surface area and areal density followed the same pattern (Figures 5.8 and 5.9), vessel S/V showed no significant differences at

T11 in both the ventral and dorsal grey matter (Figure 5.10). S/V significantly decreased at T10 in the treatment group at day 5 in the ventral (P=0.044) and dorsal (P=0.023) grey matter, however returned to sham values by day 15. In the ventral grey matter at day 5, the S/V of the vehicle group was significantly higher (P=0.0074) than the Ang1/VEGF treatment group at the injury epicentre (T10) ( $0.44 \pm 0.09 \mu\text{m}^{-1}$  in the vehicle group vs  $0.27 \pm 0.10 \mu\text{m}^{-1}$  in the treatment group). At T9, the S/V of vessels increased significantly in the vehicle group at day 5 in the ventral grey matter (P=0.013), returning to sham range by day 15.

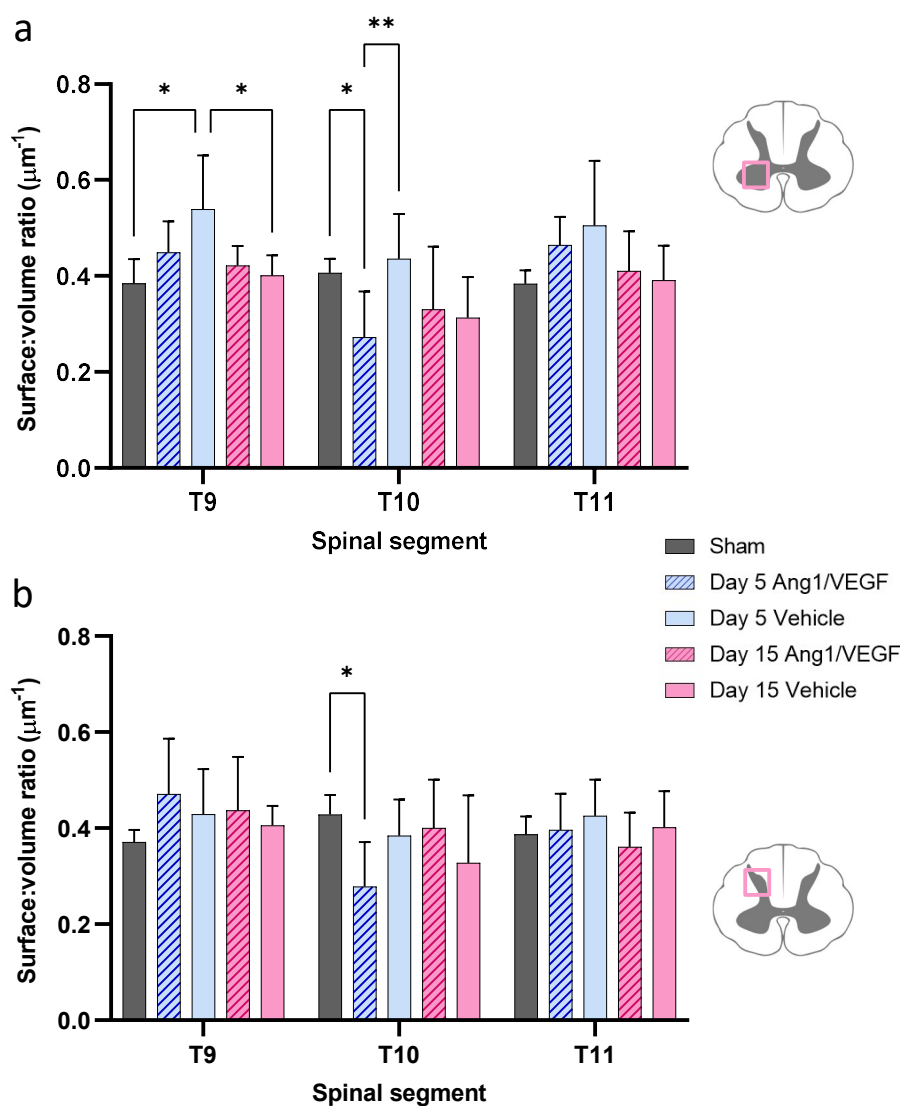


**Figure 5.10: Vessel surface:volume ratio remained stable at T11.**

Mean vessel surface:volume ratio ( $\mu\text{m}^{-1}$ ) (S/V) remained unchanged in both the ventral (a) and dorsal (b) grey matter at T11. S/V decreased at day 5 in both the ventral and dorsal grey matter at T10 in the Ang1/VEGF treatment group. Statistics: two-way ANOVA; \*  $P < 0.05$ , \*\*  $P < 0.01$ , \*\*\*  $P < 0.001$ , \*\*\*\*  $P < 0.0001$ . Error bars  $\pm$  SD.  $n=6$  for each group.

#### **5.4.4 Minimum and maximum feret diameter remains constant at T11**

Maximum feret diameter, or the maximum calliper distance of an object, and minimum feret diameter, or the minimum calliper distance of an object, can give insight into vascular remodelling. An increase in the former can imply greater obliqueness of vessels in the cross-section, which may indicate an increase in tortuosity as can occur following angiogenesis. The latter represents true capillary diameter, and endothelial cell oedema or arteriogenesis may cause an increase in minimum feret diameter. Decreased minimum and maximum feret diameter may indicate regression, early angiogenesis, or vascular collapse. No change in the measurements could be caused by adaptive remodelling including concomitant angiogenesis and arteriogenesis meaning no mean shift in peak feret diameter, or could show maintenance of existing vessel architecture with no overall regression or angiogenesis.

Analysis of the minimum feret diameter of vessels in the ventral and dorsal grey matter at T11 following Ang1/VEGF or vehicle treatment post-SCI revealed no significant difference between any groups ( $P > 0.05$ ). All conditions demonstrated the highest percentage of vessels with a minimum feret diameter of between 4 and 6  $\mu\text{m}$  (Figure 5.11 a, b). The maximum feret diameter of vessels at T11 in the dorsal grey matter showed a significant difference between sham animals and animals at day 5 following Ang1/VEGF treatment ( $P = 0.021$ ), indicating that the median, variability, or shape of the distribution was significantly different to the sham group (Figure 5.11 d). However, all other groups in the dorsal grey

matter and all groups in the ventral grey matter showed no significant difference in the maximum feret diameter (Figure 5.11 c, d) indicating that vessel architecture was maintained either by preserved microvasculature or simultaneous angiogenesis and arteriogenesis.

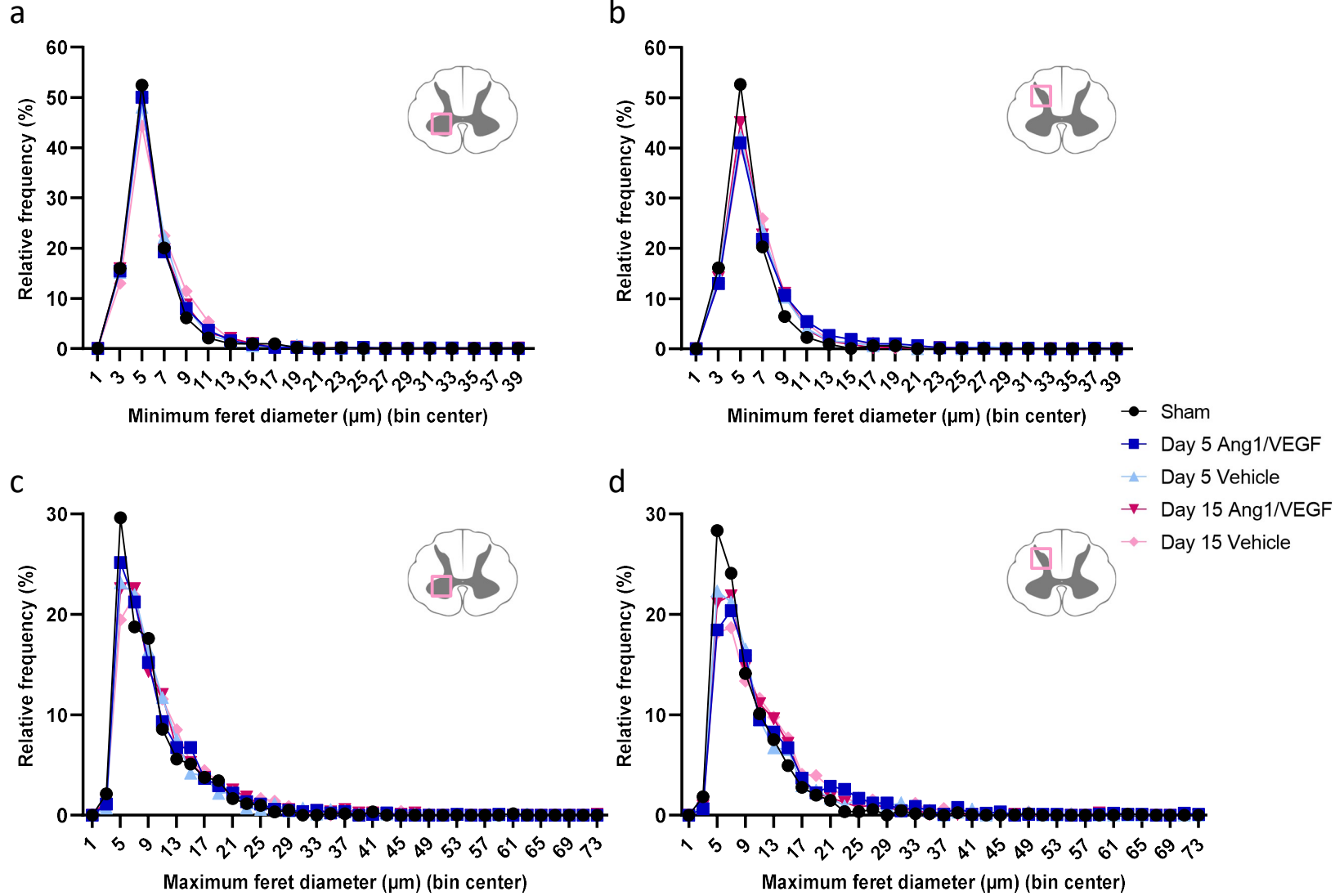


**Figure 5.11: Minimum and maximum feret diameter of vessels at T11 following Ang1/VEGF or vehicle treatment.**

The relative frequency distribution of the minimum feret diameter of vessels in the ventral (a) and dorsal (b) grey matter at T11 showed no difference between groups. The relative frequency distribution of the maximum feret diameter of vessels in the ventral grey matter (c) showed no significant differences, however the day 5 Ang1/VEGF treated group (dark blue) was significantly different to the sham group (black) in the dorsal grey matter (d). Statistics: Kolmogorov-Smirnov test. n=6 for each group.

**5.4.5 Microvascular structure varies across spinal cord regions with Ang1/VEGF treatment**

Qualitative and quantitative analysis was carried out on TEM images. Due to the limited available samples (low n number), representative sampling was used to ensure a large number of vessels from a sizeable distribution within each spinal cord area were analysed. The extent of the damage caused by the injury often meant a smaller number of vessels were present at both the T10 epicentre and T11 caudally. In one case at day 5, no vessels were observed in the dorsal grey matter at T11. Parenchyma damage was extensive, and large cavities were present in all areas imaged (Figure 5.12). Evidence of haemorrhage was commonly observed by large clusters of overlying erythrocytes. Endothelial cell oedema and frequent lack of observable basement membrane in all groups indicated potentially severe vascular dysfunction. Interestingly, structures with a morphology suggestive of loose bundles of collagen were often observed within large perivascular spaces alongside cells with an epithelial morphology (Figure 5.12). These structures were observed in both of the day 15 vehicle group spinal cords and one of the day 5 vehicle group cords, but only one of the day 15 Ang1/VEGF treatment spinal cords. Whilst the sample size is too small to draw firm conclusions, it is interesting that three of the four cords analysed in the vehicle group displayed this aberrant structure, whilst only one of the treatment group cords did.

Basement membrane thickness and intercellular cleft width measurements were used to infer microvascular integrity following Ang1/VEGF or vehicle treatment at days 5 and 15 post-SCI (Figure 5.13). Results varied across the dorsal and ventral grey matter, and between segments analysed. In all areas other than the ventral grey matter at T10 in the day 5 Ang1/VEGF treatment group, basement membrane thickness increased significantly compared to the sham group (Figure 5.13 a-d). Basement membrane thickness increased significantly in the vehicle group between days 5 and 15 in the dorsal grey matter at both T10 ( $P=0.014$ ) and T11 ( $P=0.0007$ ). An increase in basement membrane thickness was also observed in the ventral grey matter at T10 between the Ang1/VEGF treatment group at day 15 compared to day 5 ( $P<0.0001$ ). The day 5 vehicle group had significantly thicker basement membrane than the day 5 treatment group in the ventral grey matter at T10 ( $P=0.0018$ ). The basement membrane following injury was observed to be less well-defined and less electron dense, implying this increase in basement membrane thickness may lead to an increase in diffusivity.

The width of the intercellular cleft in the T10 ventral grey matter showed the opposite pattern to the T10 dorsal grey matter, with the treatment group at both timepoints displaying increased intercellular cleft width compared to the sham and vehicle groups in the ventral grey matter (Figure 5.13 e), and decreased width in the dorsal grey matter compared to the sham and vehicle groups (Figure 5.13 f). In the ventral grey matter at T11 only the Ang1/VEGF treatment group at day 15 ( $16.23 \pm 2.44$  nm) was not significantly different to the sham group ( $15.98 \pm 2.99$  nm). The day 5 treatment group displayed increased intercellular cleft width in the dorsal grey matter at T11 compared to the sham group ( $P=0.0005$ ), however by day 15 this difference was not significant

(P=0.45).

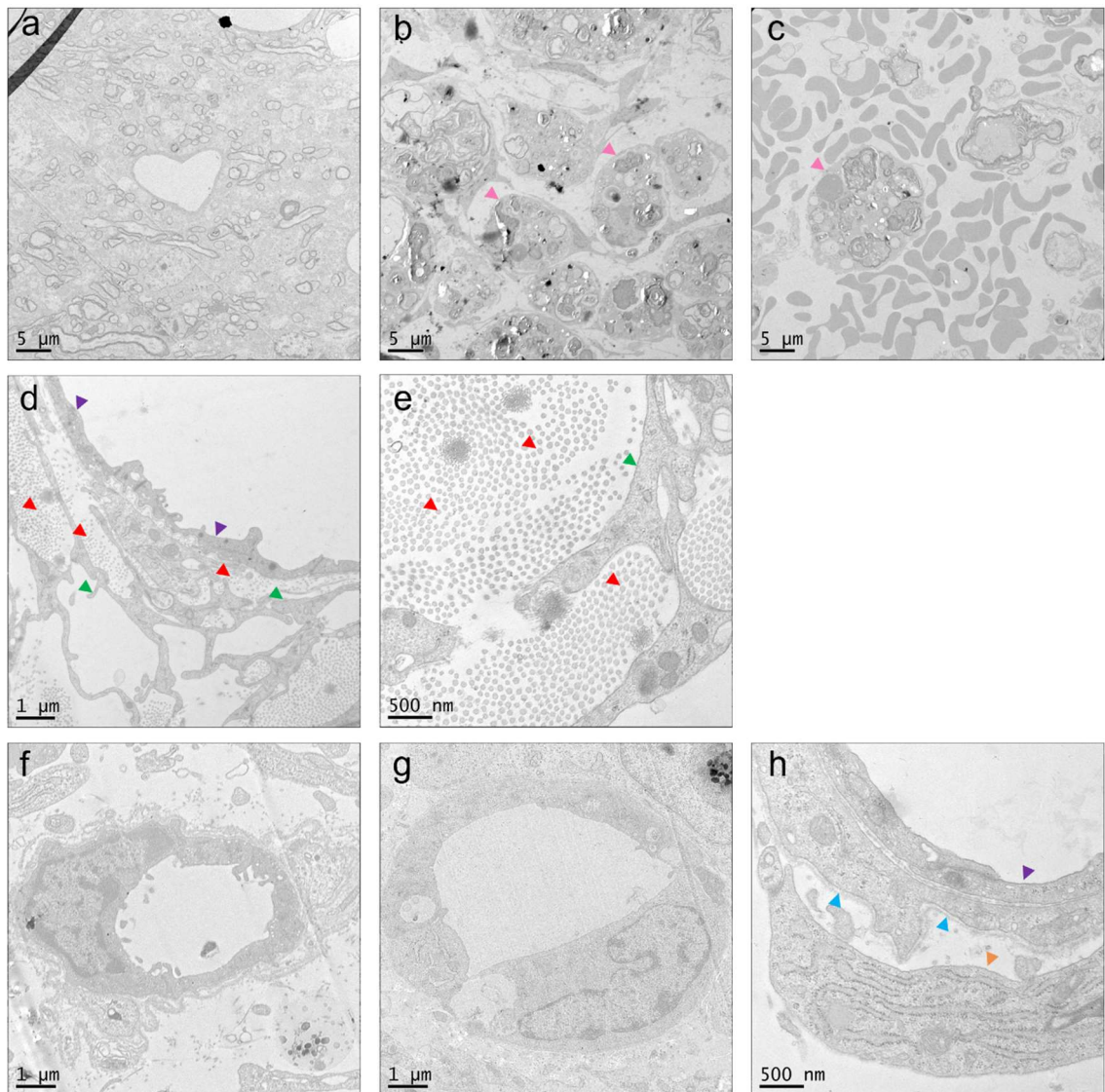


**Figure 5.12: Observational findings following Ang1/VEGF or vehicle treatment at days 5 and 15 post SCI.**

Vessels were more often surrounded by intact parenchyma in the treatment group at day 15 (a). Damage was prevalent in both groups and often included clusters of cell debris (pink arrowheads), as demonstrated in the dorsal grey matter in a vehicle treated animal at day 15 (b). Clusters of erythrocytes were observed as evidence of haemorrhage, particularly at day 5 (c). Loose bundles of collagen (red arrowheads) were frequently observed in the vehicle group interspersed between epithelial-like cells (green arrowheads) (d, e). Some capillaries demonstrated endothelial cell oedema, especially at day 5 (f, g). Pericytes (orange arrowhead) were observed detaching from the neurovascular unit, as seen in the vehicle group at day 15 (h). Endothelial cells (purple arrowheads) were often surrounded by a thickened but patchy basement membrane (blue arrowheads) (h).

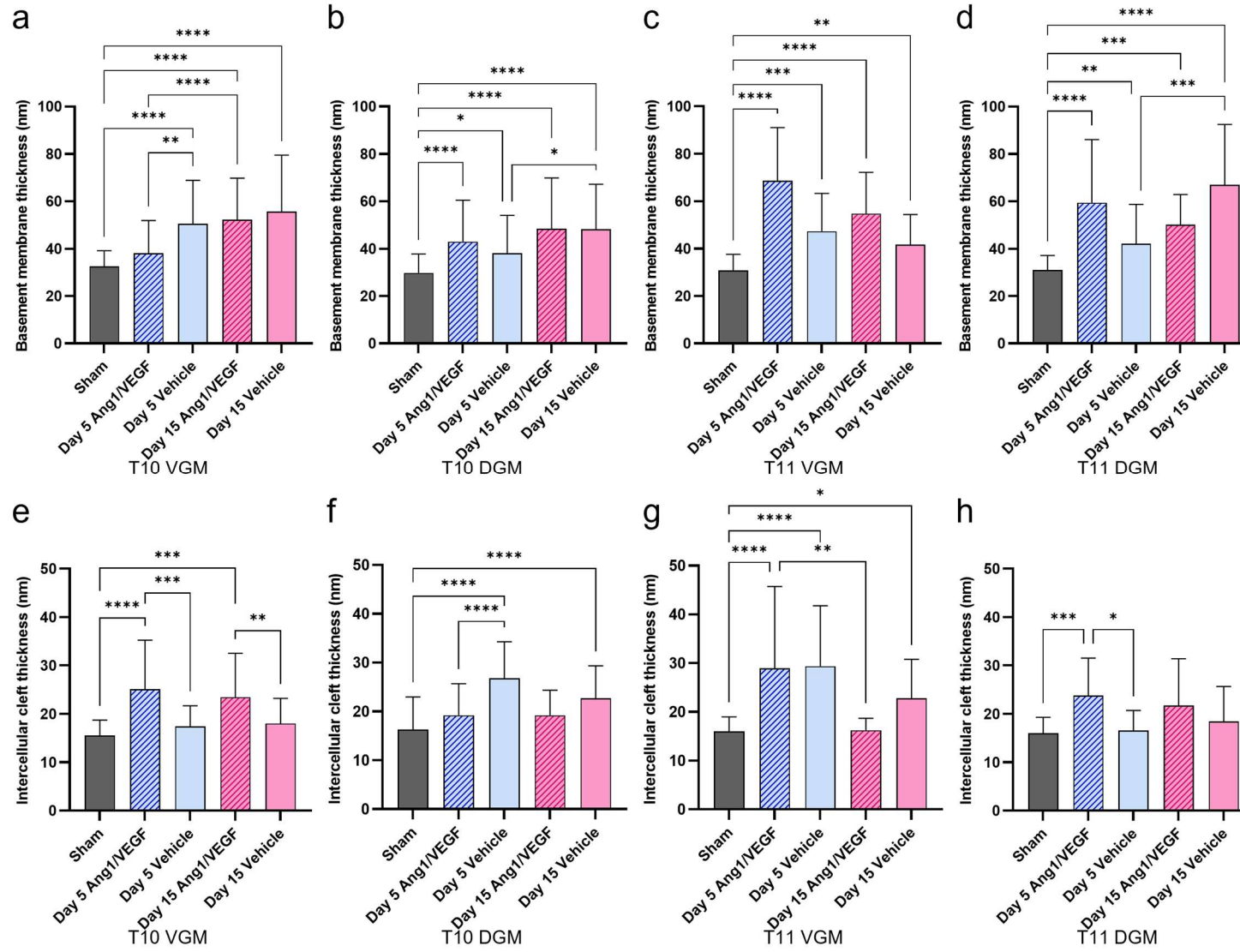


**Figure 5.13: Basement membrane thickness and intercellular cleft width of capillaries at the injury epicentre (T10) and T11.**

The basement membrane thickness (a-d) increased at day 5 and 15 in both the Ang1/VEGF treatment and vehicle groups compared to sham animals. Intercellular cleft width (e-h) increased in the day 5 treatment group in all areas other than the T10 dorsal grey matter (DGM) (f). Intercellular cleft width decreased in the Ang1/VEGF treatment group between days 5 and 15 in the ventral grey matter (VGM) at T11 (g). Statistics: two-way ANOVA; \*  $P < 0.05$ , \*\*  $P < 0.01$ , \*\*\*  $P < 0.001$ , \*\*\*\*  $P < 0.0001$ . Error bars  $\pm$  SD.  $n=2$  for each group.

## 5.5 Discussion

This study aimed to understand microvascular changes in the acute stages following SCI with Ang1/VEGF treatment. A combination of immunohistochemistry and TEM was used to examine the impact Ang1/VEGF treatment had on various microvascular characteristics. Treatment had a largely positive effect at T11, one segment caudal to the injury site, demonstrating no significant difference to sham controls in most stereological measurements at both days 5 and 15 post injury. TEM data demonstrated more variability in both measurements, and consequently, drawing broad conclusions is difficult. Interpreting these results alongside observed morphological outcomes and behavioural tests may give more insight into how the Ang1/VEGF treatment may alter SCI recovery.

In the BBB locomotor test, rats in the treatment group scored lower than the vehicle group at every timepoint, and scored significantly lower than the vehicle group at day 10. At day 15, the average vehicle treated rat was able to occasionally plantar place their paw with some weight support when stationary, whereas Ang1/VEGF rats had some sweeping with no weight support and some plantar placement of paws. The difference between these points is mild and the variance large; in both groups some animals had frequent weight supported plantar steps and occasional coordination, and some had only slight movement of all three hindlimb joints. The large number of animals required to draw conclusions from behavioural data was not feasible in this study. Consequently, there was no correlation between stereological measurements of vessels and BBB score.

More sensitive behavioural tests could be used to understand any small changes in functional outcomes. For example, the von Frey test uses small bristles or hairs to test sensation on the plantar surface of the hindlimb and assess mechanical allodynia (Ahmed et al., 2019; Deuis et al., 2017). The Randall-Selitto test measures response to mechanical pressure by applying an increasing force to the hind paw until the animal withdraws. Both of these tests measure functionality of mechano- and nociceptors following SCI. The hot plate test or Hargreaves test applies an increasing temperature to assess thermoception, using various behavioural outcomes such as stamping, licking, and jumping to judge response time (Deuis et al., 2017). All of these tests have the limitation that the end point is subjective to the observer, and many rodents develop learned behavioural responses leading to artificially small response times. Motor function tests can include the horizontal ladder rung walking test in which the rungs are unevenly and randomly spaced, or the inclined ladder test where a short ladder is placed at 55° (Ahmed et al., 2019). In both of these assessments, rats are scored for the number of times they miss or slip when placing a hindlimb on a rung, and so is a more sensitive measurement of motor function following SCI than the BBB test. These tests take a considerable amount of time to familiarise the animals and obtain data, and therefore, in the interests of time, were not included in this study.

As expected, vessels at the injury epicentre demonstrated severe damage at both timepoints regardless of treatment. All stereological measurements were significantly lower than sham values, except vessel areal density in the T10 dorsal grey matter in the vehicle group at day 15 ( $40,956 \pm 6,106 \mu\text{m}^2$  per  $\text{mm}^2$  in sham animals vs  $22,193 \pm 14,384 \mu\text{m}^2$  per  $\text{mm}^2$  in untreated animals,  $P=0.077$ ). As discussed in Chapter 4, there was significant variation between

animals at the injury epicentre. However, this improvement in areal density in the untreated group may indicate that Ang1/VEGF treatment has a detrimental effect at the injury epicentre. It is likely that the balance of Ang1 to VEGF is critical to stabilising vasculature whilst at the same time promoting angiogenesis. If the concentration of Ang1 was too low compared to VEGF, vessels may become more permeable, leading to increased extravasation and inflammation as well as an increased chance of vessel regression due to lack of a functioning BSCB. If the concentration of VEGF was too low compared to Ang1, vessel tight junctions may be too stable to allow angiogenesis to replace any severely damaged or lost vessels. A more comprehensive, detailed molecular approach to further research this is needed to understand the balance completely.

A similar molecular approach could also be used to confirm localised delivery of Ang1/VEGF in future studies. Correct delivery of growth factors in this study was inferred using several methods. Firstly, the osmotic pump at the end of the 15 day experiment was checked to be empty, and secondly, the intrathecal catheter was left in place during spinal cord preparation following perfusion so that placement at the T10 injury site could be confirmed during tissue sectioning. These assessments, combined with the demonstrable differences between treated and untreated groups, implies that the growth factors were delivered as planned. However, a direct investigation would give more insight into the exact dose delivered and the spread of Ang1/VEGF in the CNS.

Ang1/VEGF treatment appeared to have no effect on most vessel characteristics at days 5 and 15 when directly compared to the vehicle group at T9. Vessel areal density was significantly lower in the treatment group at day 5

in the dorsal grey matter of T9 ( $P=0.0031$ ), whereas the vehicle group showed no significant change compared to shams ( $P=0.077$ ). The most positive effects of Ang1/VEGF treatment occurred at T11, one segment caudal to the injury epicentre. This is encouraging as this segment showed the most significant level of damage both to the vasculature and the parenchyma, second only to the injury epicentre itself. In both the ventral and dorsal grey matter at T11, stereological analysis demonstrated an improvement in vascular characteristics at both timepoints in the Ang1/VEGF group when compared to the vehicle group. Only vessel areal density per sample area improved in the vehicle group in the dorsal grey matter of T11 at day 15 ( $P=0.87$ ). As the S/V for all groups was not significantly different compared to sham values, we can infer that vessel surface area changed in proportion to vessel areal density per sample area. This implies that there was no major change in vessel morphology, such as collapse or dilation. Minimum and maximum feret diameters showed no significant difference at T11, other than the maximum feret diameter in the dorsal grey matter of the day 5 Ang1/VEGF treatment group. This may be explained by the slight decreased peak and right shift, however as these changes are small, this is probably explained by the large biological variation between animals rather than gross remodelling.

The large variability in basement membrane thickness and intercellular cleft width between spinal cord areas, groups, and timepoints post-SCI implies that the vasculature in different areas are damaged to differing extents, and therefore may have different treatment needs. For example, vasculature at the injury site has been subjected to direct contusion force in the primary injury, as well as further compression from swelling and biochemical insult from various aspects of the secondary injury discussed previously (Chapter 1). In contrast,

vasculature at T9 and T11 has primarily only been exposed to the secondary injury. In the treatment group at day 15, the intercellular cleft width was not significantly different to the sham group in both the ventral and dorsal grey matter, and significantly reduced to the treatment group at day 5 in the ventral grey matter. As the basement membrane thickness also increased in these areas at day 5 and 15, this may imply angiogenesis at day 5 and the early stages of vessel maturation at day 15. During angiogenesis, the basement membrane breaks down to allow for endothelial cell sprouting so this may account for the patchy appearance of the basement membrane around many healthy looking vessels. Reduced intercellular cleft width implies greater tight junction stability, and therefore reduced permeability. Taken in combination with the stereology results, particularly at T11, we can infer some level of vascular protection following delivery of Ang1/VEGF, however it is difficult to understand the extent of the actions of the treatment without more extensive research.

Observational findings in TEM demonstrated significant tissue damage at all timepoints. However, of particular interest were the clearly demarcated circular structures of collagen fibres alongside cells with an epithelial morphology, usually indicative of the choroid plexus (Peters et al., 1976). This protective barrier produces cerebral spinal fluid, providing both nourishment and cushioning for the spinal cord. The choroid plexus in the spinal cord is normally located in the central canal and invaginations in the pia mater, however in this study these structures were observed in the ventral and dorsal grey matter, not close to the pia mater or central canal. Whilst these were chance observations, this phenomenon was noted in three out of four of the vehicle group at both day 5 and 15, and often in T10 and T11 sections. Reports suggest that in some cases of syringomyelia in SCI patients, choroid plexus can develop within the

cavity, although this has not been studied extensively following SCI (Shtaya et al., 2018). It is interesting that this choroid plexus-like structure developed quite extensively within 5 days of SCI as this has only been noted in rare cases at chronic timepoints previously (Jaeger and Blight, 1997). Perpendicular layers of collagen bundles with endothelial cells were observed in the perivascular space of guinea pigs 5.5 months after a T13 compression SCI (Jaeger and Blight, 1997), however a correlation between this observation and BSCB was not investigated.

Acute timepoints were chosen for this study based on the need to assess early microvascular changes following SCI with Ang1/VEGF treatment. We hypothesised that by stabilising damaged vasculature and promoting angiogenesis to replace vessels too severely damaged to recover we may be able to attenuate some of the effects of the secondary injury, namely hypoxia, ischaemia, and extravasation. Microvascular changes are likely to be observed at these acute timepoints, however behavioural changes would be expected to be more apparent at later timepoints due to the need to consolidate new neuronal connections. Therefore, a chronic timepoint, such as day 45, should be included in future experiments. This would not only enable a better understanding of functional outcomes following treatment, but also an assessment of the long-term effects of Ang1/VEGF on the microvascular system. As previously shown (Cao et al., 2017; Ng et al., 2011; Whetstone et al., 2003), neovasculature following SCI tends to undergo regression, so it would be interesting to understand if the increased vessel number, surface area, and areal density at T11 was maintained following removal of the Ang1/VEGF treatment.

This study has demonstrated further significant damage to the spinal cord following contusion injury at acute timepoints. However, Ang1/VEGF treatment appears to somewhat mitigate vascular damage, particularly caudally to the injury epicentre at T11. More significant parenchyma damage was observed in the vehicle group, which may be indicative of a more compromised vascular bed, however further research is needed to understand the microvascular changes observed with TEM. Chronic timepoints are required in future studies to comprehend how this treatment may affect microvasculature at the injury site, and how the effects may change once the stimulus is removed. This primary study into the effects of Ang1/VEGF intrathecal delivery following SCI demonstrated clear alterations to the microvasculature at acute timepoints, and so, following further research, may be a promising future treatment strategy for SCI.

***Chapter 6 : General discussion***

## **6.1 Introduction**

SCI is known to cause widespread damage to the spinal cord, but how the injury directly affects the microvasculature is relatively understudied. There are many aspects of the capillary network to consider, especially in the CNS. The number and morphology of capillaries is an important readout of vascular and tissue health, as is BSCB integrity. Research so far has mostly only investigated individual aspects at a set timepoint after injury. Understanding how the capillary network changes over time would help to fill some of the gaps in knowledge so that more specific treatments could be utilised. Targeting the microvasculature may offer new opportunities to treat SCI through improving the microenvironment by, for example, reducing inflammation and hypoxia. It is currently unknown to what extent growth factors can alter the capillary bed post-SCI, and how this may help to promote recovery.

## **6.2 Summary of key findings**

This thesis aimed to characterise the spinal cord microvasculature before, and at various acute and chronic timepoints following, SCI, and the role a vascular-focussed treatment may have on microvascular architecture. The primary subject of this latter aspect illustrates the morphological effects that Ang1/VEGF intrathecal treatment had on microvessel structure in the spinal cord; a novel approach in SCI therapy. Significant microvascular damage, including vessel regression, increased basement membrane thickness, and widened intercellular clefts, were observed at acute timepoints post-SCI indicating the need for a treatment to preserve salvageable vessels and promote angiogenesis to replace degenerated vessels. Acute intrathecal delivery of Ang1/VEGF preserved vascular integrity, particularly caudal to the injury epicentre at early timepoints following injury.

The first study in this thesis aimed to optimise methods and measurements to accurately assess the spinal cord microvasculature, and to use this to assess the potential of vascular (prazosin treatment) or more holistic (exercise training) therapies in intact uninjured animals. A protocol using immunohistochemistry and stereology was established to reliably quantify characteristics of the microvasculature in various areas of the spinal cord. Unfortunately, attempts to perfuse with a vascular marker to assess BSCB integrity were unsuccessful. Nevertheless, protocols to obtain quality tissue for visualisation of the microvasculature, stain capillaries with good specificity, and collect reliable data were developed and optimised. In this initial study using intact cords, voluntary wheel running or prazosin administration did not lead to any significant changes to the microvasculature, despite being previously shown to instigate angiogenesis in peripheral tissues (Bloor, 2005; Egginton et al., 2001; Lloyd et al., 2003). Although there may be different stimuli required for response according to endothelial phenotype, angiogenesis is a fundamental biological process that has been shown to involve conserved transduction mechanisms across both species and tissue. It may be, therefore, that the spinal cord has a lower sensitivity than other tissues, due to the delicate balance of functional requirements, and an increased stimulus over a longer period of time may be needed to initiate angiogenesis in the intact spinal cord. However using an increased dose of a vasodilator as an SCI treatment strategy may cause further harm due to the increased potential for haemorrhage and extravasation through the damaged BSCB following injury.

As there are currently limited data on the microvascular changes at various acute and chronic timepoints following SCI, the second study in this thesis aimed to develop a timeline of such changes and assess microstructural

changes to the neurovascular unit using TEM. Using methods optimised during the first study, microvessel characteristics were analysed in four areas of transverse sections in seven segments of the spinal cord at four timepoints following SCI. As expected, all vascular measurements significantly decreased at all timepoints following SCI at the injury epicentre (T10) compared to sham cords. There was some recovery by day 45, when the S/V was not significantly different to sham values at T10, however it was clear that vessel morphology was still altered at this chronic timepoint. Vessel surface area and areal density increased significantly in the ventral grey matter at T13 at day 45; an indication of larger vessels which may be dilated capillaries, or arterioles or venules. An increased number of arterioles or venules may be an early indication of an expanding vascular bed. However, combined with dilated capillaries, may also be indicative of a downstream blockage or reduction in viable capillaries causing increased pressure upstream. Vessel number, surface area, and areal density significantly decreased at acute timepoints at T9, T10, and T11 in both the ventral and dorsal grey matter indicating significant vascular damage, including collapse and regression. These data indicate a prolonged recovery period is normally required, but also that some viable vessels appear to be maintained during this period.

These findings were corroborated using TEM to assess vascular damage at day 2 post injury. Severe parenchyma damage was evident as expected, and basement membrane thickness and intercellular cleft width increased at T10 and T11 in the ventral and dorsal grey matter. Only the minor increase in intercellular cleft width in the T11 ventral grey matter was not significant, indicating capillaries in this region were perhaps slightly less severely damaged and may be maintaining the BSCB more effectively. Significant cavity formation

and cord deformation was seen in all injured cords at day 2. Cavities were present at all timepoints at T10, however did appear to spread by day 5 (Figure 6.1). Damage was highly variable between animals, although the pattern of damage spreading more severely caudally to the epicentre (Figure 6.1 c) and less severely rostrally to the fasciculus gracilis dorsal to the grey commissure (Figure 6.1 a) initially was common. This pattern of central haemorrhagic necrosis is commonly observed in spinal cord injury models and in human cases, although the cause for this fusiform pattern of damage is uncertain (Hausmann, 2003; Noble and Wrathall, 1989; Simard et al., 2007; Tator and Koyanagi, 1997).

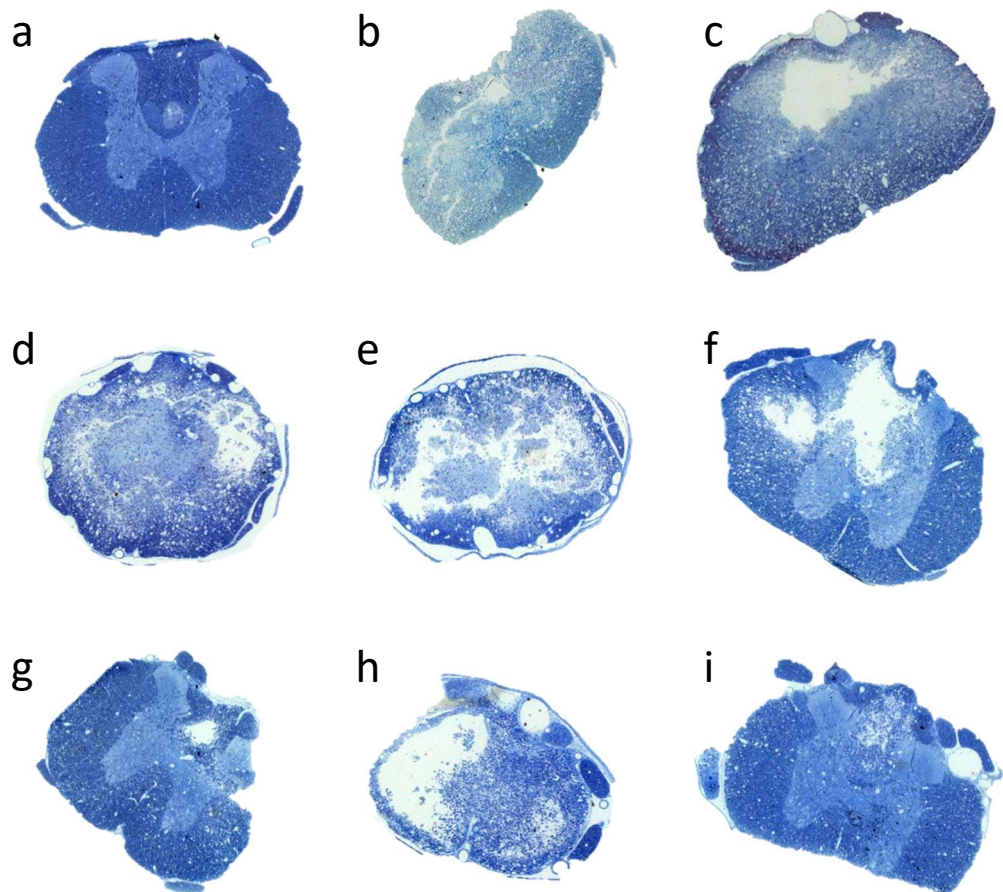


**Figure 6.1: Representative images of semi-thin sections taken for transmission electron microscopy.**

Semi-thin sections taken at T9 (a, d, g), T10 (b, e, h), and T11 (c, f, i). Cord disfigurement was evident at day 2 (a-c) with only a small amount of damage visible in the fasciculus gracilis at T9. Large cavities were observed in all segments of the cord at day 5 (untreated) (d-f), whereas damage seemed more limited to the dorsal aspect of the cord at day 15 (untreated) (g-i) away from the injury epicentre. The intrathecal catheter is visible on the dorso-lateral aspect of the cord at T10 and T11 (h, i) in this example of a vehicle treated animal.

Whilst there was clear damage to the cord at all timepoints, the difference between the appearance of the cord at day 2 and day 5 under TEM was quite striking. From the immunohistochemistry images, largely only stained to visualise the vasculature rather than the whole cord, it appeared as if there was some recovery by day 5. However, using TEM it was clear that this was not always the case. Larger and more disperse cavities were observed, as were large areas of haemorrhage and necrotic cell debris. In some areas at both days 5 and 15, parenchyma seemed relatively intact around capillaries, however in other areas the parenchyma had many gaps between cells. There was no discernible pattern between this gaping and the observable health of the nearby capillaries, although this pattern may be more evident with a higher n number. Endothelial cell oedema (measured as an increase in endothelial cell thickness) was more notable at day 5 than at days 2 or 15, however apparent pericyte detachment was seen at all timepoints. This variable cellular damage may reflect differences in macrovascular trauma and/or heterogeneity of endothelial phenotype, while perivascular disruption may suggest a potential therapeutic target.

We hypothesised that a combinatorial treatment of Ang1 (to stabilise surviving capillaries and neovasculature) and VEGF (to promote angiogenesis) may prevent or mitigate against capillary loss following SCI. As VEGF loosens tight junctions between endothelial cells during angiogenesis, it was hoped that Ang1

would limit this, and therefore reduce any increase in haemorrhage or extravasation. In the cords analysed following treatment, there was no evidence of increased extravasation following treatment. Whilst further study is needed to confirm this, the treatment group generally had a more continuous parenchyma at day 15 compared to the vehicle group, with fewer areas of gapping between cells. This implies that the Ang1/VEGF treatment is not significantly detrimental to the spinal cord in the acute period following injury. Basement membrane thickness significantly increased in all areas analysed in both the Ang1/VEGF treatment group and the vehicle group, apart from the T10 ventral grey matter at day 5 in the treatment group. This may indicate that the Ang1/VEGF treatment does not have a clear effect at these acute timepoints. As the basement membrane is digested during angiogenesis, it is difficult to tell using just this measurement if the lack of difference is due to the treatment promoting angiogenesis or having no impact on vessel regression.

For this reason, the width of the intercellular cleft was also analysed as a measurement of tight junction integrity, but this varied between spinal cord areas in the same animals, so no general conclusions could be drawn.

However, there was no significant difference between intercellular cleft width in the ventral grey matter at T11 in the sham group and the day 15 treatment group; a finding that was corroborated in the stereology data, with no significant differences between these groups in any measurement. The number, surface area, and areal density of vessels at T11 demonstrated the same patterns in the dorsal and ventral grey matter, with a trend for the treatment group to be closer to sham values in all measurements. This may imply the Ang1/VEGF treatment had the most beneficial effect one spinal segment caudal to the injury at these early timepoints. It may be that to see any significant effect at the injury

epicentre, more chronic timepoints are required to accurately assess any angiogenesis.

### **6.3 Further studies**

In order to accurately quantify microvascular characteristics, it was important to initially optimise the stereology approach in intact cords. Taking three different measurements allowed a more holistic approach to vessel remodelling, as looking at vessel number only would not give enough information to build a picture of the complex vascular changes. To further increase the understanding of vascular changes following SCI, it may be beneficial to stain for other components of the BSCB such as SMI-71 (a rat blood brain barrier marker) and glial fibrillary acidic protein (GFAP; an astrocyte marker). These may help to give more conclusive answers about the origins of BSCB disruption when combined with the TEM data.

As the balance between Ang1/VEGF is critical to promoting angiogenesis without contributing to increased BSCB permeability, further studies to optimise both the relative concentrations of these factors and the timeline of delivery would be beneficial. Delivery of Ang1/VEGF for only 14 days may not be enough to preserve and expand existing vascular beds at chronic timepoints; a more prolonged delivery may be necessary for optimal outcomes. The BBB scores may indicate that the Ang1/VEGF treatment temporarily delays functional recovery as these animals received significantly lower scores than vehicle treated animals at day 10, however this difference was resolved by day 15. Additional studies would be needed to understand any links between functional recovery and vascular measurements, and whether sequential, rather

than concomitant, treatment with angiogenic growth factors may optimise microvascular recovery.

To understand whether the results from the stereology analysis could be explained by a shift to larger vessels, increased tortuosity of vessels, or oblique sectioning, the minimum and maximum feret diameter was calculated.

Unfortunately, this analysis did not provide a clear picture of vascular changes. Alternative options to quantify vessel tortuosity would be to use either a more extensive and destructive approach to stereological analysis involving isotropic sampling of small fixed samples, or a more comprehensive coverage of the spinal cord by clearing and using Lightsheet microscopy. With optimised protocols, whole spinal segments can be turned translucent and be imaged with a Lightsheet microscope without the need for sectioning, generating a 3D image. A clearing protocol was attempted with intact cords, however this was not able to be optimised for two main reasons. Firstly, antibody penetration of RECA-1 into the centre of the cord was difficult to achieve due to the relatively large distance from the centre of the cord and contact with the antibody solution. Greater success may have been achieved in smaller mouse spinal cords, or if the vessels were able to be traced as neurons can. Secondly, due to the differing density of the grey and white matter, clearing was not sufficient in the grey matter, and as such the Lightsheet lasers were unable to adequately penetrate the tissue, leading to lower quality images. As was evident from the immunohistochemistry images, spinal cords demonstrated a higher level of background staining close to the injury post-SCI, and so as this protocol could not be optimised in intact cords, it was unlikely to generate useable images following SCI.

## 6.4 Future perspectives and clinical relevance

The studies in this thesis primarily focussed on acute timepoints post-SCI as we would expect the majority of vascular remodelling to occur within the first two weeks based on previous literature (Durham-Lee et al., 2012; Loy et al., 2002; Popovich et al., 1996). However, the chronic timepoint of day 45 indicated that the microvasculature may still not be stable even late into recovery. Future studies into the efficacy of the Ang1/VEGF treatment should therefore include more chronic timepoints to understand if the increased stability observed at acute timepoints is maintained or if, once the stimulus is removed, vessels regress. This phenomenon is seen in other pathologies where vascular treatments have been attempted (Egginton et al., 2016), so it would be vital for future treatments to understand if a similar regression effect is seen post-SCI with Ang1/VEGF treatment.

A study using microspheres loaded with VEGF, Ang1, and bFGF demonstrated an increased number of vessels per mm<sup>2</sup> at the injury epicentre at 4 and 8 weeks (Yu et al., 2016). The microspheres continually released the growth factors for the length of the study so there was no drop-off observed. Untreated animals had roughly 100-150 vessels per mm<sup>2</sup> at both timepoints, comparable to untreated animals at all timepoints in this thesis, whereas treated animals had roughly 350-400 vessels per mm<sup>2</sup> at both 4 and 8 weeks (Yu et al., 2016). This microsphere study only used vessel number as a measurement of potential angiogenesis, however this may indicate that more chronic timepoints would be beneficial to understand if a 2 week intrathecal delivery of Ang1/VEGF could promote angiogenesis and sustain these vessels.

As an initial study into the effects of Ang1/VEGF, this study assessed the number, surface area, areal density, S/V ratio, minimum and maximum feret diameters, basement membrane thickness, and intercellular cleft width of vessels, as well as locomotor function. There are always many more measurements that can be added to give a more complete picture, as discussed above. However, moving forward it would be particularly interesting to combine the Ang1/VEGF treatment with exercise training. Previous studies have combined exercise training with other treatment regimes, including epidural stimulation (Courtine et al., 2009; Harkema et al., 2011; Ichiyama et al., 2008). It is well known that exercise can help to indirectly promote healing and improve vascular health (Gibala and Little, 2020; Warburton et al., 2006). However, following SCI, exercise may have a more direct role to play. Exercise can promote and direct axonal growth (Engesser-Cesar et al., 2007; Loy et al., 2018); of particular importance its role in reducing allodynia following SCI. It may be that exercise helps to reinforce new connections following axonal remodelling, allowing the excess connections to be pruned, thus reducing unnecessary or inappropriate sensory feedback. We also know that angiogenesis and neurogenesis can be initiated and directed by many of the same growth factors, and neo-vessels and neurons often follow the same path (Herrera et al., 2010; Kundi et al., 2013; Yu et al., 2016). It is therefore reasonable to infer that exercise may directly promote angiogenesis and direct new growth.

A combinatorial treatment strategy including a vascular maintenance and/or angiogenic promotor with an exercise regime is likely to have enhanced functional outcomes. The Ang1/VEGF treatment in this study helped to preserve microvascular architecture up to day 15 post-injury, however when in

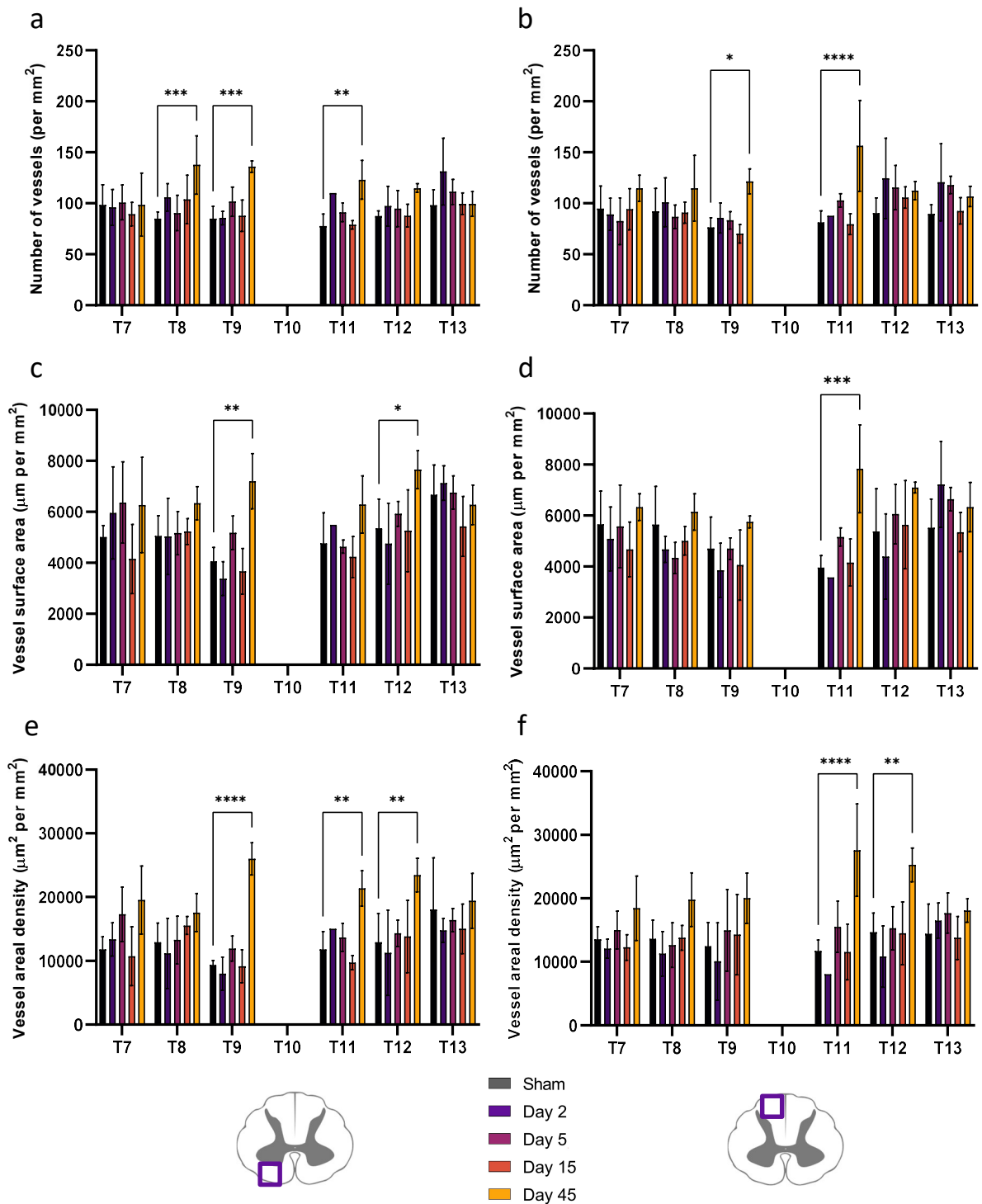
combination with exercise, a longer study would be needed to assess any meaningful effect on gross functional changes. Following a moderate/severe T10 contusion injury, rats can normally start exercise 7 days later, so the Ang1/VEGF treatment may help to maintain vasculature in the early stages of recovery when exercise is not possible. This timescale would allow a week overlap of vascular treatment and exercise, so that when the vascular treatment is stopped at day 14 the exercise regime may be able to continue to maintain the preserved and newly grown vasculature.

## **6.5 Final conclusions**

In conclusion, the studies of this thesis have achieved the aims of developing a reliable and accurate protocol to assess the microvasculature in the spinal cord, and using this to build a detailed timeline of vascular changes following SCI with and without an Ang1/VEGF treatment strategy. These studies have demonstrated that vascular damage is severe and widespread following a moderate contusion injury. Some recovery is possible over time, however the injury epicentre and adjacent segments display significant microvascular damage up to day 45 post-injury. TEM revealed that whilst capillaries at day 2 post-SCI may not be contributing to an effective BSCB, some vessels may be salvageable. A novel treatment strategy to promote stabilisation of these vessels and initiate angiogenesis to replace lost vessels was devised using an osmotic pump and intrathecal catheter to continuously and directly deliver the treatment for two weeks. It was hypothesised that the balance of Ang1 and VEGF would help to limit the damage caused by VEGF, improving tight junction integrity whilst still allowing angiogenesis. This study demonstrated no clear adverse effects of the treatment strategy, and many vascular outcome measures improved following Ang1/VEGF treatment, particularly caudal to the

injury epicentre. Interpreting vascular changes at the acute timepoints studied is complex, so it is hoped that these improvements in vascular morphology would translate at more chronic timepoints to improved capillary bed functionality, and therefore a more favourable environment for neural recovery. Due to the complexity of SCI and the effects of Ang1 and VEGF, further study is required to elucidate the most effective balance of Ang1/VEGF and better understand the significance of these vascular microstructural changes on functional outcomes.

## Appendix 1: Timeline of white matter vascular changes post-SCI (Chapter 4)



### Appendix 1 figure.

Stereological analysis of ventral (a, c, e) and dorsal (b, d, f) white matter capillaries following spinal cord injury (SCI). Vessel number, surface area, and areal density increased at day 45 compared to sham animals in some spinal segments. Statistics: two-way ANOVA; \* P<0.05, \*\* P<0.01, \*\*\* P<0.001, \*\*\*\* P<0.0001. Error bars  $\pm$  SD.

## Appendix 2: Macro written to automate vessel analysis in Chapter 4

```
input="C:/Users/nicol/OneDrive - University of Leeds/Microscope/SCI T11
feret/DG/Sham/";

output="C:/Users/nicol/OneDrive - University of Leeds/Microscope/SCI T11
feret/DG/Sham/";

list = getFileList(input);

for (i = 0; i < list.length; i++){

    action(input, output, list[i]);

}

function action(input, output, file) {

open(input + file);

selectWindow("" + file);

run("Set Scale...", "distance=582 known=100 unit=um");

run("Enhance Contrast...", "saturated=0.02");

run("Subtract Background...", "rolling=60");

run("Remove Outliers...", "radius=6 threshold=50 which=Bright");

run("8-bit");

run("Enhance Contrast...", "saturated=0.03");
```

```

setAutoThreshold("Moments dark");

setOption("BlackBackground", true);

run("Convert to Mask");

run("Remove Outliers...", "radius=6 threshold=50 which=Bright");

run("Fill Holes");

run("Analyze Particles...", "size=5-Infinity display exclude clear");

run("Read and Write Excel", "stack_results");

close(file);

}

```

```

1 input="C:/Users/nicol/OneDrive - University of Leeds/Microscope/SCI T11 feret/DG/Sham/";
2 output="C:/Users/nicol/OneDrive - University of Leeds/Microscope/SCI T11 feret/DG/Sham/";
3 list = getFileList(input);
4 for (i = 0; i < list.length; i++){
5   action(input, output, list[i]);
6 }
7 function action(input, output, file) {
8   open(input + file);
9   selectWindow("" + file);
10  run("Set Scale...", "distance=582 known=100 unit=um");
11  run("Enhance Contrast...", "saturated=0.02");
12  run("Subtract Background...", "rolling=60");
13  run("Remove Outliers...", "radius=6 threshold=50 which=Bright");
14  run("8-bit");
15  run("Enhance Contrast...", "saturated=0.03");
16  setAutoThreshold("Moments dark");
17  setOption("BlackBackground", true);
18  run("Convert to Mask");
19  run("Remove Outliers...", "radius=6 threshold=50 which=Bright");
20  run("Fill Holes");
21  run("Analyze Particles...", "size=5-Infinity display exclude clear");
22  run("Read and Write Excel", "stack_results");
23  close(file);
24 }

```

### Appendix 3: Macro written to automate vessel analysis in Chapter 5

```
input="C:/Users/nicol/OneDrive - University of Leeds/Microscope/Treatment  
T11 feret/VG/Day 5/Drug/";  
  
output="C:/Users/nicol/OneDrive - University of Leeds/Microscope/Treatment  
T11 feret/VG/Day 5/Drug/";  
  
list = getFileList(input);  
  
for (i = 0; i < list.length; i++){  
  
    action(input, output, list[i]);  
  
}  
  
function action(input, output, file) {  
  
    open(input + file);  
  
    selectWindow(" " + file);  
  
    run("Set Scale...", "distance=582 known=100 unit=um");  
  
    run("Subtract Background...", "rolling=60");  
  
    run("Enhance Contrast...", "saturated=0.02");  
  
    run("Subtract Background...", "rolling=60");  
  
    run("Remove Outliers...", "radius=6 threshold=50 which=Bright");  
  
    run("8-bit");
```

```
run("Enhance Contrast...", "saturated=0.03");

setAutoThreshold("Moments dark");

setOption("BlackBackground", true);

run("Convert to Mask");

run("Remove Outliers...", "radius=20 threshold=50 which=Bright");

run("Fill Holes");

setOption("BlackBackground", true);

run("Erode");

run("Erode");

run("Dilate");

run("Erode");

run("Dilate");

run("Erode");

run("Dilate");

run("Remove Outliers...", "radius=20 threshold=50 which=Bright");

run("Analyze Particles...", "size=10-Infinity display exclude clear");

run("Read and Write Excel", "stack_results");

close(file);
```

}

```

1 input="C:/Users/nicol/OneDrive - University of Leeds/Microscope/Treatment T11 feret/VG/Day 5/Drug/";
2 output="C:/Users/nicol/OneDrive - University of Leeds/Microscope/Treatment T11 feret/VG/Day 5/Drug/";
3 list = getFileList(input);
4 for (i = 0; i < list.length; i++){
5   action(input, output, list[i]);
6 }
7 function action(input, output, file) {}
8 open(input + file);
9 selectWindow("" + file);
10 run("Set Scale...", "distance=582 known=100 unit=um");
11 run("Subtract Background...", "rolling=60");
12 run("Enhance Contrast...", "saturated=0.02");
13 run("Subtract Background...", "rolling=60");
14 run("Remove Outliers...", "radius=6 threshold=50 which=Bright");
15 run("8-bit");
16 run("Enhance Contrast...", "saturated=0.03");
17 setAutoThreshold("Moments dark");
18 setOption("BlackBackground", true);
19 run("Convert to Mask");
20 run("Remove Outliers...", "radius=20 threshold=50 which=Bright");
21 run("Fill Holes");
22 setOption("BlackBackground", true);
23 run("Erode");
24 run("Erode");
25 run("Dilate");
26 run("Erode");
27 run("Dilate");
28 run("Erode");
29 run("Dilate");
30 run("Remove Outliers...", "radius=20 threshold=50 which=Bright");
31 run("Analyze Particles...", "size=10-Infinity display exclude clear");
32 run("Read and Write Excel", "stack_results");
33 close(file);
34 }

```

## Bibliography

Adair, T.H. and Montani, J.-P. 2011. *Angiogenesis*. San Rafael, Calif: Morgan & Claypool Life Sciences.

Ahmed, R.U., Alam, M. and Zheng, Y.P. 2019. Experimental spinal cord injury and behavioral tests in laboratory rats. *Heliyon*. **5**(3), pp.01324.

Ahuja, C.S., Wilson, J.R., Nori, S., Kotter, M.R.N., Druschel, C., Curt, A. and Fehlings, M.G. 2017. Traumatic spinal cord injury. *Nat Rev Dis Primers*. **3**, pp.17018.

Akino, M., O'Donnell, J.M., Robitaille, P.M. and Stokes, B.T. 1997. Phosphorus-31 magnetic resonance spectroscopy studies of pig spinal cord injury. Myelin changes, intracellular pH, and bioenergetics. *Invest Radiol*. **32**(7), pp.382-388.

Anderson, M.A., Burda, J.E., Ren, Y., Ao, Y., O'Shea, T.M., Kawaguchi, R., Coppola, G., Khakh, B.S., Deming, T.J. and Sofroniew, M.V. 2016. Astrocyte scar formation aids central nervous system axon regeneration. *Nature*. **532**(7598), pp.195-200.

Angeli, C.A., Edgerton, V.R., Gerasimenko, Y.P. and Harkema, S.J. 2014. Altering spinal cord excitability enables voluntary movements after chronic complete paralysis in humans. *Brain*. **137**(Pt 5), pp.1394-1409.

Balentine, J.D. 1978. Pathology of experimental spinal cord trauma. I. The necrotic lesion as a function of vascular injury. *Lab Invest*. **39**(3), pp.236-253.

Bartanusz, V., Jezova, D., Alajajian, B. and Digicaylioglu, M. 2011. The blood-spinal cord barrier: morphology and clinical implications. *Ann Neurol*. **70**(2), pp.194-206.

Basso, D.M., Beattie, M.S. and Bresnahan, J.C. 1995. A sensitive and reliable locomotor rating scale for open field testing in rats. *J Neurotrauma*. **12**(1), pp.1-21.

Baum, O., Da Silva-Azevedo, L., Willerding, G., Wöckel, A., Planitzer, G., Gossrau, R., Pries, A.R. and Zakrzewicz, A. 2004. Endothelial NOS is main mediator for shear stress-dependent angiogenesis in skeletal muscle after

prazosin administration. *Am J Physiol Heart Circ Physiol.* **287**(5), pp.H2300-2308.

Baum, O., Torchetti, E., Malik, C., Hoier, B., Walker, M., Walker, P.J., Odriozola, A., Graber, F., Tschanz, S.A., Bangsbo, J., Hoppeler, H., Askew, C.D. and Hellsten, Y. 2016. Capillary ultrastructure and mitochondrial volume density in skeletal muscle in relation to reduced exercise capacity of patients with intermittent claudication. *Am J Physiol Regul Integr Comp Physiol.* **310**(10), pp.R943-951.

Beuparlant, J., van den Brand, R., Barraud, Q., Friedli, L., Musienko, P., Dietz, V. and Courtine, G. 2013. Undirected compensatory plasticity contributes to neuronal dysfunction after severe spinal cord injury. *Brain.* **136**(Pt 11), pp.3347-3361.

Bellacen, K. and Lewis, E.C. 2009. Aortic ring assay. *J Vis Exp.* (33).

Bernacki, J., Dobrowolska, A., Nierwińska, K. and Małecki, A. 2008. Physiology and pharmacological role of the blood-brain barrier. *Pharmacol Rep.* **60**(5), pp.600-622.

Bloor, C.M. 2005. Angiogenesis during exercise and training. *Angiogenesis.* **8**(3), pp.263-271.

Breen, E.C., Johnson, E.C., Wagner, H., Tseng, H.M., Sung, L.A. and Wagner, P.D. 1996. Angiogenic growth factor mRNA responses in muscle to a single bout of exercise. *J Appl Physiol (1985).* **81**(1), pp.355-361.

Cao, Y., Zhou, Y., Ni, S., Wu, T., Li, P., Liao, S., Hu, J. and Lu, H. 2017. Three Dimensional Quantification of Microarchitecture and Vessel Regeneration by Synchrotron Radiation Microcomputed Tomography in a Rat Model of Spinal Cord Injury. *J Neurotrauma.* **34**(6), pp.1187-1199.

Carlson, G.D., Gorden, C.D., Nakazowa, S., Wada, E., Warden, K. and LaManna, J.C. 2000. Perfusion-limited recovery of evoked potential function after spinal cord injury. *Spine (Phila Pa 1976).* **25**(10), pp.1218-1226.

Carmeliet, P. and Tessier-Lavigne, M. 2005. Common mechanisms of nerve and blood vessel wiring. *Nature.* **436**(7048), pp.193-200.

- Casella, G.T., Marcillo, A., Bunge, M.B. and Wood, P.M. 2002. New vascular tissue rapidly replaces neural parenchyma and vessels destroyed by a contusion injury to the rat spinal cord. *Exp Neurol.* **173**(1), pp.63-76.
- Choi, D.W. 1987. Ionic dependence of glutamate neurotoxicity. *J Neurosci.* **7**(2), pp.369-379.
- Choi, J.S., Kim, H.Y., Cha, J.H., Choi, J.Y., Park, S.I., Jeong, C.H., Jeun, S.S. and Lee, M.Y. 2007. Upregulation of vascular endothelial growth factor receptors Flt-1 and Flk-1 following acute spinal cord contusion in rats. *J Histochem Cytochem.* **55**(8), pp.821-830.
- Cotman, C.W. and Berchtold, N.C. 2002. Exercise: a behavioral intervention to enhance brain health and plasticity. *Trends Neurosci.* **25**(6), pp.295-301.
- Courtine, G., Gerasimenko, Y., van den Brand, R., Yew, A., Musienko, P., Zhong, H., Song, B., Ao, Y., Ichiyama, R.M., Lavrov, I., Roy, R.R., Sofroniew, M.V. and Edgerton, V.R. 2009. Transformation of nonfunctional spinal circuits into functional states after the loss of brain input. *Nat Neurosci.* **12**(10), pp.1333-1342.
- Dale-Nagle, E.A., Satriotomo, I. and Mitchell, G.S. 2011. Spinal vascular endothelial growth factor induces phrenic motor facilitation via extracellular signal-regulated kinase and Akt signaling. *The Journal of neuroscience : the official journal of the Society for Neuroscience.* **31**(21), pp.7682-7690.
- Davis, G.E., Norden, P.R. and Bowers, S.L. 2015. Molecular control of capillary morphogenesis and maturation by recognition and remodeling of the extracellular matrix: functional roles of endothelial cells and pericytes in health and disease. *Connect Tissue Res.* **56**(5), pp.392-402.
- De Laporte, L., des Rieux, A., Tuinstra, H.M., Zelivyanskaya, M.L., De Clerck, N.M., Postnov, A.A., Pr at, V. and Shea, L.D. 2011. Vascular endothelial growth factor and fibroblast growth factor 2 delivery from spinal cord bridges to enhance angiogenesis following injury. *J Biomed Mater Res A.* **98**(3), pp.372-382.

- Deuis, J.R., Dvorakova, L.S. and Vetter, I. 2017. Methods Used to Evaluate Pain Behaviors in Rodents. *Front Mol Neurosci.* **10**, p284.
- Deveza, L., Choi, J. and Yang, F. 2012. Therapeutic angiogenesis for treating cardiovascular diseases. *Theranostics.* **2**(8), pp.801-814.
- Dias, D.O., Kim, H., Holl, D., Werne Solnestam, B., Lundeberg, J., Carlén, M., Göritz, C. and Frisén, J. 2018. Reducing Pericyte-Derived Scarring Promotes Recovery after Spinal Cord Injury. *Cell.* **173**(1), pp.153-165.e122.
- Dietz, V., Colombo, G., Jensen, L. and Baumgartner, L. 1995. Locomotor capacity of spinal cord in paraplegic patients. *Annals of Neurology.* **37**(5), pp.574-582.
- Dobkin, B., Apple, D., Barbeau, H., Basso, M., Behrman, A., Deforge, D., Ditunno, J., Dudley, G., Elashoff, R., Fugate, L., Harkema, S., Saulino, M. and Scott, M. 2006. Weight-supported treadmill vs over-ground training for walking after acute incomplete SCI. *Neurology.* **66**(4), pp.484-493.
- Duan, H., Ge, W., Zhang, A., Xi, Y., Chen, Z., Luo, D., Cheng, Y., Fan, K.S., Horvath, S., Sofroniew, M.V., Cheng, L., Yang, Z., Sun, Y.E. and Li, X. 2015. Transcriptome analyses reveal molecular mechanisms underlying functional recovery after spinal cord injury. *Proc Natl Acad Sci U S A.* **112**(43), pp.13360-13365.
- Duijvestijn, A.M., van Goor, H., Klatter, F., Majoor, G.D., van Bussel, E. and van Breda Vriesman, P.J. 1992. Antibodies defining rat endothelial cells: RECA-1, a pan-endothelial cell-specific monoclonal antibody. *Lab Invest.* **66**(4), pp.459-466.
- Dumont, R.J., Okonkwo, D.O., Verma, S., Hurlbert, R.J., Boulos, P.T., Ellegala, D.B. and Dumont, A.S. 2001. Acute spinal cord injury, part I: pathophysiologic mechanisms. *Clin Neuropharmacol.* **24**(5), pp.254-264.
- Dunford, E.C., Mandel, E.R., Mohajeri, S., Haas, T.L. and Riddell, M.C. 2017. Metabolic effects of prazosin on skeletal muscle insulin resistance in glucocorticoid-treated male rats. *American journal of physiology. Regulatory, integrative and comparative physiology.* **312**(1), pp.R62-R73.

Durham-Lee, J.C., Wu, Y., Mokkaapati, V.U., Paulucci-Holthauzen, A.A. and Nestic, O. 2012. Induction of angiopoietin-2 after spinal cord injury.

*Neuroscience*. **202**, pp.454-464.

Egginton, S. 2009. Invited review: activity-induced angiogenesis. *Pflugers Arch*. **457**(5), pp.963-977.

Egginton, S. 2016. In Vivo Models of Muscle Angiogenesis. In: Martin, S.G. and Hewett, P.W. eds. *Angiogenesis Protocols*. New York, NY: Springer New York, pp.355-373.

Egginton, S., Hussain, A., Hall-Jones, J., Chaudhry, B., Syeda, F. and Glen, K.E. 2016. Shear stress-induced angiogenesis in mouse muscle is independent of the vasodilator mechanism and quickly reversible. *Acta Physiol (Oxf)*. **218**(3), pp.153-166.

Egginton, S., Zhou, A.L., Brown, M.D. and Hudlická, O. 2001. Unorthodox angiogenesis in skeletal muscle. *Cardiovasc Res*. **49**(3), pp.634-646.

Engesser-Cesar, C., Ichiyama, R.M., Nefas, A.L., Hill, M.A., Edgerton, V.R., Cotman, C.W. and Anderson, A.J. 2007. Wheel running following spinal cord injury improves locomotor recovery and stimulates serotonergic fiber growth. *Eur J Neurosci*. **25**(7), pp.1931-1939.

Ermak, G. and Davies, K.J. 2002. Calcium and oxidative stress: from cell signaling to cell death. *Mol Immunol*. **38**(10), pp.713-721.

Erschbamer, M., Oberg, J., Westman, E., Sitnikov, R., Olson, L. and Spenger, C. 2011. <sup>1</sup>H-MRS in spinal cord injury: acute and chronic metabolite alterations in rat brain and lumbar spinal cord. *Eur J Neurosci*. **33**(4), pp.678-688.

Fitch, M.T., Doller, C., Combs, C.K., Landreth, G.E. and Silver, J. 1999. Cellular and molecular mechanisms of glial scarring and progressive cavitation: in vivo and in vitro analysis of inflammation-induced secondary injury after CNS trauma. *J Neurosci*. **19**(19), pp.8182-8198.

Giaume, C., Koulakoff, A., Roux, L., Holcman, D. and Rouach, N. 2010. Astroglial networks: a step further in neuroglial and gliovascular interactions. *Nature Reviews Neuroscience*. **11**(2), pp.87-99.

- Gibala, M.J. and Little, J.P. 2020. Physiological basis of brief vigorous exercise to improve health. *The Journal of Physiology*. **598**(1), pp.61-69.
- Goldsmith, H.S. 1994. Brain and spinal cord revascularization by omental transposition. *Neurol Res*. **16**(3), pp.159-162.
- Gómez-Pinilla, F., Ying, Z., Opazo, P., Roy, R.R. and Edgerton, V.R. 2001. Differential regulation by exercise of BDNF and NT-3 in rat spinal cord and skeletal muscle. *Eur J Neurosci*. **13**(6), pp.1078-1084.
- Goritz, C., Dias, D.O., Tomilin, N., Barbacid, M., Shupliakov, O. and Frisen, J. 2011. A pericyte origin of spinal cord scar tissue. *Science*. **333**(6039), pp.238-242.
- Guimarães, C.F., Gasperini, L., Marques, A.P. and Reis, R.L. 2020. The stiffness of living tissues and its implications for tissue engineering. *Nature Reviews Materials*. **5**(5), pp.351-370.
- Guo, M., Ricardo, S.D., Deane, J.A., Shi, M., Cullen-McEwen, L. and Bertram, J.F. 2005. A stereological study of the renal glomerular vasculature in the db/db mouse model of diabetic nephropathy. *J Anat*. **207**(6), pp.813-821.
- Halder, S.K., Kant, R. and Milner, R. 2018. Chronic mild hypoxia promotes profound vascular remodeling in spinal cord blood vessels, preferentially in white matter, via an  $\alpha 5\beta 1$  integrin-mediated mechanism. *Angiogenesis*. **21**(2), pp.251-266.
- Han, S., Arnold, S.A., Sithu, S.D., Mahoney, E.T., Geraldts, J.T., Tran, P., Benton, R.L., Maddie, M.A., D'Souza, S.E., Whittemore, S.R. and Hagg, T. 2010. Rescuing vasculature with intravenous angiopoietin-1 and alpha v beta 3 integrin peptide is protective after spinal cord injury. *Brain*. **133**(Pt 4), pp.1026-1042.
- Hanahan, D. 1997. Signaling vascular morphogenesis and maintenance. *Science*. **277**(5322), pp.48-50.
- Hansen-Smith, F., Egginton, S., Zhou, A.L. and Hudlicka, O. 2001. Growth of arterioles precedes that of capillaries in stretch-induced angiogenesis in skeletal muscle. *Microvasc Res*. **62**(1), pp.1-14.

- Harkema, S., Gerasimenko, Y., Hodes, J., Burdick, J., Angeli, C., Chen, Y., Ferreira, C., Willhite, A., Rejc, E., Grossman, R.G. and Edgerton, V.R. 2011. Effect of epidural stimulation of the lumbosacral spinal cord on voluntary movement, standing, and assisted stepping after motor complete paraplegia: a case study. *Lancet*. **377**(9781), pp.1938-1947.
- Hausmann, O.N. 2003. Post-traumatic inflammation following spinal cord injury. *Spinal Cord*. **41**(7), pp.369-378.
- Hayakawa, Y. and Wang, T.C. 2017. Nerves switch on angiogenic metabolism. *Science*. **358**(6361), pp.305-306.
- Herrera, J.J., Nestic, O. and Narayana, P.A. 2009. Reduced vascular endothelial growth factor expression in contusive spinal cord injury. *J Neurotrauma*. **26**(7), pp.995-1003.
- Herrera, J.J., Sundberg, L.M., Zentilin, L., Giacca, M. and Narayana, P.A. 2010. Sustained expression of vascular endothelial growth factor and angiopoietin-1 improves blood-spinal cord barrier integrity and functional recovery after spinal cord injury. *J Neurotrauma*. **27**(11), pp.2067-2076.
- Howard, C.V. and Reed, M.G. 1998. *Unbiased stereology: three-dimensional measurement in microscopy (advanced methods)*. 1st edition ed. Taylor & Francis.
- Hu, J.Z., Wu, T.D., Zhang, T., Zhao, Y.F., Pang, J. and Lu, H.B. 2012. Three-dimensional alteration of microvasculature in a rat model of traumatic spinal cord injury. *J Neurosci Methods*. **204**(1), pp.150-158.
- Ichiyama, R.M., Courtine, G., Gerasimenko, Y.P., Yang, G.J., van den Brand, R., Lavrov, I.A., Zhong, H., Roy, R.R. and Edgerton, V.R. 2008. Step training reinforces specific spinal locomotor circuitry in adult spinal rats. *J Neurosci*. **28**(29), pp.7370-7375.
- Iizuka, K., Machida, T. and Hirafuji, M. 2014. Skeletal Muscle Is an Endocrine Organ. *Journal of Pharmacological Sciences*. **125**(2), pp.125-131.

Imperato-Kalmar, E.L., McKinney, R.A., Schnell, L., Rubin, B.P. and Schwab, M.E. 1997. Local changes in vascular architecture following partial spinal cord lesion in the rat. *Exp Neurol.* **145**(2 Pt 1), pp.322-328.

Isaacs, K.R., Anderson, B.J., Alcantara, A.A., Black, J.E. and Greenough, W.T. 1992. Exercise and the brain: angiogenesis in the adult rat cerebellum after vigorous physical activity and motor skill learning. *J Cereb Blood Flow Metab.* **12**(1), pp.110-119.

Jaeger, C.B. and Blight, A.R. 1997. Spinal cord compression injury in guinea pigs: structural changes of endothelium and its perivascular cell associations after blood-brain barrier breakdown and repair. *Exp Neurol.* **144**(2), pp.381-399.

Jensen, R., Ortenblad, N., Stausholm, M.H., Skjaerbaek, M.C., Larsen, D.N., Hansen, M., Holmberg, H.C., Plomgaard, P. and Nielsen, J. 2020. Heterogeneity in subcellular muscle glycogen utilisation during exercise impacts endurance capacity in men. *J Physiol.* **598**(19), pp.4271-4292.

Jin, L.Y., Li, J., Wang, K.F., Xia, W.W., Zhu, Z.Q., Wang, C.R., Li, X.F. and Liu, H.Y. 2021. Blood-Spinal Cord Barrier in Spinal Cord Injury: A Review. *J Neurotrauma.* **38**(9), pp.1203-1224.

Kaneko, S., Iwanami, A., Nakamura, M., Kishino, A., Kikuchi, K., Shibata, S., Okano, H.J., Ikegami, T., Moriya, A., Konishi, O., Nakayama, C., Kumagai, K., Kimura, T., Sato, Y., Goshima, Y., Taniguchi, M., Ito, M., He, Z., Toyama, Y. and Okano, H. 2006. A selective Sema3A inhibitor enhances regenerative responses and functional recovery of the injured spinal cord. *Nat Med.* **12**(12), pp.1380-1389.

Kermani, P. and Hempstead, B. 2007. Brain-derived neurotrophic factor: a newly described mediator of angiogenesis. *Trends in cardiovascular medicine.* **17**(4), pp.140-143.

Kissane, R.W.P., Wright, O., Al'Joboori, Y.D., Marczak, P., Ichiyama, R.M. and Egginton, S. 2019. Effects of treadmill training on microvascular remodeling in the rat after spinal cord injury. *Muscle & Nerve.* **59**(3), pp.370-379.

- Kumar, H., Choi, H., Jo, M.-J., Joshi, H.P., Muttigi, M., Bonanomi, D., Kim, S.B., Ban, E., Kim, A., Lee, S.-H., Kim, K.-T., Sohn, S., Zeng, X. and Han, I. 2018a. Neutrophil elastase inhibition effectively rescued angiotensin-1 decrease and inhibits glial scar after spinal cord injury. *Acta neuropathologica communications*. **6**(1), pp.73-73.
- Kumar, R., Lim, J., Mekary, R.A., Rattani, A., Dewan, M.C., Sharif, S.Y., Osorio-Fonseca, E. and Park, K.B. 2018b. Traumatic Spinal Injury: Global Epidemiology and Worldwide Volume. *World Neurosurg*. **113**, pp.345-363.
- Kundi, S., Bicknell, R. and Ahmed, Z. 2013. The role of angiogenic and wound-healing factors after spinal cord injury in mammals. *Neurosci Res*. **76**(1-2), pp.1-9.
- Levick, J.R. 2010. *An introduction to cardiovascular physiology*. Fifth edition. ed. London: Hodder Arnold.
- Li, Y., Lucas-Osma, A.M., Black, S., Bandet, M.V., Stephens, M.J., Vavrek, R., Sanelli, L., Fenrich, K.K., Di Narzo, A.F., Dracheva, S., Winship, I.R., Fouad, K. and Bennett, D.J. 2017. Pericytes impair capillary blood flow and motor function after chronic spinal cord injury. *Nat Med*. **23**(6), pp.733-741.
- Lima, C., Pratas-Vital, J., Escada, P., Hasse-Ferreira, A., Capucho, C. and Peduzzi, J.D. 2006. Olfactory Mucosa Autografts in Human Spinal Cord Injury: A Pilot Clinical Study. *The Journal of Spinal Cord Medicine*. **29**(3), pp.191-203.
- Liu, Y., Figley, S., Spratt, S.K., Lee, G., Ando, D., Surosky, R. and Fehlings, M.G. 2010. An engineered transcription factor which activates VEGF-A enhances recovery after spinal cord injury. *Neurobiology of Disease*. **37**(2), pp.384-393.
- Lladó, J., Tolosa, L. and Olmos, G. 2013. Cellular and molecular mechanisms involved in the neuroprotective effects of VEGF on motoneurons. *Front Cell Neurosci*. **7**, pp.181.
- Lloyd, P.G., Prior, B.M., Yang, H.T. and Terjung, R.L. 2003. Angiogenic growth factor expression in rat skeletal muscle in response to exercise training. *Am J Physiol Heart Circ Physiol*. **284**(5), pp.1668-1678.

Long, H.Q., Xie, W.H., Chen, W.L., Xie, W.L., Xu, J.H. and Hu, Y. 2014. Value of micro-CT for monitoring spinal microvascular changes after chronic spinal cord compression. *Int J Mol Sci.* **15**(7), pp.12061-12073.

Loy, D.N., Crawford, C.H., Darnall, J.B., Burke, D.A., Onifer, S.M. and Whittemore, S.R. 2002. Temporal progression of angiogenesis and basal lamina deposition after contusive spinal cord injury in the adult rat. *J Comp Neurol.* **445**(4), pp.308-324.

Loy, K., Schmalz, A., Hoche, T., Jacobi, A., Kreuzfeldt, M., Merkler, D. and Bareyre, F.M. 2018. Enhanced Voluntary Exercise Improves Functional Recovery following Spinal Cord Injury by Impacting the Local Neuroglial Injury Response and Supporting the Rewiring of Supraspinal Circuits. *J Neurotrauma.* **35**(24), pp.2904-2915.

Mauter, A.E., Weinzierl, M.R., Donovan, F. and Noble, L.J. 2000. Vascular events after spinal cord injury: contribution to secondary pathogenesis. *Phys Ther.* **80**(7), pp.673-687.

Meinild Lundby, A.K., Jacobs, R.A., Gehrig, S., de Leur, J., Hauser, M., Bonne, T.C., Fluck, D., Dandanell, S., Kirk, N., Kaech, A., Ziegler, U., Larsen, S. and Lundby, C. 2018. Exercise training increases skeletal muscle mitochondrial volume density by enlargement of existing mitochondria and not de novo biogenesis. *Acta Physiol (Oxf).* **222**(1), pp.12195.

Miyamoto, N., Pham, L.D., Seo, J.H., Kim, K.W., Lo, E.H. and Arai, K. 2014. Crosstalk between cerebral endothelium and oligodendrocyte. *Cell Mol Life Sci.* **71**(6), pp.1055-1066.

Moisan, A., Favre, I.M., Rome, C., Grillon, E., Naegele, B., Barbieux, M., De Fraipont, F., Richard, M.J., Barbier, E.L., Remy, C. and Detante, O. 2014. Microvascular plasticity after experimental stroke: a molecular and MRI study. *Cerebrovasc Dis.* **38**(5), pp.344-353.

Muhlfeld, C., Papadakis, T., Krasteva, G., Nyengaard, J.R., Hahn, U. and Kummer, W. 2010. An unbiased stereological method for efficiently quantifying the innervation of the heart and other organs based on total length estimations. *J Appl Physiol (1985).* **108**(5), pp.1402-1409.

Mukoyama, Y.S., Shin, D., Britsch, S., Taniguchi, M. and Anderson, D.J. 2002. Sensory nerves determine the pattern of arterial differentiation and blood vessel branching in the skin. *Cell*. **109**(6), pp.693-705.

Muoio, V., Persson, P.B. and Sendeski, M.M. 2014. The neurovascular unit – concept review. *Acta Physiologica*. **210**(4), pp.790-798.

Nahirney, P.C., Reeson, P. and Brown, C.E. 2016. Ultrastructural analysis of blood-brain barrier breakdown in the peri-infarct zone in young adult and aged mice. *J Cereb Blood Flow Metab*. **36**(2), pp.413-425.

Navaratna, D., Guo, S., Arai, K. and Lo, E.H. 2009. Mechanisms and targets for angiogenic therapy after stroke. *Cell adhesion & migration*. **3**(2), pp.216-223.

Neeper, S.A., Gómez-Pinilla, F., Choi, J. and Cotman, C.W. 1996. Physical activity increases mRNA for brain-derived neurotrophic factor and nerve growth factor in rat brain. *Brain Res*. **726**(1-2), pp.49-56.

Ng, M.T., Stammers, A.T. and Kwon, B.K. 2011. Vascular disruption and the role of angiogenic proteins after spinal cord injury. *Transl Stroke Res*. **2**(4), pp.474-491.

Noble, L.J., Donovan, F., Igarashi, T., Goussev, S. and Werb, Z. 2002. Matrix metalloproteinases limit functional recovery after spinal cord injury by modulation of early vascular events. *J Neurosci*. **22**(17), pp.7526-7535.

Noble, L.J. and Wrathall, J.R. 1989. Distribution and time course of protein extravasation in the rat spinal cord after contusive injury. *Brain Res*. **482**(1), pp.57-66.

Noorafshan, A., Khazraei, H., Mirkhani, H. and Karbalay-Doust, S. 2013. Stereological study of the diabetic heart of male rats. *Lab Anim Res*. **29**(1), pp.12-18.

NSCIB, N.S.C.I.S.B. 2012. *The Initial Management of Adults with Spinal Cord Injuries. Advice for Major Trauma Networks and SCI Centres on the Development of Joint Protocols*. [Leaflet].

- Ohab, J.J., Fleming, S., Blesch, A. and Carmichael, S.T. 2006. A neurovascular niche for neurogenesis after stroke. *The Journal of neuroscience : the official journal of the Society for Neuroscience*. **26**(50), pp.13007-13016.
- Olfert, I.M. and Birot, O. 2011. Importance of anti-angiogenic factors in the regulation of skeletal muscle angiogenesis. *Microcirculation*. **18**(4), pp.316-330.
- Ouma, G.O., Jonas, R.A., Usman, M.H.U. and Mohler, E.R., 3rd. 2012. Targets and delivery methods for therapeutic angiogenesis in peripheral artery disease. *Vascular medicine (London, England)*. **17**(3), pp.174-192.
- Perrin, L.A., June, J.E., Rosebury, W., Robertson, A., Kovesdi, I., Bruder, J.T., Kessler, P.D., Keiser, J.A. and Gordon, D. 2004. Increased revascularization efficacy after administration of an adenovirus encoding VEGF(121). *Gene Ther*. **11**(6), pp.512-521.
- Peters, A., Palay, S.L. and Webster, H.d. 1976. The fine structure of the nervous system: neurons and their supporting cells. Third edition. *Ann Neurol*.
- Popovich, P.G., Horner, P.J., Mullin, B.B. and Stokes, B.T. 1996. A quantitative spatial analysis of the blood-spinal cord barrier. I. Permeability changes after experimental spinal contusion injury. *Exp Neurol*. **142**(2), pp.258-275.
- Prior, B.M., Yang, H.T. and Terjung, R.L. 2004. What makes vessels grow with exercise training? *J Appl Physiol (1985)*. **97**(3), pp.1119-1128.
- Prockop, L.D., Naidu, K.A., Binard, J.E. and Ransohoff, J. 1995. Selective permeability of [3H]-D-mannitol and [14C]-carboxyl-inulin across the blood-brain barrier and blood-spinal cord barrier in the rabbit. *J Spinal Cord Med*. **18**(4), pp.221-226.
- Rauch, M.F., Hynes, S.R., Bertram, J., Redmond, A., Robinson, R., Williams, C., Xu, H., Madri, J.A. and Lavik, E.B. 2009. Engineering angiogenesis following spinal cord injury: a coculture of neural progenitor and endothelial cells in a degradable polymer implant leads to an increase in vessel density and formation of the blood-spinal cord barrier. *Eur J Neurosci*. **29**(1), pp.132-145.
- Ready, T. 2001. Limited gene therapy trials to restart. *Nature Medicine*. **7**(3), pp.265-265.

Rolls, A., Shechter, R. and Schwartz, M. 2009. The bright side of the glial scar in CNS repair. *Nature Reviews Neuroscience*. **10**(3), pp.235-241.

Rust, R., Gantner, C. and Schwab, M.E. 2019. Pro- and antiangiogenic therapies: current status and clinical implications. *The FASEB Journal*. **33**(1), pp.34-48.

Sandoo, A., van Zanten, J.J., Metsios, G.S., Carroll, D. and Kitas, G.D. 2010. The endothelium and its role in regulating vascular tone. *Open Cardiovasc Med J*. **4**, pp.302-312.

Sandvig, A., Berry, M., Barrett, L.B., Butt, A. and Logan, A. 2004. Myelin-, reactive glia-, and scar-derived CNS axon growth inhibitors: expression, receptor signaling, and correlation with axon regeneration. *Glia*. **46**(3), pp.225-251.

Serini, G. and Bussolino, F. 2004. Common cues in vascular and axon guidance. *Physiology (Bethesda)*. **19**, pp.348-354.

Sharma, H.S. 2005. Pathophysiology of blood-spinal cord barrier in traumatic injury and repair. *Curr Pharm Des*. **11**(11), pp.1353-1389.

Shen, Q., Goderie, S.K., Jin, L., Karanth, N., Sun, Y., Abramova, N., Vincent, P., Pumiglia, K. and Temple, S. 2004. Endothelial Cells Stimulate Self-Renewal and Expand Neurogenesis of Neural Stem Cells. *Science*. **304**(5675), pp.1338-1340.

Shigematsu, H., Yasuda, K., Iwai, T., Sasajima, T., Ishimaru, S., Ohashi, Y., Yamaguchi, T., Ogihara, T. and Morishita, R. 2010. Randomized, double-blind, placebo-controlled clinical trial of hepatocyte growth factor plasmid for critical limb ischemia. *Gene Ther*. **17**(9), pp.1152-1161.

Shtaya, A., Sadek, A.R., Nicoll, J.A.R. and Nader-Sepahi, A. 2018. Choroid Plexus in the Central Canal of the Spinal Cord Causing Recurrent Syringomyelia. *World Neurosurg*. **111**, pp.275-278.

Simard, J.M., Tsybalyuk, O., Ivanov, A., Ivanova, S., Bhatta, S., Geng, Z., Woo, S.K. and Gerzanich, V. 2007. Endothelial sulfonylurea receptor 1-regulated NC Ca-ATP channels mediate progressive hemorrhagic necrosis

following spinal cord injury. *The Journal of clinical investigation*. **117**(8), pp.2105-2113.

Singh, A., Tetreault, L., Kalsi-Ryan, S., Nouri, A. and Fehlings, M.G. 2014. Global prevalence and incidence of traumatic spinal cord injury. *Clin Epidemiol*. **6**, pp.309-331.

Sköld, M., Cullheim, S., Hammarberg, H., Piehl, F., Suneson, A., Lake, S., Sjögren, A., Walum, E. and Risling, M. 2000. Induction of VEGF and VEGF receptors in the spinal cord after mechanical spinal injury and prostaglandin administration. *European Journal of Neuroscience*. **12**(10), pp.3675-3686.

Slomnicki, L.P., Myers, S.A., Saraswat Ohri, S., Parsh, M.V., Andres, K.R., Chariker, J.H., Rouchka, E.C., Whittemore, S.R. and Hetman, M. 2020. Improved locomotor recovery after contusive spinal cord injury in Bmal1(-/-) mice is associated with protection of the blood spinal cord barrier. *Sci Rep*. **10**(1), pp.14212.

Smith, R.R., Brown, E.H., Shum-Siu, A., Whelan, A., Burke, D.A., Benton, R.L. and Magnuson, D.S. 2009. Swim training initiated acutely after spinal cord injury is ineffective and induces extravasation in and around the epicenter. *J Neurotrauma*. **26**(7), pp.1017-1027.

Spampinato, S.F., Bortolotto, V., Canonico, P.L., Sortino, M.A. and Grilli, M. 2019. Astrocyte-Derived Paracrine Signals: Relevance for Neurogenic Niche Regulation and Blood–Brain Barrier Integrity. *Frontiers in Pharmacology*. **10**(1346).

Squair, J.W., West, C.R., Popok, D., Assinck, P., Liu, J., Tetzlaff, W. and Krassioukov, A.V. 2017. High Thoracic Contusion Model for the Investigation of Cardiovascular Function after Spinal Cord Injury. *J Neurotrauma*. **34**(3), pp.671-684.

Stratman, A.N., Malotte, K.M., Mahan, R.D., Davis, M.J. and Davis, G.E. 2009. Pericyte recruitment during vasculogenic tube assembly stimulates endothelial basement membrane matrix formation. *Blood*. **114**(24), pp.5091-5101.

- Streijger, F., So, K., Manouchehri, N., Tigchelaar, S., Lee, J.H.T., Okon, E.B., Shortt, K., Kim, S.E., McInnes, K., Cripton, P. and Kwon, B.K. 2017. Changes in Pressure, Hemodynamics, and Metabolism within the Spinal Cord during the First 7 Days after Injury Using a Porcine Model. *J Neurotrauma*. **34**(24), pp.3336-3350.
- Sun, Y., Jin, K., Xie, L., Childs, J., Mao, X.O., Logvinova, A. and Greenberg, D.A. 2003. VEGF-induced neuroprotection, neurogenesis, and angiogenesis after focal cerebral ischemia. *J Clin Invest*. **111**(12), pp.1843-1851.
- Sundberg, L.M., Herrera, J.J. and Narayana, P.A. 2011. Effect of vascular endothelial growth factor treatment in experimental traumatic spinal cord injury: in vivo longitudinal assessment. *J Neurotrauma*. **28**(4), pp.565-578.
- Swain, R.A., Harris, A.B., Wiener, E.C., Dutka, M.V., Morris, H.D., Theien, B.E., Konda, S., Engberg, K., Lauterbur, P.C. and Greenough, W.T. 2003. Prolonged exercise induces angiogenesis and increases cerebral blood volume in primary motor cortex of the rat. *Neuroscience*. **117**(4), pp.1037-1046.
- Tang, Y., Nyengaard, J.R., Andersen, J.B., Baandrup, U. and Gundersen, H.J. 2009. The application of stereological methods for estimating structural parameters in the human heart. *Anat Rec (Hoboken)*. **292**(10), pp.1630-1647.
- Tator, C.H. and Koyanagi, I. 1997. Vascular mechanisms in the pathophysiology of human spinal cord injury. *J Neurosurg*. **86**(3), pp.483-492.
- Tsilibary, E.C. 2003. Microvascular basement membranes in diabetes mellitus. *J Pathol*. **200**(4), pp.537-546.
- van den Brand, R., Heutschi, J., Barraud, Q., DiGiovanna, J., Bartholdi, K., Huerlimann, M., Friedli, L., Vollenweider, I., Moraud, E.M., Duis, S., Dominici, N., Micera, S., Musienko, P. and Courtine, G. 2012. Restoring Voluntary Control of Locomotion after Paralyzing Spinal Cord Injury. *Science*. **336**(6085), pp.1182-1185.
- van Hinsbergh, V.W. and Koolwijk, P. 2008. Endothelial sprouting and angiogenesis: matrix metalloproteinases in the lead. *Cardiovasc Res*. **78**(2), pp.203-212.

Vasiliadis, A.V., Zafeiridis, A., Dipla, K., Galanis, N., Chatzidimitriou, D., Kyparos, A., Nikolaidis, M.G. and Vrabas, I.S. 2014. Circulating angiogenic biomolecules at rest and in response to upper-limb exercise in individuals with spinal cord injury. *The Journal of Spinal Cord Medicine*. **37**(2), pp.226-232.

Vink, H. and Duling, B.R. 1996. Identification of distinct luminal domains for macromolecules, erythrocytes, and leukocytes within mammalian capillaries. *Circ Res*. **79**(3), pp.581-589.

Wang, H., Liu, N.K., Zhang, Y.P., Deng, L., Lu, Q.B., Shields, C.B., Walker, M.J., Li, J. and Xu, X.M. 2015. Treadmill training induced lumbar motoneuron dendritic plasticity and behavior recovery in adult rats after a thoracic contusive spinal cord injury. *Exp Neurol*. **271**, pp.368-378.

Warburton, D.E., Nicol, C.W. and Bredin, S.S. 2006. Health benefits of physical activity: the evidence. *Cmaj*. **174**(6), pp.801-809.

Ward, P.J., Herrity, A.N., Harkema, S.J. and Hubscher, C.H. 2016. Training-Induced Functional Gains following SCI. *Neural Plast*. **2016**, pp.4307694.

Weibel, E.R. 1980. Theoretical foundations. *Stereological Method*. **2**, pp.1-348.

Wernig, A. and Müller, S. 1992. Laufband locomotion with body weight support improved walking in persons with severe spinal cord injuries. *Paraplegia*. **30**(4), pp.229-238.

West, C.R., Mills, P. and Krassioukov, A.V. 2012. Influence of the neurological level of spinal cord injury on cardiovascular outcomes in humans: a meta-analysis. *Spinal Cord*. **50**(7), pp.484-492.

West, M.J. 2012. *Basic Stereology for Biologists and Neuroscientists*. Cold Spring Harbor Laboratory Press.

Whetstone, W.D., Hsu, J.-Y.C., Eisenberg, M., Werb, Z. and Noble-Haeusslein, L.J. 2003. Blood-spinal cord barrier after spinal cord injury: relation to revascularization and wound healing. *Journal of neuroscience research*. **74**(2), pp.227-239.

Willison, A.G., Smith, S., Davies, B.M., Kotter, M.R.N. and Barnett, S.C. 2020. A scoping review of trials for cell-based therapies in human spinal cord injury. *Spinal Cord*. **58**(8), pp.844-856.

Wirz, M., Zemon, D.H., Rupp, R., Scheel, A., Colombo, G., Dietz, V. and Hornby, T.G. 2005. Effectiveness of automated locomotor training in patients with chronic incomplete spinal cord injury: a multicenter trial. *Arch Phys Med Rehabil*. **86**(4), pp.672-680.

Wolman, L. 1965. The disturbance of circulation in traumatic paraplegia in acute and late stages: A pathological study. *Spinal Cord*. **2**(4), pp.213-226.

Xu, J., Long, H., Chen, W., Cheng, X., Yu, H., Huang, Y., Wang, X. and Li, F. 2017. Ultrastructural Features of Neurovascular Units in a Rat Model of Chronic Compressive Spinal Cord Injury. *Front Neuroanat*. **11**, pp.136.

Xu, Y., He, Q., Wang, M., Wang, X., Gong, F., Bai, L., Zhang, J. and Wang, W. 2019. Quantifying blood-brain-barrier leakage using a combination of evans blue and high molecular weight FITC-Dextran. *J Neurosci Methods*. **325**, pp.108349.

Yin, J., Yin, Z., Wang, B., Zhu, C., Sun, C., Liu, X. and Gong, G. 2019. Angiotensin-1 Protects Spinal Cord Ischemia and Reperfusion Injury by Inhibiting Autophagy in Rats. *Neurochemical Research*. **44**(12), pp.2746-2754.

Ying, X., Xie, Q., Li, S., Yu, X., Zhou, K., Yue, J., Chen, X., Tu, W., Yang, G. and Jiang, S. 2020. Water treadmill training attenuates blood-spinal cord barrier disruption in rats by promoting angiogenesis and inhibiting matrix metalloproteinase-2/9 expression following spinal cord injury. *Fluids and Barriers of the CNS*. **17**(1), pp.70.

Ying, Z., Roy, R.R., Zhong, H., Zdzunowski, S., Edgerton, V.R. and Gomez-Pinilla, F. 2008. BDNF-exercise interactions in the recovery of symmetrical stepping after a cervical hemisection in rats. *Neuroscience*. **155**(4), pp.1070-1078.

- Ylä-Herttuala, S., Bridges, C., Katz, M.G. and Korpisalo, P. 2017. Angiogenic gene therapy in cardiovascular diseases: dream or vision? *European Heart Journal*. **38**(18), pp.1365-1371.
- Yu, S., Yao, S., Wen, Y., Wang, Y., Wang, H. and Xu, Q. 2016. Angiogenic microspheres promote neural regeneration and motor function recovery after spinal cord injury in rats. *Sci Rep*. **6**, pp.33428.
- Zakrzewicz, A., Secomb, T.W. and Pries, A.R. 2002. Angioadaptation: keeping the vascular system in shape. *News Physiol Sci*. **17**, pp.197-201.
- Zhan, Y., Li, M.-Z., Yang, L., Feng, X.-F., Zhang, Q.-X., Zhang, N., Zhao, Y.-Y. and Zhao, H. 2019. An MRI Study of Neurovascular Restorative After Combination Treatment With Xiaoshuan Enteric-Coated Capsule and Enriched Environment in Rats After Stroke. *Frontiers in neuroscience*. **13**, pp.701-701.
- Zhang, Z.G., Zhang, L., Croll, S.D. and Chopp, M. 2002. Angiopoietin-1 reduces cerebral blood vessel leakage and ischemic lesion volume after focal cerebral embolic ischemia in mice. *Neuroscience*. **113**(3), pp.683-687.
- Zonta, M., Angulo, M.C., Gobbo, S., Rosengarten, B., Hossmann, K.-A., Pozzan, T. and Carmignoto, G. 2003. Neuron-to-astrocyte signaling is central to the dynamic control of brain microcirculation. *Nature Neuroscience*. **6**(1), pp.43-50.